

Tormod Selbekk

# Ultrasound imaging in neurosurgery

Delineation of tumours for resection control

Thesis for the degree of Philosophiae Doctor

Trondheim, March 2013

Norwegian University of Science and Technology  
Faculty of Medicine  
Department of Circulation and Medical Imaging



**NTNU – Trondheim**  
Norwegian University of  
Science and Technology

**NTNU**

Norwegian University of Science and Technology

Thesis for the degree of Philosophiae Doctor

Faculty of Medicine

Department of Circulation and Medical Imaging

© Tormod Selbekk

ISBN 978-82-471-4270-7 (printed ver.)

ISBN 978-82-471-4271-4 (electronic ver.)

ISSN 1503-8181

Doctoral theses at NTNU, 2013:85

Printed by NTNU-trykk

## **Ultralyd avbildning i nevrokirurgi - avgrensning av svulster for reseksjonskontroll**

Ved operasjon av svulster ønsker man som regel å fjerne så mye av svulstvevet som mulig. Hvor mye av svulstvevet som fjernes under en operasjon, kan ha stor betydning for pasienten. Fullstendig fjerning, i motsetning til delvis fjerning av all makroskopisk svulstvev er for de fleste hjernesvulster assosiert med lengre overlevelse. Ultralyd er en avbildningsteknikk som kan gi økt reseksjonsgrad og dermed økt overlevelse, samt tryggere kirurgi med mindre sjanse for nevrologiske utfall. Det forutsetter imidlertid at ultralyd er i stand til å avbilde utbredelsen av svulsten på en sannferdig måte, under hele operasjonsforløpet.

Studiene inkludert i avhandlingen tar for seg hvordan overgangen mellom hjernesvulster og normalt hjernevev avbildes med ultralyd. I to studier har vi samlet inn biopsier periferet i hjernesvulster ved hjelp av navigasjonsteknologi og 3D ultralyd, for å sammenligne histologi og ultralyd bildefunn. Resultatene fra biopsistudiene viser at det er godt samsvar mellom histologi og bildefunn, for biopsier samlet inn før påbegynt reseksjon. Resultatene viser også at kvaliteten på ultralydbildene kan påvirkes av selve operasjonsforløpet. Ultralyd bildevolum samlet inn før man begynner å fjerne svulsten gir en svært god avbildning av svulstens utbredelse, mens ultralyd samlet inn underveis og helt i slutten av operasjonsforløpet kan være vanskeligere å tolke for kirurgen. Kirurgien vil i seg selv føre til mer støy og forstyrrelser i ultralydbildene, som dermed kan bli mindre spesifikke i å skille mellom svulst og normalt hjernevev. Årsakene til dette blir diskutert i avhandlingen, og det blir foreslått hvordan man kan identifisere og redusere støy i bildene.

I tre andre studier har vi prosessert ultralyddata og beregnet relativ tøyning i vevet. Hensikten har vært å undersøke om prosessering av ultralyd-data kan brukes som metode for å finne vevshastighet og beregne tøyning i vevet, og i så fall om dette kan skille mellom svulst og normalt hjernevev. Arbeidet førte til den første artikkelen, etter det vi kjenner til, som viste at det er mulig å skille hjernesvulster fra normalvev ved hjelp av ultralyd elastogrammer, dvs. bilder som viser ulik tøyning i vevet. De små tøyningene som ble detektert i vevet er forårsaket av at arteriene pulserer, og dermed gir bevegelse i det omliggende hjernevevet. Videre viste resultatene at graden av tøyning er signifikant mindre i svulstvev enn i normalt hjernevev. Analyser viste også at det er signifikant høyere kontrast mellom svulstvev og normal hjerne i elastogrammene enn i konvensjonelle ultralydbilder. Ultralyd avbildning av tøyning har derfor et potensial til å skille bedre mellom patologisk vev og normalt hjernevev enn konvensjonell ultralyd.

Tormod Selbekk

Institutt for sirkulasjon og bildediagnostikk, NTNU

Hovedveileder: Prof. Toril A. Nagelhus Hernes

Biveiledere: Prof. Geirmund Unsgård, Prof. Hans Torp

Finansiering: Nasjonalt kompetansesenter for 3D ultralyd i nevrokirurgi, samt SINTEF gjennom strategiske midler for samarbeid med Medical Imaging Lab, NTNU

*Ovennevnte avhandling er funnet verdig til å forsvares offentlig  
for graden Philosophiae Doctor (PhD) i medisinsk teknologi.  
Disputas finner sted i Auditoriet Geitfjellet, 2. etg. Øya Helsehus, mandag  
11. mars 2013, kl. 12:15*



## **Acknowledgement**

This thesis is a result of studies conducted at the *National Centre of Competence in Ultrasound and Image-guided Therapy* at St. Olavs University Hospital, which is continuing the activities in the previous National centre for 3D ultrasound in neurosurgery (1996-2011). The centre is a fruitful cross-disciplinary collaboration between the Norwegian University of Science and Technology (Norges teknisk-naturvitenskapelige universitet, NTNU), the research foundation SINTEF and St. Olavs University Hospital. I was formally enrolled as a PhD student at NTNU in February 2009. The PhD has been financed the National Centre for 3D ultrasound in Neurosurgery and by SINTEF through strategic collaboration with Medical Imaging Lab, NTNU.

It has been a great privilege to do research within the framework of the National Centre. The spirit of the team when it comes to research and development is astonishing, and there is a common goal to seek improved solutions for image guidance in neurosurgery and to evaluate clinical outcome by performing clinical studies. The studies included in this thesis would of course not have been possible to perform without the efforts and support by the staff at the neurosurgical department, St. Olavs Hospital. I wish to express my thankfulness to the staff at the neurosurgical department, including all the surgeons, nurses, assistants, technicians and other personnel that have made the research possible to do. In particular I would like to thank my co-supervisor Professor Geirmund Unsgård, for his endurance and enthusiasm when it comes to the research activities, for his believe in cross-disciplinary research, and for all the interesting discussions. I would also express my gratitude to Ole Solheim, consultant neurosurgeon, for his contributions and willingness to help in the studies included in my PhD as well as in other projects. Together with Asgeir S. Jakola, resident neurosurgeon, Linda Nordtvedt and Lisa M. Sagberg, research nurses, who are important contributors in on-going research activity, they form a strong academic team with an unique flair for generating and conducting studies that are highly publishable. I would also like to thank Ola M. Rygh for valuable collaboration and discussions while he was working at St. Olavs Hospital.

I am thankful to all my colleagues at the department of Medical Technology, SINTEF for their valuable skills and knowledge, and for providing a positive work atmosphere. I wish to express my gratitude to supervisor Professor Toril A. N. Hernes for her valuable guidance and encouragement throughout my PhD, and for suggesting practical solutions to manage both my SINTEF-job and my PhD-studies. My sincere thanks goes to Reidar Brekken for substantial contributions, by implementing in Matlab methods for analysis of ultrasound data and elastograms, and for valuable discussions during the studies. Thanks to former colleague Jon Bang, for implementing the first version of the strain processing in Matlab. Thanks also to Frank Lindseth, Ingerid Reinertsen and all the other scientists at SINTEF that are significantly contributing to the research within image guided neurosurgery.

I would also express my gratitude to my co-supervisor Hans Torp at the department of Circulation and Medical Imaging for discussions about ultrasound elastography and not at least for supervising student projects about ultrasound strain imaging of brain tumours.

I am very thankful to my co-authors Sverre H. Torp, Stian Lydersen, Steinar Ommedal (who was also my valuable mentor when I started working at SINTEF), Tomm B. Müller, Marit Indergaard, and Gunnar Myhr for their efforts and important contributions.

At last, but not least, I am grateful for the support from my family. Especially the useful discussions about neurosurgery and image guided therapy with my wife Oddrun Fredriksli. I am very grateful for my sons, Hallvard and Åsmund, and the patience they have with their father.

## Table of contents

Abbreviations .....	9
List of publications .....	11
Summary .....	13
1.0 Introduction .....	15
2.0 Ultrasound imaging .....	19
2.1 Sound and ultrasound .....	19
2.2 Resolution in the ultrasound images .....	20
2.3 Attenuation and depth penetration .....	22
2.4 Reflection and scattering of sound .....	22
2.5 Ultrasound imaging techniques .....	24
3.0 Tissue elasticity and ultrasound imaging .....	27
3.1 Longitudinal and transverse waves in soft tissue .....	27
3.2 Elastic moduli .....	28
3.3 Ultrasound imaging of tissue strain and elasticity .....	30
4.0 Navigation and ultrasound imaging in brain surgery .....	35
4.1 Brain tumours .....	35
4.2 Neuronavigation systems .....	36
4.3 Neuronavigation and intraoperative ultrasound .....	38
5.0 Aims .....	41
6.0 Summary of papers .....	43
6.1 Paper 1 .....	43
6.2 Paper 2 .....	43
6.3 Paper 3 .....	44
6.4 Paper 4 .....	45
6.5 Paper 5 .....	46
7.0 Discussion .....	49
7.1 Ultrasound for resection control .....	49
7.1.1 Ultrasound artefacts in intraoperative imaging .....	51
7.1.2 How to minimize surgically induced ultrasound artefacts .....	54
7.2 Ultrasound strain imaging of brain tumours .....	57
7.2.1 The relative hardness of tissue .....	57
7.2.2 Assessment of B-mode and strain image quality .....	59
7.2.3 Is ultrasound strain imaging suitable for resection control? .....	60
8.0 Intraoperative ultrasound - future perspectives .....	65
9.0 References .....	67

Appendix: Paper 1 - 5



## **Abbreviations**

2D - Two dimensional

3D - Three dimensional

A-mode - Amplitude Mode

B-mode - Brightness Mode

M-mode - Motion Mode

CSF - Cerebrospinal fluid

CT - Computed Tomography

Hz - Hertz

MHz - Megahertz (1.000.000 Hz)

MR - Magnetic Resonance

MRI - Magnetic Resonance Imaging

RF - Radio Frequency

ROC - Receiver Operating Characteristics



## List of publications

- 1) **Selbekk T**, Bang J, Unsgaard G. Strain processing of intraoperative ultrasound images of brain tumours: initial results. *Ultrasound Med Biol.* 2005; 31(1): 45-51
- 2) **Selbekk T**, Brekken R, Solheim O, Lydersen S, Hernes TAN, Unsgård G. Tissue motion and strain in the human brain assessed by intraoperative ultrasound in glioma patients. *Ultrasound Med Biol*; 36(1): 2-10, 2010
- 3) **Selbekk T**, Brekken R, Indergaard M, Solheim O, Unsgård G. Comparison of Contrast in Brighness Mode and Strain Ultrasonography of Glial Brain Tumours. *BMC Medical Imaging*, 2012, May 23; 12:11
- 4) Unsgård G, **Selbekk T**, Müller TB, Ommedal S, Torp HS, Myhr G, Bang J, Nagelhus Hernes TA. Ability of navigated 3D ultrasound to delineate gliomas and metastases - comparison of image interpretations with histopathology. *Acta Neurochirurgica*, 2005; 147(12):1259-69.
- 5) Rygh OM, **Selbekk T**, Torp S, Lydersen S, Hernes TAN, Unsgaard G. Comparison of ultrasound findings with histopathology in subsequent phases of glioblastoma resection. *Acta Neurochir (Wien)*, 2008; 150(10):1033-41.

## Contributions in relevant papers that are not included in the PhD thesis

1. Reinertsen I, Jakola AS, Friderichsen P, Lindseth F, Solheim O, **Selbekk T** and Unsgård G. A new system for 3D ultrasound guided placement of cerebral ventricular catheters. *International Journal of Computer Assisted Radiology and Surgery* 2012; 7(1): 151-157.
2. Unsgård G, Solheim O, Lindseth F, **Selbekk T**: Intraoperative Imaging with 3D Ultrasound in Neurosurgery. *Acta Neurochir Suppl.* 2011, Volume 109, Part 6, 181-186
3. Solheim O, **Selbekk T**, Jakola AS, Unsgård G. Ultrasound-guided operations in unselected high-grade gliomas—overall results, impact of image quality and patient selection. *Acta Neurochirurgica* 2010; 152(11): 1873-1886.
4. Våpenstad C, Rethy A, Lango T, **Selbekk T**, Ystgaard B, Hernes TAN, et al. Laparoscopic ultrasound: a survey of its current and future use, requirements, and integration with navigation technology. *Surg Endosc.* 2010, 24(12), 2944-2953.
5. Berntsen EM, Gulati S, Solheim O, Kvistad KA, Torp SH, **Selbekk T**, Unsgård G, Håberg AK. BOLD fMRI and Diffusion Tensor Tractography Incorporated into a 3D Ultrasound-based Intra-operative Imaging Navigation System: Impact on Therapeutic Strategies, Extent of Resection and Clinical Outcome. *Neurosurgery* 2010; 67(2): 237-250
6. Solheim O, **Selbekk T**, Løvtakken L, Tangen GA, Solberg OV, Johansen TF, Cappelen J, Unsgård G. Intracellular ultrasound in transsphenoidal surgery - a novel technique. *Neurosurgery*, 2010; 66:173-186
7. Solheim O, **Selbekk T**, Lindseth F, Unsgaard G, Intraoperative navigated 3D ultrasound in giant intracranial meningiomas. *Acta Neurochirurgica*, 2009; 151:1143-1151
8. Gulati S, Berntsen EM, Solheim O, Kvistad KA, Håberg A, **Selbekk T**, Lindseth F, Torp SH, Unsgaard G. Surgical resection of high grade gliomas in eloquent regions guided by blood oxygenation level dependent functional magnetic resonance imaging, diffusion tensor tractography, and intraoperative navigated 3D ultrasound. *Minimally Invasive Neurosurgery*, 2009; 52:1: 17-24
9. Rasmussen I-A, Lindseth F, Rygh OM, Berntsen EM, **Selbekk T**, Xu J, Hernes TAN, Harg E, Håberg A, Unsgaard G. Improved neuronavigation by use of combined intraoperative 3D ultrasound and brain shift corrected functional MRI and DTI-based tractograms: Initial experiences during surgical resections close to eloquent cerebrocortical areas. *Acta Neurochir.* 149:365-378, 2007
10. Rygh OM, **Selbekk T**, Lindseth F, Müller TB, Hernes TAN, Unsgaard G. Intraoperative navigated 3D ultrasound angiography in surgery. *Surgical Neurology*. 66:581-592, 2006
11. Hernes TAN, Lindseth F, **Selbekk T**, Rygh OM, Tangen GA, Rasmussen I, Wollf A, Rasmussen I, Solberg OV, Harg E, Augdal S, Couweleers F, Unsgaard G. Technical developments for improved 3D ultrasound guided neurosurgery - Computer-assisted 3D ultrasound-guided neurosurgery: technological contributions, including multimodal registration and advanced display, demonstrating future perspectives. *International Journal of Medical Robotics and Computer Assisted Surgery*, 2:1:45-59, 2006
12. Kolstad F, Rygh OM, **Selbekk T**, Unsgaard G, Nygaards OP. Three-dimensional ultrasonography navigation in spinal cord tumor surgery. Technical note. *J Neurosurg: Spine*, 5:3:264-70, 2006
13. Unsgaard G, Rygh OM, **Selbekk T**, Müller TB, Kolstad F, Lindseth F, Hernes TAN. Intraoperative 3D ultrasound in neurosurgery. *Acta Neurochirurgica*, 148:3:235-53, 2006
14. Rygh OM, Cappelen J, **Selbekk T**, Lindseth F, Hernes TAN, Unsgård G. Endoscopy guided by an intraoperative 3D ultrasound based neuronavigation system. *Minim Invasive Neurosurg*, February, 49:1:1-9, 2006.
15. Hernes TAN, **Selbekk T**, Lindseth F, Rygh OM, Muller T, Unsgård G. Navigated neurosurgery with intraoperative 3D ultrasound. *Indian Clinical Neurosurgery*, vol 5, 2005

## Summary

Complete removal, as opposed to only partial removal, of all macroscopic tumor tissue is associated with longer survival for most of the brain tumours. Ultrasound is an imaging technique that can contribute to increase the degree of tumour being removed by the surgeon, and thereby indirectly contribute to increased survival. Ultrasound may also contribute to safer surgery and less risk for neurological damage. However, this requires that the ultrasound images are able to depict the tumour in an adequate manner, throughout the whole operation.

The studies included in the thesis investigate whether or not ultrasound is able to adequately depict the transition between tumour and normal brain. In two studies we have used 3D ultrasound and a navigated biopsy forceps to collect biopsies in the peripheral tumor in order to compare ultrasound image findings and histology.

The results of the biopsy studies show that there is a high correspondence between histology and ultrasound findings, for biopsies sampled prior to start of resection. However, the quality of the ultrasound images is affected by the progress of the surgery. Ultrasound image volumes acquired before start of resection show a realistic delineation of the solid tumour. The images from 3D ultrasound volumes acquired during and at the end of surgery are somewhat more difficult to interpret for the surgeon. The surgery itself introduces more noise and interference in the ultrasound images, making the images less specific in separating normal tissue from tumour. The reasons for the increased noise are discussed, and it is suggested how the noise can be identified and reduced.

In three other studies ultrasound data has been processed off-line to estimate strain in the brain tissue. The aim was to investigate whether or not processing of ultrasound data could detect different elasticity in tumor tissue and normal brain, and if so, check if this could differentiate between tumor and normal brain. The work led to the first article, of our knowledge, demonstrating that it is possible to image brain tumors using ultrasonic elastograms, i.e. images depicting strain in the tissue. The pulsation of the arteries during a cardiac cycle impose movements of the surrounding

brain tissue, and this was found to cause sufficient deformation to allow generation of strain images. Furthermore, the results showed that the degree of strain is significantly less in tumor tissue than in normal brain tissue. Analysis of image contrast, showed that the strain images have significantly higher contrast between tumor and normal brain than conventional ultrasound images. Ultrasound imaging of strain has thereby the inherent potential to differentiate better between pathological and normal brain tissue than conventional ultrasound. The results suggest that ultrasound elastography methods should be further developed for intraoperative use. This could complement the future use of ultrasound imaging in neurosurgery.

## **1.0 Introduction**

Medical imaging has throughout the last decades changed the way surgery is being performed. The introduction of imaging technology in the operating room has made it possible to perform less invasive procedures, and has significantly advanced the field of surgery. Intraoperative imaging is so established in many therapeutic treatments today that it would be difficult to do even simple interventional or surgical procedures without the guidance and monitoring being offered by medical imaging technology. In interventional radiology instruments are guided inside the body by medical images. This has in some fields replaced traditional open surgery, and thereby offers less invasive treatment of the patients. In traditional surgical disciplines the use of intraoperative imaging has led to surgery being performed through smaller openings in the body, and to less traumatization of healthy tissue.

The technology used for the image-guided procedure may in general be either Magnetic Resonance Imaging (MRI), Computed Tomography / X-ray imaging or ultrasound imaging. The choice of technology is in large part determined by the technology's ability to provide images of satisfactory quality for the given procedure, but it is also affected by the availability of the technology and practical and economical factors.

Ultrasound (US) imaging is one of the most widespread diagnostic imaging techniques that is used in clinical practice. The popularity of the imaging technology is probably related to the affordable cost, its versatility, simplicity and safety in use, and its ever improving image quality. The ultrasound systems are adaptable to a wide range of clinical purposes, and ultrasound is used for percutaneous imaging in different medical specialities as e.g. obstetrics, cardiology and gastroenterology (abdominal imaging). Endocavity ultrasound transducer probes are used for imaging from within the natural body cavities/openings in fields like gynaecology, urology (prostate) and oesophagus. Ultrasound may also be used for imaging during interventional procedures (intravascular ultrasound) and during surgery.

The National Centre of Competence in Ultrasound and Image-guided Therapy at St. Olavs University Hospital is conducting research and development of technology and

clinical procedures for image guided treatment in clinical fields like laparoscopic surgery, endovascular treatment and neurosurgery. In neurosurgery the centre has advanced the use of ultrasound imaging and navigation technology for intraoperative guidance and resection control. The research contributed to the technology that has been commercialized by the company Sonowand AS (Trondheim, Norway), which with their system (Sonowand Invite) is integrating ultrasound and navigation technology for use in brain tumour surgery. The research at the National Centre has generated new knowledge and publications related to optimization of ultrasound for the purpose of imaging of brain tumours [1], clinical evaluation of the feasibility of the technology in different neurosurgical procedures [2-7], development of method for navigation based on preoperative functional magnetic resonance images (fMRI) and diffusion tensor imaging (DTI) based tractography [8-10], development and evaluation of technology for intraoperative use in neurosurgery [11-13] and evaluation of clinical outcome for patients operated with the technology [14-16].

This thesis is also a result of the activity of the centre. Thematically it includes both clinical biopsy studies and feasibility studies exploring the use of ultrasound strain imaging in neurosurgery. Some would perhaps say that biopsy studies comparing 3D ultrasound image findings and histopathology has little in common with studies investigating the feasibility of ultrasound strain imaging of brain tumours. However, it may also be considered as two different approaches in a unified goal to gain more knowledge about how ultrasound is able to delineate various brain tumours for the purpose of resection control. The outcome of the biopsy studies included in this thesis provide a basis for understanding the clinical reliability of using ultrasound volumes for navigational guidance, in various stages of the operation. The papers also contribute to increased understanding of ultrasound artefacts that can be observed during the surgery, and thereby the knowledge on how image artefacts may be reduced.

The work related to the evaluation of an ultrasound strain processing method is an example on how emerging ultrasound techniques can be used as a conjunction to conventional ultrasound B-mode imaging in depicting the tumour. The results of the

strain processing work will hopefully motivate for further research on imaging of tissue strain and elasticity in brain tumour surgery.

Although the work has an overall context of ultrasound delineation of brain tumours, the papers have somewhat different perspectives. The following sections (2-4) will provide relevant background for both the biopsy studies and the strain imaging studies.



## 2.0 Ultrasound imaging

This section is aiming to provide some theoretical background in ultrasound that might be helpful in understanding the papers included in the thesis, and to understand the difference between the generation of conventional ultrasound images and ultrasound strain images.

### 2.1 Sound and ultrasound

Sound is mechanical vibrations that propagate in a given medium, which may be fluids, gases, solids and plasma. In gases, fluids and plasma the sound travels as compressional waves (also called longitudinal waves), which means that all particles in the medium will move along, or in parallel, to the direction of travel for the wave energy. In solids the sound may in addition also travel as transverse waves, in which particles vibrate in direction perpendicular to the direction of the wave energy (Fig. 1).

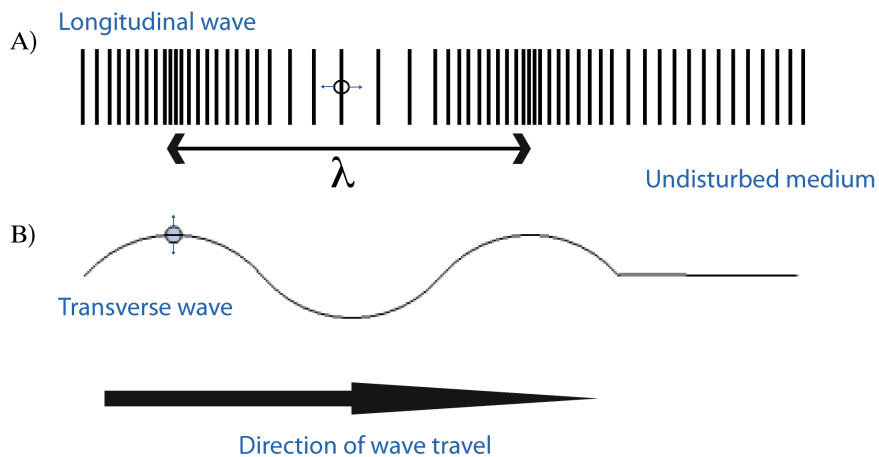


Figure 1. Illustration of longitudinal wave propagation (A) and transverse wave propagation (B) in a solid medium. For longitudinal waves, a given particle in the medium will move in the direction of the travelling wave. For transverse waves, a given particle in the medium will move perpendicular to the direction of the travelling wave. The direction of movement around the steady state position for a given particle in the medium is indicated as a circle with arrows in A) and B).

Sound in the human audible range have frequencies between approximately 20 Hz to 20 000 Hz. Ultrasound is defined as sound with frequencies above 20 kHz. In medical imaging the ultrasound frequency range is between 2-40 MHz, with the highest frequencies currently used in intravascular ultrasound (IVUS).

The relationship between the spatial wavelength  $\lambda$ , the frequency  $f$  and the speed of sound  $c$  is given as:

$$\lambda = \frac{c}{f} \quad (1)$$

The speed of sound is media dependent, which implies that also the spatial wavelength is dependent on the media in which the sound travels. Speed of sound is approx. 330 m/s in air and 1480 m/s in fresh water. In biological tissue the speed of sound varies from approx. 600 m/s in lung tissue to ca. 4000 m/s in bone. A standard setting in commercial medical ultrasound scanners is a constant speed of sound of 1540 m/s for soft biological tissue. A sound wave of frequency 10 MHz propagating in soft tissue will accordingly have a spatial wavelength of 0.154 mm.

## 2.2 Resolution in the ultrasound images

Resolution defines the ability to separate two closely spaced objects from one another. For the ultrasound image the resolution can be defined for three axes relative to the transducer surface (Fig 2).

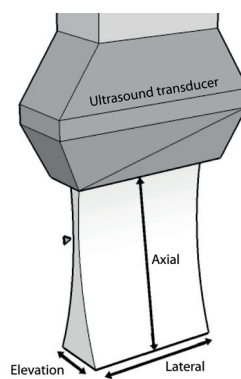


Figure 2: Axial, lateral and elevation axes as defined relative to the transducer surface. Courtesy of Ole V. Solberg (modified).

The resolution in the axial direction, i.e. along the axis of wave travel, is defined by the time duration of the transmitted pulse. The pulse duration (PD) is defined by the number of cycles in the transmitted pulse (n) multiplied by the period (T) of the cycles,  $PD = n \cdot T$ . The axial resolution  $\Delta z$  can be expressed by the equation:

$$\Delta z = c * PD / 2 = \frac{nc}{2f} = \frac{n\lambda}{2} \quad (2)$$

Two objects spaced more than half the spatial pulse length apart in the axial direction will be resolved as two separate reflectors.

The resolution in the lateral direction defines the ability to separate two laterally closely spaced objects, perpendicular to the beam. Lateral resolution  $\Delta l$  is related to the width of the ultrasound beam, which can be expressed by the transducer aperture D, the focal depth F and the wavelength  $\lambda$ :

$$\Delta l = \frac{\lambda F}{D} \quad (3)$$

The lateral resolution improves (lower number) with shorter wavelengths (higher frequency) and larger transducer aperture.

The resolution in the elevation direction, perpendicular to the image plane, is also referred to as the ultrasound slice thickness. The elevation resolution is related to the height of the transducer elements and the focusing in the elevation plane. The slice thickness may vary substantially with depth.

The resolution of the ultrasound image is usually highest in the axial direction, followed by the lateral direction and then the elevation direction.

### **2.3 Attenuation and depth penetration**

The amplitude of the ultrasound pulse will gradually decrease as it propagates in the tissue. The attenuation of a given media is given by the attenuation coefficient  $\alpha$ , which usually is expressed as a damping value in decibel per centimetre per MegaHertz [dB/(cm \* MHz)]. For soft biological tissue a value of  $\alpha= 0.5$  dB/(MHz cm) is often used.

There have been a few papers reporting measurements of attenuation in brain tissue. Bamber *et al.* reported measurements of attenuation on fresh human brain tissue acquired from autopsy [17]. These measurements found that attenuation in predominately white matter was higher than the attenuation in mixed grey and white matter with a ratio of 1.4. The attenuation, reported in dB/cm, ranged from 0.58 in mixed grey and white matter to 0.8 in tissue containing mostly white matter. Kremkau *et al.* reported measurements of attenuation and sound speed of fresh tissue from five different anatomical locations of the brain provided by autopsy of four adults [18]. The average attenuation of the measurements was 0.87 dB/cm. The attenuation was found to be higher in white matter than in mixed tissue (white and grey) and in grey matter, with attenuation coefficients of approx. 0.97, 0.87 and 0.75 dB/cm, respectively. He reported a ratio of 1.5 between attenuation in white and grey matter at a frequency of 2.5 MHz. Strowitzki *et al.* measured the attenuation of brain tissue *in vivo* from spectral analysis of ultrasound radiofrequency data acquired in 20 brain operations [19]. The slope of attenuation in the subcortical tissue with white matter dominance was found to be  $0.94 \pm 0.13$  dB/(MHz cm).

The large attenuation coefficient for brain found in the above-mentioned studies suggest that the ultrasound pulses will be more damped in brain than in most other soft tissues.

### **2.4 Reflection and scattering of sound**

Ultrasound imaging is a pulse-echo technique. The generation of the ultrasound images are based upon transmission of a sound pulse and receiving of echoed events that have

been reflected from tissue boundaries or scattered from smaller objects. In conventional scanners today, a narrow ultrasound beam is transmitted from the ultrasound transducer. When the transmitted pressure pulse meets a hinder in form of a boundary between different soft tissues, or scatter points within the tissue with different acoustic properties, some of the energy of the transmitted sound pulse is echoed back to the transducer.

The acoustic impedance is a measure that describes the opposition to the flow of sound through a surface in the substance. For a plane wave with a given frequency the acoustic impedance  $Z$  of a medium can be defined as the product of *mass density*  $\rho$  and *speed of sound*  $c$ :

$$Z = \rho c \quad (4)$$

The strength of the reflected echo originating from a *boundary* between different tissues is determined by the differences in the characteristic acoustic impedances of the tissues. The reflection coefficient  $R$  describes the relative amplitude of a reflected wave relative to the amplitude of the incoming wave, at a given boundary that is wider than the ultrasound wavelength. For the simplified case of a normal incidence sound wave the reflection coefficient  $R$  between two plane layers can be expressed as:

$$R = \frac{Z_2 - Z_1}{Z_2 + Z_1} = \frac{\rho_2 c_2 - \rho_1 c_1}{\rho_2 c_2 + \rho_1 c_1} \quad (5)$$

The above equation states that the amplitude of the sound wave being reflected from the interface is dependent on the media properties mass density  $\rho$  and the speed of sound  $c$  in addition to the amplitude of the incoming sound wave.

The speed of sound  $c$  in a fluid is defined by:

$$c = \sqrt{\frac{\kappa}{\rho}} \quad (6)$$

where  $\kappa$  is the bulk modulus of elasticity. Thus, substituting Eq. (6) in Eq. (5) the reflection coefficient R can be entirely expressed by the material properties mass density and bulk modulus.

In addition to reflections from tissue interfaces that are larger in size than the wavelength  $\lambda$  as described above, smaller inclusions in the tissue may act as scatter points and cause backscattering of sound to the ultrasound transducer. For spherical particles with radius  $a$  much smaller than the acoustic wavelength  $\lambda$ , the ultrasonic backscatter coefficient  $\eta$  as a function of angular frequency  $\omega$  is proportional to [20]:

$$\eta(\omega) \propto k^4 a^6 \left( \frac{\kappa_1 - \kappa_0}{\kappa_0} - \frac{\rho_1 - \rho_0}{\rho_0} \right)^2 \quad (7)$$

where  $k$  is the wave number  $2\pi/\lambda$ ,  $\kappa_1$  is the bulk modulus of the scatterer,  $\kappa_0$  is the bulk modulus of the surrounding medium,  $\rho_1$  is the mass density of the scatterer and  $\rho_0$  is the density of the surrounding medium.

To summarize this subsection, the ultrasound images are generated by compressional sound waves that have been echoed from tissue interfaces or scatterer points. The brightness of the various events seen in the images is dependent on the strength of the echoes. In a fluid medium the strength of the reflected echoes are related to the material properties mass density and bulk modulus.

## 2.5 Ultrasound imaging techniques

Medical examinations by ultrasound can be performed in several different ways. In the last two decades there has been a substantial increase in the number of ultrasound imaging techniques. This section will provide a brief and general overview of the most common ultrasound display modes and imaging techniques, and provide some background on how they have been explored for diagnosis of neurological conditions.

The simplest and historically oldest display mode is the Amplitude mode (A-mode). In this mode the horizontal axis represent the time required from transmitting the ultrasound pulse to the echo to be returned and the vertical axis represent the strength of the echo. The single line (1 dimensional) technique was the first modality to be used in clinical examinations, and it has also been used for detection of neurological disease. Karl Theodore Dussik suggested the use of transcranial ultrasound examinations for detection of the ventricles and brain tumours in 1942 [21]. This is regarded as the first experiment that demonstrates the possibility of using ultrasound for diagnostic purposes. Together with his brother Friederich, a physicist, he continued the development and experiments during the 1940ies [22]. During the 1950ies the use of transcranial A-mode ultrasound was further explored for assessment of tumour localization and gross assessment of size [23-25].

The development of brightness mode (B-mode) percutaneous ultrasound imaging in the late 1960ies enabled 2D images of internal body organs. In the B-mode images the brightness of an image pixel corresponds to the amplitude of the reflected echo. The vertical position of each pixel with a given brightness is determined by the time delay from pulse transmission to echo receive, and the horizontal position is determined by the location of the receiving transducer elements. In the 1980ies the use of B-mode images for intraoperative imaging of brain tumours was first reported [26-28].

Motion mode (M-mode) ultrasound can be used for analysis of moving body parts. The brightness of the reflected echoes along a single beam of an ultrasound scan is plotted versus time. As the reflection from a moving organ is changing in depth relative to the transducer surface, the movement can typically be seen as an oscillating curve in the M-mode display. Thus, the displacement and velocity of the specific organ structure can be calculated from the M-mode curves.

The Doppler Mode is used for measuring and visualization of blood flow, based on the Doppler effect. The Doppler frequency shift  $f_D$  for a signal with frequency  $f_0$  being reflected from an object with velocity  $v$  propagating with an angle  $\theta$  relative to the sound beam is provided by:

$$f_D = 2f_0 \frac{vcos\theta}{c} \quad (8)$$

The Doppler shift can be analysed along a single beam or by providing a 2D image. The feasibility of Transcranial Doppler for assessment of intracerebral blood circulation was demonstrated by Aaslid *et al.* in 1982 [29] and has since gained widespread use and acceptance. In neurosurgery it is important for the surgeon to know the localisation of vital blood vessels, and ultrasound Doppler methods may be used for this purpose. The 2D images of blood flow by either Colour Doppler (where the mean velocity is encoded in a colour code) or Power Doppler (where the Power of the Doppler signal is encoded in a colour code) has been reported utilized for intraoperative imaging of intracerebral blood vessels [5, 7, 30].

Ultrasound techniques targeted for imaging of objects with non-linear acoustic responses have also been developed. Such techniques have been used in combination with micro-bubbles for transcranial and intraoperative imaging of cerebral blood vessels [31-33]. In the latter case the contrast was applied to improve delineation of tumours by identifying hypervascular regions.

Harmonic mode imaging is perhaps the most established technique for non-linear imaging, in which the system transmits on one frequency but is tuned to receive on the second harmonic of the transmitted frequency. Another technique is known as pulse-inversion imaging; where two consecutive pulses of opposite polarity are transmitted into the tissue, and the resulting echoes are added during receive. A novel and interesting technique for non-linear ultrasound imaging has recently been developed by NTNU and is referred to as SURF imaging [34].

Ultrasound elastography is an imaging mode for assessment of soft tissue strain and elasticity, and is now used as a broad term covering a wide range of strain or elasticity imaging techniques. Ultrasound elastography is further elaborated in section 3.3.

## 3.0 Tissue elasticity and ultrasound imaging

### 3.1 Longitudinal and transverse waves in soft tissue

In section 2 we considered how the material properties of a fluid would affect the speed of sound, reflection and scattering of sound. Soft biological tissue may for simplicity be considered as a fluid, but there are some important differences. One of them is that shear waves can propagate in solids but not in fluids. Shear waves (or transverse waves) can propagate in soft biological tissues, along with compressional waves (Fig. 1). The compressional waves are propagating by inducing *volume changes* in the media, as the material is compressed and expanded in the direction of travel. The particle motion is thereby in the direction of the wave travel. The shear waves propagate by inducing disturbances in the material, but without inducing volume changes. The disturbance is an elastic deformation (shear) in the direction perpendicular to wave travel, i.e. the particle motion is perpendicular to wave travel. The shear deformation in tissue is an important prerequisite for ultrasound elastography methods. The strain occurring from one image frame to another can be found along the axial direction of the image by processing of the data to find local time delays, with subsequent differentiation to obtain strain values.

Strain is a unit less measure of relative tissue deformation. For a media segment with the equilibrium length of  $L_0$  the longitudinal strain  $\varepsilon$  may be expressed by:

$$\varepsilon = \frac{L-L_0}{L_0} = \frac{\Delta L}{L_0} \quad (9)$$

where  $\Delta L$  denotes the differential length of the segment after compression or rarefaction of the medium.

The equations shown in section 2 are based on wave propagation in fluids. For solids the shear stiffness of the media will also affect the wave propagation.

The phase velocity  $c_p$  for a compressional (longitudinal) plane wave propagating in an isotropic medium can be expressed by:

$$c_p = \sqrt{\frac{\kappa + 2G}{\rho}} \quad (10)$$

where  $\kappa$  is the bulk modulus and  $G$  is the *shear modulus*.

The phase velocity  $c_s$  for a shear wave propagating in an isotropic medium can be defined by the expression:

$$c_s = \sqrt{\frac{G}{\rho}} \quad (11)$$

From Eq. 10-11 we observe that the velocities are dependent on the material properties like the elastic moduli  $G$ ,  $\kappa$  and the mass density  $\rho$ . For the compressional waves the velocity  $c_p$  in soft biological tissue varies from ca. 1412 m/s in fat to ca. 1629 m/s in muscle, while the corresponding figures for mass density  $\rho$  is from 916 kg/m<sup>3</sup> to 1050 kg/m<sup>3</sup> [35]. The relative velocity difference in normal and abnormal tissue is generally expected to be small. The shear wave velocity  $c_s$  is very low in normal soft biological tissue. Reported values for healthy tissue are typically within the order of approximately 1 - 6.5 m/s, depending on the organ [36, 37]. However, the velocity  $c_s$  may increase to the double and more in tumours [38]. In abnormal tissue, the relative velocity change for the shear wave is therefore usually more profound than the relative change in velocity for the compressional wave. The reason for this is that pathology often leads to a marked alternation of the elastic shear modulus of tissue, which again will affect the shear wave velocity of the tissue. The elastic moduli and their values for soft tissue is the topic of the next section.

### 3.2 Elastic moduli

Manduca *et al.* stated " It is generally agreed that no other physical parameter of tissue is changed by pathological or physiological processes to as great an extent as its elasticity" [39]. There are several coefficients that are used to describe the elastic

properties of a material. The three coefficients most frequently used to describe the stiffness of the material are the bulk modulus ( $\kappa$ ), the shear modulus (G) and Young's modulus (E).

The bulk (or volume) modulus  $\kappa$  is a coefficient of elasticity defining how an increase in uniform pressure will lead to a decrease in volume for a substance (with unit volume V). The bulk modulus is expressed in Pascal (Pa,  $\text{Nm}^{-2}$ ,  $\text{kg m}^{-1}\text{s}^{-2}$ ). A high value for the bulk modulus will indicate a high resistance towards change in volume, i.e. a low compressibility. Soft biological tissue is often considered to be an almost incompressible medium, like water. The bulk modulus of soft biological tissue is accordingly very high. For brain tissue the values estimated for use in numerical simulations has been reported to be from 2.19 GPa [40] to 2.3 GPa [41]. As the bulk modulus in normal tissue is very high, the relative change in value due to the presence of pathology as tumours is generally expected to be small.

The shear modulus G (modulus of rigidity) is a coefficient of elasticity describing how a substance responds to shear stress and is defined as the ratio of shear stress to the shear strain. In soft tissue the shear modulus is in general low compared to the bulk modulus. The average shear modulus in brain has in one study been measured in vivo by Magnetic Resonance Elastography (MRE) of 25 healthy volunteers to be 13.6 kPa in white matter and 5.22 kPa in grey matter [42]. Another group reported somewhat other results from a MRE study involving 5 volunteers, with an average G of 3.1 kPa in grey matter, and 2.7 kPa in white matter [43]. It is generally considered that pathologic processes like tumours will significantly alter the shear modulus of tissue. In pathologic tissue the shear modulus may be much higher than in the surrounding normal tissue, in the order of several magnitudes. This may be exemplified by a MRE study of liver, which reported an average shear modulus for normal liver parenchyma of 2.3 kPa, while it was found to be 10.1 kPa in malignant tumours [44].

The relation between longitudinal stress  $\sigma$  and longitudinal strain  $\epsilon$  is expressed by the Young's modulus E:

$$E = \sigma / \epsilon \quad (12)$$

For a sample object being stretched or compressed, the Poisson's ratio  $\nu$  is the ratio of transverse strain  $\epsilon_x$  to the axial strain  $\epsilon_z$ . For soft tissue the Poisson's ratio  $\nu$  can be approximated to  $\approx 0.5$ . Soft tissue has as previously stated a low shear modulus  $G$ , and thereby a low resistance towards shear deformation. This means that large deformations can occur when uniaxial stress  $\sigma$  is applied to a sample object, but with practically no change in volume. Thus, the uniaxial stress  $\sigma$  will produce a large transverse contraction or expansion, and will result in mainly shear deformations [45]. For soft tissue assuming  $\nu \approx 0.5$  the Young's modulus in Eq. 12 can also be approximated to:

$$E \approx 3G \quad (13)$$

Substituting this approximation into Eq. 11, we find that the strain  $\epsilon$  is equal to the stress  $\sigma$  applied to the tissue, divided by a constant that is proportional to the shear modulus of the tissue.

To conclude this section, we have stated that soft tissue may be considered as a nearly incompressible medium, with a correspondingly high bulk modulus. The Young's modulus is related to the shear modulus by approximately a factor 3. The shear modulus (and the Young's modulus) has the largest dynamic range and can potentially be used for identification of diseased tissue. Ultrasound can be used for exploring the elastic properties of tissue by methods often referred to as ultrasound elastography imaging or ultrasound strain imaging, which is the subject of the next section.

### **3.3 Ultrasound imaging of tissue strain and elasticity**

Ultrasound may be used to image the tissue deformation that occurs when some kind of stress is acting on the tissue. The concept of ultrasound imaging of tissue strain or elasticity is in general terms often referred to as *ultrasound elastography* and the corresponding 2D images are frequently called *elastograms*. However, the imaging of tissue strain is also referred to as *ultrasound strain imaging* or by more method-specific terms, as shown in later in this section.

Magnetic Resonance Elastography (MRE) methods have also been developed to investigate tissue elasticity in different organs of the body, as referred to in the previous section. Although MRE is a very interesting topic, this section will focus on ultrasound methods only.

The theoretical framework for the study of behaviour of vibrating soft tissue was established already in the early 1950ies, for example by von Gierke *et al.* publication titled *Physics of vibrations in living tissues* in 1952 [46]. However, it was not until 30 years later that the measurements of tissue movements was first explored for clinical purposes, by using ultrasound for study of tissue motion in liver caused by vascular pulsation [47, 48].

In the late 1980ies techniques for *vibration elastography imaging*, also known as *vibration amplitude sonoelastography* or simply *sonoelasticity imaging* was developed [49]. In this technique a low frequency vibration (20-1000 Hz) is externally applied to the skin surface to investigate the subcutaneous structures. The internal motion of the tissue is investigated with a pulsed Doppler technique. Stiff tissue responds differently to the vibrations than softer tissue, and would therefore become apparent in the real-time images.

In the early 1990-ies the development of *compression elastography*, also referred to as *quasi-static elasticity imaging*, begun. Ophir published a paper in 1991 where ultrasound radio frequency (RF) data before and after applying compression were compared and processed using cross-correlation to obtain the time-shifts of the echoes. This allowed the subsequent calculation of elastograms [50]. The quasi-static elasticity imply that the force is applied for a sufficiently long time for the tissue strain to stabilize, and the resulting difference in echo traveltime between ultrasound data acquired prior and after compression can be calculated. The tissue may be excited by applying forces at the surface (manually or by electromechanical devices) or by physiological processes within the organ, as e.g. the pulsation of the arteries. The generated elastograms are usually displayed as a colour coded overlay on the

conventional ultrasound brightness mode image. The colour mapping may cover a range of unit-less strain values as percentages from minimum (negative) strain to maximum (positive) strain. Alternatively it may also be mapped from "soft" to "hard" tissue, thereby not quantifying the strain range displayed. The processing performed on the ultrasound data covered in this thesis is within the category of quasi-static elasticity imaging. We have in our papers referred to the method as ultrasound strain imaging.

Quasi-static elasticity imaging has been evaluated in a broad range of clinical applications. It has been reported used in diagnostics of tumours in e.g. breast, prostate, liver, the thyroid gland and in brain [51-56]. Quasi-static elasticity imaging is an emerging ultrasound imaging modality, now becoming more and more available as an option on commercial ultrasound systems.

As previously explained, the elastography methods require that the tissue is excited by some means. The tissue movement can be caused by physiological processes internally in the organ, as e.g. pulsation of arteries. The tissue can also be externally excited by manually pushing the tissue or by using an electromechanical vibrating device. An alternative approach is to use the acoustic radiation force of an ultrasonic focused beam to generate displacements in the tissue, with subsequent detection of mechanical properties. One example of such an approach is the Acoustic Radiation Force Impulse (ARFI) method developed at Duke University [57]. In this technique short duration acoustic pulses (push pulses) are used to generate smaller localized displacements deep in the tissue. These displacements are tracked by ultrasonic cross correlation, in a similar fashion as for the quasi-static elasticity imaging. The method has been investigated for imaging of focal liver lesions, prostate and breast [58-60].

A second example is the innovative Supersonic Shear Imaging (SSI) method developed by the research group at the Laboratoire Ondes et Acoustique headed by Mathias Fink [61]. In SSI the acoustic radiation force is used to generate low-frequency shear waves (50-500 Hz) remotely in the tissue. The shear modulus of the tissue can be quantified by imaging the shear wave propagating in the tissue by using ultrasound frame rates of several kHz. The method has been explored for diagnosis of liver fibrosis, breast lesions and cornea [62-64].

For further reading about methods for ultrasound elasticity imaging and its clinical use I would recommend the recent review papers by Wells and Liang [35] and Parker, Doyley and Rubens [65].



## **4.0 Navigation and ultrasound imaging in brain surgery**

### **4.1 Brain tumours**

Intracranial tumours include primary and secondary tumours in the brain, dura and cranium. Primary tumours are neoplasms originating from the brain itself or blood vessels, meninges and bone in the intracranial space. The secondary brain tumours are metastases that are originating from a primary tumour situated in another organ of the body.

The incidence of primary intracranial tumours is 3 per 100.000 for children (0-14 years), 8-10 per 100.000 for adults and increasing with age to 20 per 100.000 for the age of 70 year [66]. The most common primary tumours are gliomas (about 50%), meningiomas (about 20%) and pituitary adenomas (about 10%), but there are close to 100 different types of primary brain tumours. The tumours can be classified as benign (non-cancerous) or malignant (cancerous) depending on the behaviour and type of cells. Benign tumours are relatively slow growing and do not infiltrate the surrounding tissue. Malignant tumours are relatively fast growing and will infiltrate the surrounding tissue. The brain tumours are classified by histology, i.e. the cells are examined under the microscope. Primary brain tumours can be classified in one of four different histology grades according to criteria established by the World Health Organization (WHO) [67]. Grade I-II are often referred to as low-grade tumours and grade III-IV are referred to as high-grade tumours, with the high-grade tumours being the most malignant.

Medical imaging studies are important for diagnosis of intracranial growing processes. A CT scan may be done as the initial imaging study, but MRI is the most common imaging modality used for diagnostic imaging of brain tumours and is currently considered the 'gold standard'.

The different brain tumours respond differently to treatment, and this will affect the treatment regime for the individual patient. Surgery is still the primary treatment for most brain tumours. Small low-grade tumours may as an alternative be monitored for growth progression, and some tumours may be deemed inoperable due to the location or the general state of the patient. Smaller tumours (<3 cm) may also be treated by stereotactic radiotherapy as an alternative to surgery, and this may be an option for

secondary brain tumours and smaller benign brain tumours. In surgery, the goal is usually to perform a total extirpation of the tumour. If this is not achievable due to the tumour being located in eloquent area, the goal is to remove as much of the tumour as possible without causing functional damage. The rationale for the resection strategy is that the prognosis for survival is for many tumours related to the degree of resection [68-70]. If there is no apparent tumour tissue seen in the early post-operative MRI, this is often referred to as 'gross total tumour resection'. However, for the diffuse infiltrating malignant tumours, scattered tumour cells are bound to be present in the brain parenchyma even when gross total resection is achieved. Diffuse infiltrating tumours like gliomas will therefore at some stage start to grow again. The prognosis for patients with grade IV tumours is unfortunately still very poor.

#### **4.2 Neuronavigation systems**

Neuronavigation is the term used to describe the use of computer-assisted methods to guide or navigate instruments within the confinements of the skull (or spinal column) during surgery. Neuronavigation requires a means to acquire the positions of the navigated instruments, in addition to software that is able to display the position of the instrument in the patient-specific images. The images of the patient used for navigation purposes can be acquired prior to or during surgery. When using preoperative images for navigation both Computed Tomography (CT) and Magnetic Resonance imaging (MRi) can be used, but MR images are usually the preferred choice for navigation in brain tumour surgery. The preoperative image volumes should for registration purposes cover the complete head of the patient. An image volume is registered to the patient by using anatomical features or by using a set of skin adhesive fiducial markers that are attached to the patient's head prior to imaging.

For the biopsy studies included in this thesis, the preoperative MR-data was usually registered to the patient using 5 fiducial markers, and in a few cases using anatomical landmarks. The position of the fiducial markers were identified and registered in the image volumes. When the patient was anaesthetised and positioned on the operating

table, the surgeon used a navigation instrument (a pointer device) to sample the position of the fiducial markers attached to the patient's head. A minimum of four corresponding points was used in the image-to-patient registration. After the registration was performed, the preoperative images could be used for planning the craniotomy.

There are also navigation systems that have implemented semiautomatic methods for image-to-patient registration. This means that the operator of the navigation system does not have to manually identify landmarks (anatomical/fiducial markers) in the preoperative images. These methods usually involve automatic segmentation of the patient's skin surface as shown in the preoperative images. The sampling of the patient's skin when positioned on the operating table may be performed with a navigated laser pointer device or other navigated pointer devices, enabling acquisition of a larger amount of sample points. The registration of the images to the patient is then performed with a points-to-surface registration method. The surface based methods involving automatic segmentation of MR-data and sampling with a laser pointer device, may by some users be experienced as user-friendlier than the conventional fiducial based registration method. However, the laser surface scanning (or points-to-surface) method has been reported to be less accurate than the conventional fiducially based point-to-point method [71, 72]. The target registration error (TRE) is defined as the three dimensional Euclidean distance between the coordinates of the target in image space and in the physical space. The two last above-cited papers reported mean TRE of 1.0 mm and 2.5 mm for fiducial based registration, compared to mean TRE of 1.8 mm and 5.0 mm for surface based methods, respectively.

The neuronavigation system should ideally provide high navigation accuracy throughout the surgical procedure. However, the anatomy of brain is known to shift position after opening of the dura mater due to drainage of cerebro-spinal fluid (CSF), gravity effects and removal of tumour mass. This shift in the position of the anatomy is often referred to as *brain shift* and has been shown to occur in the early stage of the surgery with displacement values ranging up to several centimetres [73-75]. The brain

shift may therefore significantly impair the accuracy of navigation based on preoperative images as the surgery proceeds.

Intraoperative imaging provides a solution to the brain shift problem, and is used for guidance and resection control. In surgery of brain tumours the most commonly used imaging technologies are magnetic resonance imaging (MRI) or ultrasound. Compared to using only preoperative image data for navigation, the navigation of instruments based on recently acquired intraoperative images can potentially be performed with higher accuracy and precision [76].

#### **4.3 Neuronavigation and intraoperative ultrasound**

Intraoperative ultrasound facilitates imaging of anatomy, while clinical navigation systems facilitate guidance of surgical tools based on images. The combined use of ultrasound imaging and navigation technology has been explored since the early 1990ies. The University of Oulu was one of the frontiers and demonstrated the clinical use of a passive mechanical arm-based navigation system, which could display reconstructions of preoperative images (CT/MR) and corresponding real-time intraoperative ultrasound images [77].

By attaching position sensors (also referred to as 3D localizers) on the ultrasound probe it is possible to establish the relative spatial position of the image pixels, and it is possible to reconstruct 2D images into an image volume, hence the term 3D ultrasound. The localizer attached to the probe is usually ultrasonic, electromagnetic or optic, and the two latter options (optic, electromagnetic) are currently the most established in commercial systems. Hata *et al.* described in a paper from 1997 the initial clinical experience with a frame- and armless navigation system incorporating an ultrasound scanner and an ultrasound probe equipped with an ultrasonic positioning sensor [78]. In 1998 Jödicke *et al.* presented a system for detection of brain shift, by comparing preoperative MR images and intraoperative 3D ultrasound [79]. The integration of ultrasound and navigation technology was also explored in Trondheim, and a system with the feasibility of 3D ultrasound and navigation guidance was

developed. Geirmund Unsgård performed the first brain tumour operation with 3D ultrasound guidance in 1997, and the system development and clinical experience was described in several later papers [6, 80, 81]. The technology was further developed and commercialized by the company Sonowand AS (Trondheim, Norway), which is a spin-off company from the research activities of the previous National Centre for 3D Ultrasound in Neurosurgery (1995-2011) at St. Olavs Hospital. The technology has been explored for use in several neurosurgical procedures, but its predominant use is within resection of brain tumours [82]. The Sonowand system allows navigation of pre-calibrated tools equipped with an optic localizer, or it allows tools like biopsy forceps to be calibrated to the navigation system *in situ* in the operating room (Fig. 3).

The 3D ultrasound data is acquired by freehand tilting and/or translation of the pre-calibrated ultrasound probe. If repeated 3D ultrasound acquisitions are performed during brain tumour surgery, the system will solve the brain shift problem, facilitate imaging of residual tumour, and provide navigated image guidance for surgical instruments. In addition, there is no need to register the ultrasound image volumes to the patient, as with preoperative images. This is because the acquisition of 3D ultrasound data and the subsequent navigation of instruments based on the 3D ultrasound images are performed in the same physical space, i.e. within the same coordinate system. Frank Lindseth *et al.* published an accuracy evaluation of the first version of the Sonowand system, and found a TRE accuracy of 1.4 mm ( $\pm 0.45$  mm) [83]. In a clinical setting the navigation based on 3D ultrasound should be more accurate, than navigation based on preoperative images.

On the Sonowand system the 3D ultrasound data can be displayed as reformatted image slices along with corresponding image slices of preoperative MR. The system facilitates concomitant comparison of image findings in intraoperative ultrasound and any preoperative MR series like T1, T2, FLAIR, etc. that has been registered to the patient. The position of navigated instruments as e.g. a biopsy forceps are indicated in the displayed image slices. This display feature has been used in the biopsy studies included in the thesis, for direct comparison of image findings (intraoperative ultrasound, preoperative MR) and histology for a given biopsy.

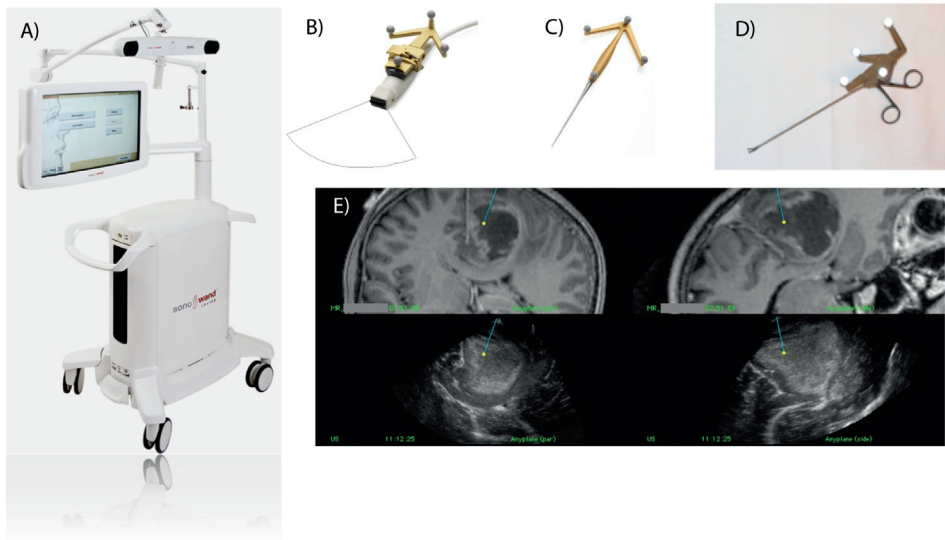


Figure 3. A commercial 3D ultrasound based navigation system (Sonowand Invite®) for intraoperative ultrasound imaging and navigation (A), various tools of the navigation system equipped with optical localizer units showing one phased array ultrasound probe (B), a navigation pointer (C), a biopsy forceps (D), and a screen dump of the navigation display showing reformatted MR images in top row, and corresponding reformatted ultrasound images in bottom row (E). The tip of the navigated instrument is indicated with a bright spot in the reformatted image slices.

## 5.0 Aims

The PhD project assesses the use of ultrasound for imaging of brain tumours during surgery. The overall aim was to 1) investigate the reliability of intraoperative 3D ultrasound imaging for detection of pathologic tissue, both prior to start of resection and in subsequent phases of the surgery, and 2) evaluate whether strain processing could generate images that are able to differentiate between pathologic tissue and normal brain.

The secondary goals were:

- Evaluate if the delineation of tumour as depicted by 3D ultrasound images acquired prior to resection is in agreement with histology
- Evaluate if the delineation of tumour as depicted by 3D ultrasound images acquired prior to, during and after resection is in agreement with histology
- Evaluate if it is possible to obtain strain images of brain tumours
- Evaluate if strain magnitude is different in tumour and the adjacent normal brain tissue
- Evaluate if strain magnitude images possesses higher image contrast than conventional B-mode images



## **6.0 Summary of papers**

### **6.1 Paper 1**

Strain processing of intraoperative ultrasound images of brain tumours: initial results.

Selbekk T, Bang J, Unsgaard G.

*Ultrasound Med Biol*; 31(1): 45-51, 2005

The purpose of the study was to explore whether or not a method for strain processing could be used to detect strain in brain and generate strain images of brain tumours.

Ultrasound radio frequency data was acquired in two patients, operated for a glial tumour and a metastasis respectively. A flat linear 10 MHz array (GE Vingmed, Horten, Norway) was kept motionless on intact dura during data acquisition. Electrocardiograph (ECG) data was recorded with the ultrasound data. The processing was performed in Matlab (MathWorks Inc., MA, USA) and consisted of 1) calculation of travel time differences between consecutive ultrasound frames, 2) calculation of axial strain, 3) rectification and filtering before display.

The results show that it was possible to calculate time delays between frames with the implemented method. The image frames of the calculated time delays showed a periodic appearance in the results that correlated well with the period of the QRS complex in ECG data. It was possible to generate strain images of the brain tumours. Strain magnitude images could be obtained, that showed the magnitude of the strain to be lower in the tumour than in adjacent normal tissue.

The paper concludes that it is possible to generate ultrasound strain images based on the tissue displacement introduced by the vascular pulsation. The resulting strain magnitude images seem able to differentiate between tumour and normal brain.

### **6.2 Paper 2**

Tissue motion and strain in the human brain assessed by intraoperative ultrasound in glioma patients.

Selbekk T, Brekken R, Solheim O, Lydersen S, Hernes TAN, Unsgård G.

*Ultrasound Med Biol*; 36(1): 2-10, 2010

The purpose of the study was to investigate the magnitude of tissue velocity and strain imposed during a cardiac cycle, especially to analyse the differences in normal tissue and solid tumour.

Ultrasound radiofrequency (RF) data were acquired during surgery of 16 patients with glial tumours, using a handheld 10 MHz flat linear probe. Data were retrospectively processed to obtain measurements of axial tissue velocity and axial local strain. There were 4 regions of interest selected across the ultrasound visible tumour border; two regions expected to be in solid tumour tissue and two regions expected to contain normal tissue with possible tumour infiltration. The measurements were compared using the paired Wilcoxon sign rank test.

The results shown no statistically significant difference between maximum velocities for any of the four regions investigated ( $p>0.05$ ). The strain magnitudes are significantly different between all of the four regions investigated. However, the difference in strain level between two regions located on opposite side of the ultrasound visible tumour border is much higher than the difference in strain level for two regions located on the same side.

The paper concludes that the quantified strain magnitudes differentiate between regions of solid tumour and regions with expected normal tissue as seen in the ultrasound image, and imaging of tissue elasticity can therefore potentially contribute as a diagnostic tool in conjunction with conventional B-mode ultrasound imaging.

### **6.3 Paper 3**

Comparison of Contrast in Brightness Mode and Strain Ultrasonography of Glial Brain Tumours

Selbekk T, Brekken R, Indergaard M, Solheim O, Unsgård G. BMC Medical Imaging, 2012, May 23; 12:11.

The purpose of the study was to perform a direct comparison of image contrast between tumour and the surrounding tissue with presumably normal brain for conventional brightness mode (B-mode) ultrasound images and for strain magnitude images.

Ultrasound radiofrequency (RF) data acquired during surgery of 15 patients with glial tumours (8 low-grade, 7 high-grade) were included in the study. The RF-data were subsequently processed to provide strain magnitude images. The contrast between tumour and the surrounding normal brain was calculated for both the B-mode and the strain magnitude images, using identical regions of interest for the calculations. Three contrast measurements at different locations were performed for each image. The t-tests were used for statistical comparison.

The results show that the contrasts in the strain magnitude images are significantly higher than in the conventional ultrasound B-mode images (N=45,  $P < 0.0001$ ). There is not a significant difference in contrast between the sub-groups of low-grade and high-grade gliomas, neither for the strain images ( $P = 0.49$ ) nor the B-mode images ( $P = 0.25$ ).

The conclusion is that the ultrasound strain images provide higher image contrast and thereby better discrimination between normal brain tissue and glial tumour tissue than the conventional ultrasound images. Ultrasound strain imaging holds the potential to become a valuable adjunct to conventional ultrasound when it comes to identification of resectable tumour tissue during brain surgery.

#### **6.4 Paper 4**

Ability of navigated 3D ultrasound to delineate gliomas and metastases - comparison of image interpretations with histopathology.

Unsgård G, Selbekk T, Müller TB, Ommedal S, Torp HS, Myhr G, Bang J, Hernes TAN

*Acta Neurochirurgica*, 147(12):1259-69, 2005.

The objective of this study was to investigate if the delineation of tumour as seen in 3D ultrasound images was in agreement with histopathology.

A system combining ultrasound imaging and navigation technology was used in surgery of 28 patients (7 low-grade astrocytomas, 8 anaplastic astrocytomas, 7 glioblastomas and 6 metastases). A navigated biopsy forceps was used for image-guided biopsy sampling, using the simultaneous display of intraoperative ultrasound and

preoperative MR image volumes. A total of 87 navigated biopsies were sampled within a distance of 2-7 mm from the ultrasound visible tumour border. The surgeon's interpretation of the image findings was recorded and later compared with histopathology.

The results show that the interpreted ultrasound findings of biopsies sampled close to the tumour border were in agreement with histopathology in 74% for low-grade astrocytomas (n=31), 83% for anaplastic astrocytoma (n=18), 77% for glioblastoma multiforme (n=26) and 100% for metastases (n=10). Infiltrating tumour cells were found outside the ultrasound visible tumour border, particularly for low-grade astrocytomas.

We conclude that the reformatted images from 3D ultrasound acquired prior to start of resection provide a good delineation of metastases and the solid compartments of glial tumours, and may therefore be used for navigation purposes.

## **6.5 Paper 5**

Comparison of ultrasound findings with histopathology in subsequent phases of glioblastoma resection

Rygh OM, Selbekk T, Torp S, Lydersen S, Hernes TAN, Unsgård G.

Acta Neurochir (Wien), 2008; 150(10):1033-41.

The objective of the study was to investigate the ability of navigated 3D ultrasound to distinguish tumour and normal tissue in three stages of surgery: before start of resection, during resection and after resection. Ultrasound is used for image guidance in brain tumour surgery. The ultrasound image quality might be affected by artefact caused by the resection of the tumour.

A total of 186 biopsies from 19 glioblastoma patients were included in the study. The navigated biopsies were sampled in the tumour border zone before and during resection, while after resection the biopsies were sampled in the resection cavity wall. The surgeon's interpretation of the image findings was compared with histopathology.

The image findings of biopsies and ultrasound volumes acquired prior to resection of tumour had a high sensitivity and specificity of 95% (n=61). For ultrasound

volumes and biopsies acquired during surgery the sensitivity was 88% while the specificity dropped to 42% (n= 52). For ultrasound volumes acquired after finalized tumour resection the image findings of biopsies sampled in the resection wall had a sensitivity of 26% while specificity was 88% (n= 73).

The results suggest that the image interpretation and navigation guidance are in good agreement with histopathology prior to surgery, with good ultrasound delineation of tumour. During resection the sensitivity is still high, while some of the biopsies with tumour image findings had a histopathology of normal tissue resulting in a poor specificity of 42%. The image findings for biopsies sampled in the cavity after completed resection had a sensitivity of 26%, indicating it may be difficult to identify small tumour remnants or infiltration that may be present in the resection cavity. It was concluded that the ultrasound image quality might degrade during resection. However, the results are probably also affected by navigation inaccuracies caused by the manipulation of tissue with the biopsy forceps.



## **7.0 Discussion**

The main purpose of this thesis was to investigate if ultrasound is able to depict brain tumours in an adequately manner, and thereby serve as a tool for resection control and hence improved patient treatment.

Based on the results included in the thesis it is fair to say that 3D ultrasound is able to delineate the tumour margins of glial brain tumours in an adequately manner, and is also suitable for resection control. However, surgically induced image artefacts may degrade the image quality during the operation. It is also fair to say that ultrasound elastography holds the potential to become a valuable adjunct to conventional B-mode ultrasound, providing a relatively higher image contrast between tumour lesions and adjacent normal brain tissue.

The clinical implications of using ultrasound for intraoperative imaging and resection control have partly been discussed in the papers included in the thesis. The findings of the biopsy study in subsequent phases of surgery have also been discussed in the thesis for the degree philosophiae doctor by Ola Morten Rygh [84]. Several clinical studies investigating e.g. survival and quality of life for patients operated for intracranial tumours at St. Olavs hospital has recently been published. These have been part of the PhD thesis of Ole Solheim and Sasha Gulati, as well as Asgeir Jakola's ongoing PhD study [14-16, 70, 85-90]. The following sections will therefore mainly focus on issues related to ultrasound image generation and the impact of surgical resection on image quality.

### **7.1 Ultrasound for resection control**

Although ultrasound is an established image technology in neurosurgery, there are only a limited number of published studies that have investigated resection control by comparing ultrasound with histopathological findings. LeRoux *et al.* and Woydt *et al.* compared real-time 2D ultrasound images of gliomas with histopathology, and concluded that intraoperative US could improve gross total resection [91, 92]. Chacko

*et al.* compared 2D ultrasound images at the end of tumour resection with histopathology and found that of the 79 samples taken from the tumour-brain interface that were reported as tumour on ultrasound, 66 had histopathological evidence of tumour while 13 samples were negative for tumour [93], giving a positive predictive value of 0.84.

Ultrasound imaging and navigation based on 3D ultrasound is deemed to be valuable for resection control, but it is also clear that the ultrasound images acquired at the end of surgery must be interpreted carefully in order to avoid false interpretation due to image artefacts. Surgically induced image artefacts are not solely associated with ultrasound technology, but also with imaging techniques like MRI. In 1999 Knauth *et al.* explored image artefacts in intraoperative MRI of 51 patients with brain tumours and found that surgically induced enhancement could be observed in the MR images of all patients [94]. In 41 (80.4%) of the patients an enhancement at the resection margins was visible and became more profound with increasing time elapsed from the injection of contrast agent. In 5 patients (9.8%) an intraparenchymal signal enhancements were seen in already the first post-contrast study, and showed little time dependence thereafter. This latter kind of image artefacts had a similar appearance as enhancing residual tumour, and could thereby involve an increased risk of false image interpretation.

However, the outcome of the biopsy studies included in the thesis is not only affected by the image quality of 3D ultrasound. The navigation accuracy of the biopsy forceps used in the studies may also affect the end results. The interpretation of the images (tumour/not tumour) is based on the position of the biopsy forceps as marked in the reformatted images displayed on the navigation system. If the navigation is inaccurate, the position of the biopsy forceps as indicated in the respective image volumes will not be identical to the true physical position in the brain. The biopsy forceps might manipulate and displace the tissue during sampling, even if the biopsy sampling is carefully performed to avoid spatial shifts of anatomy. This source of navigation inaccuracy might increase with resection as the tissue is more easily manipulated when part of the solid tumour is removed. Real-time ultrasound imaging was not used to monitor the position of the biopsy forceps during sampling. We cannot exclude the

possibility that the results of the comparison between ultrasound findings and histology are affected by navigation inaccuracies. However, it is difficult in retrospect to assess the true navigation accuracy for each of the acquired biopsies. We will therefore focus the further discussions on factors related to ultrasound image quality, rather than factors affecting navigation accuracy.

The next subsections will discuss ultrasound artefacts; how they are affected by surgery, and how artefacts can be dealt with to reduce the risk of misinterpreting the images.

### **7.1.1 Ultrasound artefacts in intraoperative imaging**

The process of acquisition and generation of ultrasound images may itself introduce noise and distorted representations of the true anatomy in the ultrasound images. This is referred to as ultrasound artefacts. The reason for the imperfect ultrasound image is the violation of one or more of the following assumptions:

1. The ultrasound beam is narrow with uniform width
2. The ultrasound waves travels in a straight line directly to the reflecting object and back to the transducer
3. The speed of sound is constant in soft tissue
4. The attenuation of ultrasound is constant and uniform

The violation of the assumptions may become more pronounced as surgery progresses. Thus, the surgical resection of tumour may result in increased image artefacts and more challenges related to the interpretation of the ultrasound images.

Assumption No. 1 is violated by the ultrasound beam being not infinitely thin, but is having a spatial extent as can be described by the axial, lateral and elevation resolution. The violation of the assumption can be seen in images as smearing of objects that are smaller than the actual beam width. The beam profile is mainly determined by the specifications of the ultrasound transducer array, and the spatial extent of the ultrasound beam should not be much affected by surgery.

Violation of assumption No. 2 can cause reverberations and mirror image artefacts. Neither of these two artefacts can be said to pose a significant problem in

intraoperative imaging of brain tumours, but reverberations may in some cases be observed. Reverberations are caused by the ultrasound pulse being reflected multiple times, i.e. that the echoed sound received by the transducer has been reflected more than once. Reverberations are seen in the ultrasound images as succession of reflected events following a primary reflection of a structure or anatomical feature. In neurosurgery these artefacts have very seldom the potential to be mistaken for remaining tumour, but may degrade the overall image quality. Reverberations might be observed to occur between the transducer surface and the sterile drape that covers the ultrasound probe, or between the sterile drape and the brain cortex. Ensuring proper acoustic coupling between the surfaces can reduce the noise caused by reverberations.

Reverberations can be seen as multiple reflections of the bottom of resection cavity, so the artefact may become more apparent during surgery. This may or may not be considered to hamper the image quality, dependent on the localisation of the multiple reflections in the images. If the reverberations are appearing deeper in the images than the deepest target of interest, the added noise will probably not significantly degrade the clinical usefulness of the images. If reverberating events are appearing in the same depth and location as the primary reflection of a target of interest, this may be considered to degrade the ultrasound image quality. However, violation of assumption No. 2 alone should not impose a huge risk of generating artefacts that may be mistaken as remaining tumour tissue.

Assumption 3, the speed of sound  $c$  is constant in soft tissue, is to some extent always violated in medical ultrasound imaging (section 2.1). This may cause improper delineation of geometry, depth range errors and phase aberration. The latter phenomena refer to defocusing of the ultrasound beam caused by distortions of the ultrasound wavefront due to differences in the speed of sound. Portions of the propagating wavefront will be advanced or retarded depending on the speed of sound, and this may cause distortions in the focusing and steering of the ultrasound beam. This may in turn lead to reduced resolution and contrast in the ultrasound images. Violation of assumption 3 is not a major issue when it comes to intraoperative ultrasound imaging of the brain, as the brain is a quite homogenous organ. The resection of tumour may potentially introduce slightly more artefacts due to the violation of the constant speed of

sound assumption. The saline water used for filling up the resection cavity will have a velocity  $c$  that is likely to be about 1525 m/s compared to about 1550 m/s as have been stated for brain [95].

The assumption No04 stating that the attenuation of tissue is constant and uniform, is the one that is most severely violated by surgery. The attenuation coefficient  $\alpha$  may vary between different substances or tissues (section 2.3). In brain tissue it has been measured to be in the range from approximately 0.65 to 0.95 dB/(MHz cm). Apart from the obvious loss of frequency content with depth, the absorption of the brain does not induce any major ultrasound artefacts for imaging performed prior to resection. The Time-Gain-Control (TGC) of the scanner can be adjusted to compensate for the attenuation of the ultrasound waves with distance.

After start of resection, the presence of a resection cavity will introduce significant alternations in the attenuation of the imaged media. The resection cavity needs to be filled with saline water, which has an attenuation coefficient  $\alpha$  in the range of 0.002 dB/(MHz cm). The very large difference in absorption between brain and saline water might have a large negative impact on ultrasound images of the operation area. The difference in absorption is causing the most common and dominant image artefact in intraoperative ultrasound imaging of brain tumours; the brightness (or enhancement) artefact. The artefact may be seen in the images as an artificial increased brightness below the bottom of the water filled cavity, which during brain surgery will be the resection cavity (Fig. 4).

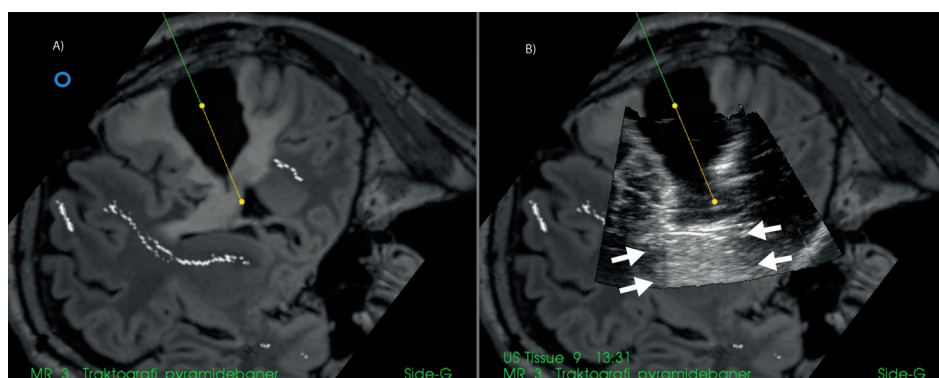


Figure 4. A screen dump from a 3D ultrasound based navigation system (Sonowand Invite<sup>®</sup>) showing a reformatted image slice from the preoperative MRI volume (A), and the same slice with the corresponding ultrasound image as overlay on the MR image (B). The enhancement artefact below the bottom of the long resection cavity is marked with bright arrows in B).

If brightness artefacts hamper the images, it may mask the presence of possible tumour remnants. It is therefore vital that the surgeon know how to identify this artefact, so the noise in the images is not interpreted to be remaining tumour tissue that may be resected.

### 7.1.2 How to minimize surgically induced ultrasound artefacts

It is important that the surgeon is able to determine whether or not a feature in the ultrasound images represent true anatomy or a likely surgically induced artefact. In real-time 2D imaging the location of the artefact in the image will move when the probe is moved or altered in position and angle. Thus, the ultrasound artefacts will appear at different locations when imaging is done from different angles. The acquisition of 3D ultrasound volumes allows comparison of different vintages of ultrasound datasets. This allows the surgeon to compare the most recently acquired data with a baseline image volume acquired before start of resection. If a feature is seen in the most current ultrasound volume but not in the previously acquired image volumes, the feature is likely to be an artefact. However, this requires that the surgeon acquire several ultrasound image volumes at different stages of the tumour resection. It is especially important to acquire an ultrasound volume at a stage before the tumour is completely resected. It is easier for the surgeon to recognise the tumour border shown in the

intraoperative ultrasound images, if the progress of the tumour removal is monitored by acquisition of 3D ultrasound volumes at regular intervals throughout surgery.

It is important for safe resection of tumours that image artefacts are recognized, since these may be more pronounced in the images acquired at the end of surgery.

As pointed out in previous section, the most pronounced ultrasound artefact that can be observed in intraoperative ultrasound imaging in brain tumour surgery is the enhancement artefact caused by different absorption in the media investigated. The damping of the ultrasound pulse is related to the absorption coefficient  $\alpha$  of the media and the distance travelled. The enhancement artefact can be minimized by either reducing the distance to the imaged region of interest, or by making the absorption coefficient  $\alpha$  equal in the whole imaged area.

During surgery the ultrasound probes are usually positioned at the brain cortex. When an operating channel and a resection cavity have been established, it could also be possible to insert probes with a small physical size and a small footprint into the resection cavity (Fig. 5). In this way the probe can be brought within close distance to the bottom of the resection cavity to inspect the tissue of the resection margins. This approach will reduce or remove the enhancement artefacts. A possible drawback is that the width of the ultrasound image is bound to be limited due to the small size of the ultrasound probe. Only small sections of the resection margin can be investigated at a time. If 3D ultrasound acquisition is enabled, moving the probe back and forth over the area with possible tumour remnants may still provide an ultrasound volume covering the region of interest.

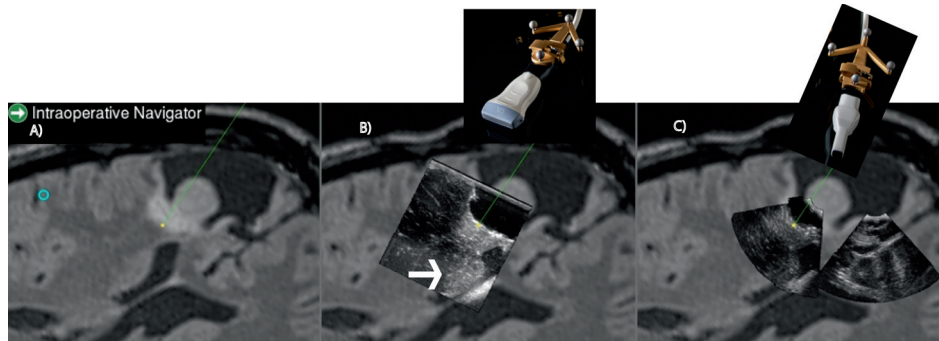


Figure 5. Screen dump from a 3D ultrasound based navigation system (Sonowand Invite<sup>®</sup>) showing the reformatted image slice of preoperative MR (A), the reformatted image slice from a ultrasound volume acquired with a flat linear array probe (shown above for illustration) positioned at the brain cortex (B), the reformatted ultrasound image slice from a ultrasound volume acquired with a phased array probe (shown above) with a small footprint inserted in the resection cavity (C). In B and C) the ultrasound volumes are acquired after part of the tumour is removed. Notice brightness artefact in B) marked with a bright arrow, which is not present in C) where the data has been acquired with the probe in close distance to the bottom of the cavity.

Acquisition of 3D ultrasound data in this study was usually performed with linear array or phased array probes placed on the brain cortex. When acquiring data during tumour resection the probe may partly be placed over the resection cavity filled with saline water. To avoid the enhanced brightness below the resection cavity, the ultrasound pulses propagating in the saline water need to have a similar damping as the brain itself. There is a difference between the absorption coefficient  $\alpha$  in white and grey brain matter (Section 2.3), but relative to the absorption coefficient of saline water this difference is very small.

The research group forming the National Centre of Competence in Ultrasound and Image Guided Therapy has in the last two years developed a fluid with absorption coefficient  $\alpha$  similar to the brain. This effort has resulted in a fluid that has the potential to replace saline water as an acoustic coupling medium for intraoperative ultrasound imaging (Figure 6). The fluid has an absorption coefficient  $\alpha$  targeted at 0.80 dB/(MHz cm), which is in the same order as  $\alpha$  of the adult human brain. Further, the fluid is sufficiently viscous to allow easy removal from the resection cavity with a suction device after imaging is finished. The fluid is based on substances that are approved for intravascular use. The fluid has been investigated for harmful effects by injection in brain parenchyma of rats and by injection of the fluid in the cerebrospinal space in pigs.

Papers about the development of the fluid and the results of the animal experiments are currently in writing, and a patent application has been submitted. The fluid represents a potential future tool to obtain ultrasound images of highest quality throughout the surgical procedure.

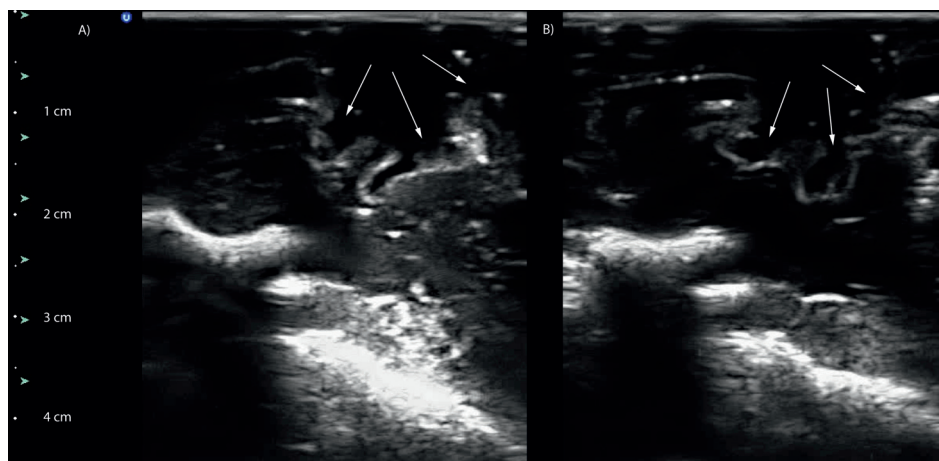


Figure 6. Resection cavity (marked with arrows) made in a fresh piglet brain, imaged using normal physiological saline to fill the resection cavity (A) and imaged using the developed acoustic coupling fluid (B). The acquisition parameters are identical in both cases. Note the difference in intensity of the bone below the resection cavity, seen in the deeper parts of the image of A) and B).

## 7.2 Ultrasound strain imaging of brain tumours

The first paper included in this PhD-thesis showed that it was possible to generate strain images of brain tumours. Later papers from other research groups have confirmed that it is possible to generate images related to strain in brain from intraoperative ultrasound data acquired during surgery of brain tumours. The next subsections will discuss how the strain magnitude images and measurements in our published studies compare to the findings of the other studies.

### 7.2.1 The relative hardness of tissue

A group from the Ruhr University Bochum, Germany, developed a method for imaging of tissue elasticity, in which a low frequent (5-10 Hz) vibration with amplitude 0.3 mm was applied to the brain while imaging local strain [96]. In the "vibrography" images,

the strain level in the tumour was by visual inspection categorized as having i) equal strain level as normal tissue but with a high strain rim in the peripheral tumour, ii) higher strain than the normal brain parenchyma and iii) lower strain than the brain parenchyma. In their series of 20 patients with heterogeneous tumours, it was possible to generate elastograms in 18 patients, in which 3 tumours were of category i), 6 tumours were of category ii) and 7 tumours were in category iii). Two cases could not be put in one of these categories. Quantitative measures of strain were not obtained in the study.

Another paper from a research team in London, UK, reports the experience with ultrasound elastography in 31 patients with brain tumours [97]. Two different ultrasound systems were used in the series, and the ultrasound transducers were used to palpate the brain tissue during elastography imaging. The elastograms were categorised as showing the lesions being a) less stiff, b) equally stiff and c) stiffer than the surrounding normal brain. The surgeon was in a blinded manner asked to characterise the tumour being resected in the same groups. The paper states that there was agreement between the elastograms and the surgeon's assessment in 25 of 31 cases. Unfortunately the paper does not quantify the number of cases in each category.

In our research group we have obtained strain images of 19 cases with intracerebral tumours. In the strain magnitude images of all 19 cases the tumour shows as being harder (lower strain) than the surrounding normal brain. However, in some cases the images are heterogeneous with smaller regions within the lesion showing up as softer tissue.

It may seem that there is a discrepancy between our findings regarding hardness of brain tumours compared to normal brain and the two other studies. The difference in apparent hardness of brain tumours observed between the studies might partly be explained by differences in the acquisition and processing of data. The challenge for all measurement methods is how to measure a system without affecting the very same system by the measurement technique. Our measurements are performed with the surgeon gently placing the ultrasound probe at or close to the brain cortex. Saline or sterile acoustic gel was used in order to achieve proper acoustic contact between the transducer and the brain. This ensures that there is negligible pressure or load applied

to the brain from the transducer. The stress applied to the parenchyma is originating from the cardiac pulsation, with most of the tissue movement probably being introduced by the larger arteries of the brain. This is in contrast to the measurements reported in the two other publications. The probes were in both cases in firm contact with the brain cortex, as the probes were used to apply a light compression to the brain. The degree of static preloading applied to the tissue before acquisition of elastograms is difficult to assess and might vary from case to case. The precompression will apply a load to the tissue being below the transducer and might thereby affect the assessment of relative tissue hardness. Krouskop *et al.* found by measurements in biological tissue that the level of static preloading had marked impact on the measured value of Young's modulus [98].

Differences in preload applied during image acquisition may therefore be one factor explaining why some studies report that the apparent hardness of tumour relative to normal brain seem to differ from patient to patient, even for tumours within the same WHO-grade.

In addition the relative tissue hardness is very likely to be affected by the heterogeneity in tumour origin (glioma, metastases, meningioma, etc.), the localisation of tumour relative to anatomy like e.g. the ventricles, and the presence of oedema. Tumours like glioblastoma multiforme may have compartments with softer and harder tissue, and the presence of necrosis or cysts will affect the apparent hardness of the tumour compared to the surrounding normal brain tissue.

Thus, the relative hardness of tissue as seen in ultrasound elastograms may be affected by factors related to the acquisition and generation of images, and by factors related to pathology and anatomy.

### **7.2.2 Assessment of B-mode and strain image quality**

In medical imaging the term image quality is related to quantitative assessment or subjective measure on how accurately an image of a body actually represent that body with respect to visibility of anatomy and signs of disease. Image quality can be described by suitable variables calculated directly from the images, such as signal-to-noise ratio (SNR), contrast-to-noise ratio (CNR) or assessment of spatial resolution with

the aid of resolution phantoms for the given image modality. The image quality may also be qualitatively defined and ranged by studies involving human observers. The image quality is for medical purposes often indirectly assessed by evaluating the diagnostic performance of the given images.

We have in all papers I-III included in this thesis performed some kind of comparison between strain magnitude and conventional B-mode ultrasound. Paper I presented merely display of both modalities for visual comparison in two different cases of brain tumours. Paper II included 16 patients with glial tumour, and a receiver operating characteristics (ROC) curve was used to compare strain magnitude levels with B-mode echogenicity (low or high) indicating either normal parenchyma or tumour tissue. In paper III the image contrast between lesion and adjacent normal tissue was assessed and compared for strain magnitudes and B-mode echo intensity.

It could be argued that the analyses of the images included in the study are more focused on the potential benefit and strength of the ultrasound strain magnitude images rather than exploring the weaknesses of the, in terms of clinical use, relatively new image modality. This is partly true. As discussed in the papers the strain images are prone to noise due to decorrelation effects in parts of the ultrasound image showing very low echo intensity. Selecting these regions for e.g. SNR analyses would certainly provide results that would be in disfavour of the strain images compared to the conventional ultrasound images. However, it is possible to filter out or remove parts in the strain images that are obviously erroneous and false. The strain images would even so contain information that could be of potential benefit when it comes to discrimination between lesions and normal tissue. In the analyses we have therefore focused on the potential strength of the strain images as a useful conjunction to conventional B-mode ultrasound imaging, rather than the possible weaknesses of the image modality.

### **7.2.3 Is ultrasound strain imaging suitable for resection control?**

Based on the data acquired in relation to the studies included in this thesis, we have observed that the strain magnitude images acquired prior to start of resection are

capable of delineating the extent of brain tumours. In some patients data was also acquired during resection. In these cases we could also generate strain magnitude images showing areas with residual tumour (Figure 7). The strain processing will produce erroneous results for the ultrasound RF-data originating from the water-filled resection cavity areas. However, the processing method used in our study was still able to produce strain images of residual tumour and brain parenchyma. This indicates that ultrasound strain imaging may serve as a tool for monitoring progress of tumour resection and thereby serve as a tool for resection control.

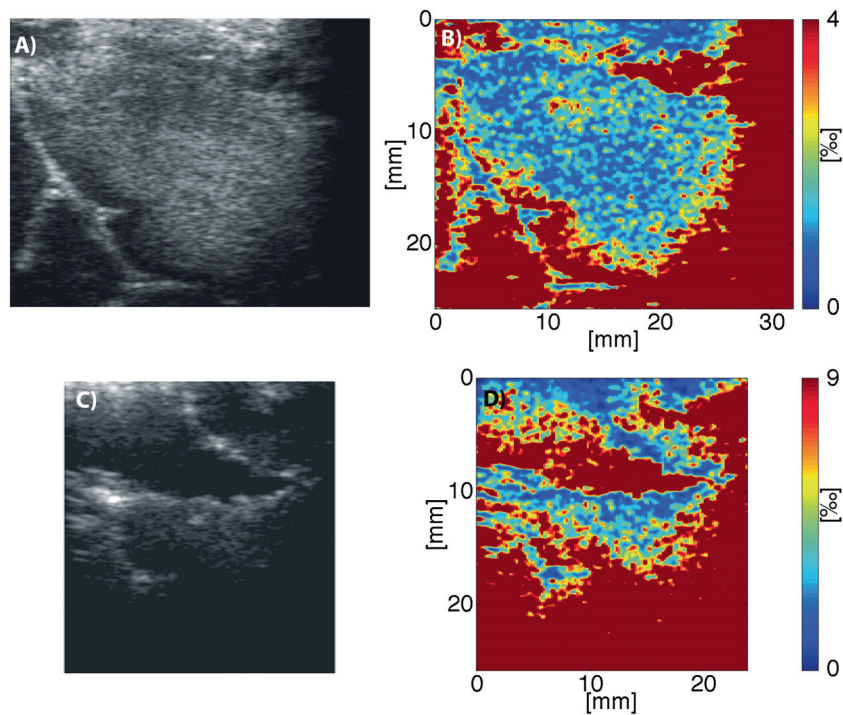


Figure 7. Ultrasound RF-data of a brain tumour (glioblastoma) before start of resection (A), and the corresponding strain magnitude image (B). Ultrasound RF-data from the same operation acquired after some resection of tumour (C) and the corresponding strain magnitude image (D). In the strain magnitude images a blue colour indicate low strain, i.e. harder tissue, than areas with yellow and red colour. In these images the blue colour is showing the falx cerebri and tissue that is likely to be tumour.

The research group has also made initial tests on freehand acquisition of 3D ultrasound elastography during brain tumour surgery. Data was acquired using the Ultrasonix MDP scanner (Vancouver, BC, Canada) with a flat linear probe (L14-5/38) and the standard

elastography module. The navigation system consisted of the in-house developed CustusX research navigation software and the Polaris tracking system (NDI, Ontario, Canada). The real time ultrasound elastograms were video-grabbed and fed to the navigation system.

In two patients (meningioma, glioma) having operation for the first time, the 3D elastography volumes seem to be able to depict the whole tumour in a consistent manner. Volume rendering of the ultrasound elastography volume could be done, as well as conventional displays of reformatted image slices (Fig 8). The reformatted images may be patient oriented (coronal, sagittal, axial) or tool oriented (arbitrary angles according to the orientation of the navigation tool). In a third patient the 3D elastography did not provide any meaningful images of the tumour. This patient had been operated multiple times, had previously received radiation therapy, and the small tumour was located on top of a large cavity from previous operations. We assume that for this patient there was not sufficient tissue pulsation in the proximity of the tumour to generate the elastograms. However, it should be kept in mind that this patient case was not very representative for the typical brain tumour operation.

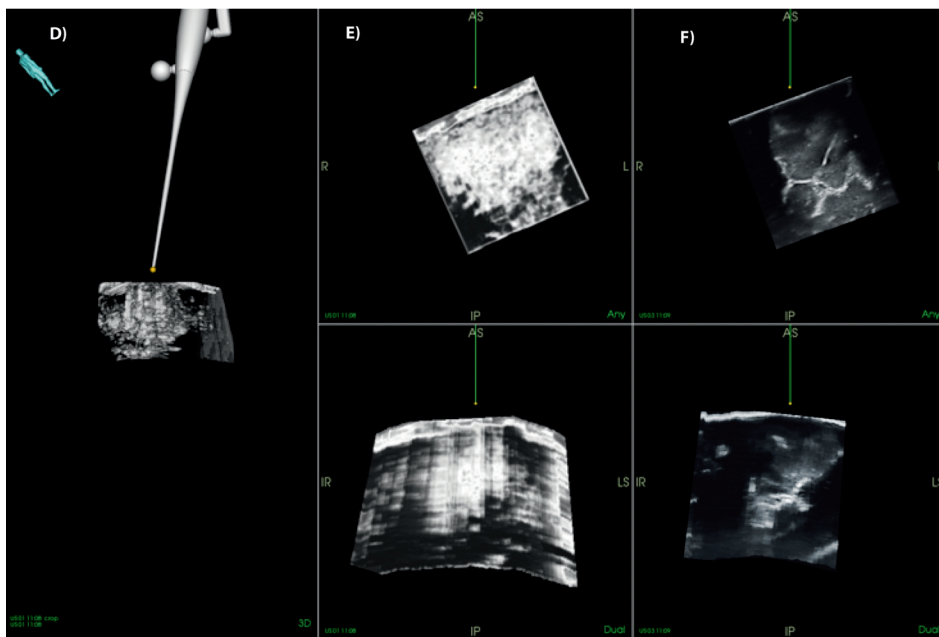
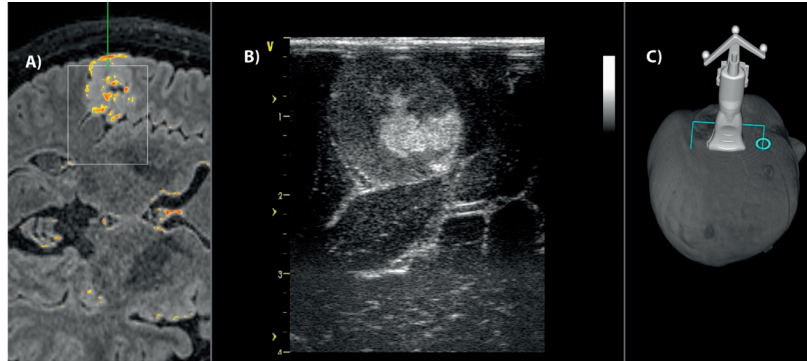


Figure 8. Screen dump from a 3D ultrasound navigation system (Sonowand Invite<sup>®</sup>) showing reformatted MR image slice (A), the corresponding real-time ultrasound image (B) and volume rendering of the MR data and the ultrasound probe as position during real-time imaging (C). The next row shows a screen dump of the same patient using the CustusX navigation system with the volume rendered ultrasound elastography volume and navigation tool (D), the instrument oriented reformatted image slices of the ultrasound elastography volume (E), and corresponding image slices of the ultrasound B-mode image volume (F). The two reformatted image slices in column E) and F) are perpendicular to each other, i.e. two reformatted image slices are shown for each volume.

The generation of elastography images of brain tumours using the elastography module of the Ultrasonix scanner suggests that the method used for elastography processing is not very critical for a successful result. This is in line with the findings of Thomas Børstad's master thesis, which explored several methods for calculating *time*

*delays* between ultrasound image frames, that could be used for obtaining elastograms of brain tumours [99]. It is therefore likely that it is possible to further optimize acquisition parameters and processing parameters to obtain high quality ultrasound elastograms of brain tumours. This does not guarantee that the image modality provides a significant positive effect on the outcome for the patient. The potential clinical benefit of ultrasound elastography as a conjunction to conventional intraoperative ultrasound imaging must be further investigated in properly designed future studies.

## **8.0 Intraoperative ultrasound - future perspectives**

It is fair to assume that medical images will be increasingly important for guidance of therapy and surgical treatment in the years to come. The trend towards less invasive procedures for treatment is likely to continue. Surgical treatment will be performed through smaller accesses to cause less harm to normal tissue, but still with the surgical aim of complete lesion removal. The minimal invasive approach necessitates the use of medical imaging technology to compensate the loss of direct sight in the operating field relative to open surgery procedures.

Ultrasound is a technology that should be well positioned for increased use in the operating room. The ultrasound transducers will gradually go from 1D arrays to 2D arrays, enabling acquisition of ultrasound image volumes in real-time, often referred to as 4D ultrasound imaging (3D + time). In combination with the expected increase in computer performance this may lead to more sophisticated methods for beam steering and beam forming, resulting in higher resolution and better images. The development of 2D arrays may also pave the way for more sophisticated ultrasound modalities and rapid generation of ultrasound image volumes as e.g. ultrasound elastography image volumes.

Ultrasound arrays today are mostly based on piezoelectric materials. The recent commercial release of a CMUT (capacitive micromachined ultrasound transducer) transducer by Hitachi, paves the way for silicon-based arrays. This may introduce probes that are cheaper, more customizable and have higher frequencies and bandwidth compared to piezoelectric transducers. In combination with the everlasting trend of miniaturization, the CMUTs may in a long-term perspective allow complete ultrasound systems to be seamlessly integrated with surgical tools. It may very well be that the future surgical instrument for resection of brain tumours has an ultrasound transducer integrated on the tip, with ultrasound modalities as B-mode and strain images shown on a smaller display unit attached to the handle.

It is also sound to assume that the current basic research on the combined use of ultrasound and micro-bubbles for therapeutic purposes will gradually evolve into clinical applications. The release of drugs contained in the micro-bubbles using ultrasound pulses could be a future treatment options for patients with cancer or other diseases. It may be that other imaging technologies than ultrasound will perform

monitoring of such therapy, or that hybrid imaging systems will be developed for this purpose.

It is difficult to definitely predict the discoveries that will form the future of ultrasound imaging and how it will be used for monitoring and guidance of therapeutic procedures. However, ultrasound technology will continue to develop resulting in more adaptive systems with lower cost that provide better image quality and more information about the state of the tissue. The clinical importance and use of ultrasound is likely to increase in the coming years. Research within technical development and clinical use of ultrasound and navigation technology as currently done in Trondheim and other places, should therefore be considered as a great asset to the society and a prerequisite to the development of future patient treatment.

## 9.0 References

1. Unsgaard G, Gronningsaeter A, Ommedal S, Nagelhus Hernes TA. Brain operations guided by real-time two-dimensional ultrasound: New possibilities as a result of improved image quality. *Neurosurgery*. 2002;51:402-412
2. Kolstad F, Rygh OM, Selbekk T, Unsgaard G, Nygaard OP. Three-dimensional ultrasonography navigation in spinal cord tumor surgery. Technical note. *J Neurosurg Spine*. 2006;5:264-270
3. Rygh OM, Cappelen J, Selbekk T, Lindseth F, Hernes TA, Unsgaard G. Endoscopy guided by an intraoperative 3F ultrasound-based neuronavigation system. *Minim Invasive Neurosurg*. 2006;49:1-9
4. Rygh OM, Nagelhus Hernes TA, Lindseth F, Selbekk T, Brostrup Muller T, Unsgaard G. Intraoperative navigated 3-dimensional ultrasound angiography in tumor surgery. *Surg Neurol*. 2006;66:581-592; discussion 592
5. Solheim O, Selbekk T, Lindseth F, Unsgard G. Navigated resection of giant intracranial meningiomas based on intraoperative 3F ultrasound. *Acta Neurochir (Wien)*. 2009;151:1143-1151
6. Unsgaard G, Ommedal S, Muller T, Gronningsaeter A, Nagelhus Hernes TA. Neuronavigation by intraoperative three-dimensional ultrasound: Initial experience during brain tumor resection. *Neurosurgery*. 2002;50:804-812; discussion 812
7. Unsgaard G, Ommedal S, Rygh O, Lindseth F. Operation of CXO s assisted by stereoscopic navigation–controlled display of preoperative OT angiography and intraoperative ultrasound angiography. *Neurosurgery*. 2005;56:S2:281-290
8. Berntsen EM, Gulati S, Solheim O, Kvistad KA, Torp SH, Selbekk T, Unsgard G, Haberg AK. Functional magnetic resonance imaging and diffusion tensor tractography incorporated into an intraoperative 3-dimensional ultrasound-based neuronavigation system: Impact on therapeutic strategies, extent of resection, and clinical outcome. *Neurosurgery*. 2010;67:251-264
9. Gulati S, Berntsen EM, Solheim O, Kvistad KA, Haberg A, Selbekk T, Torp SH, Unsgaard G. Surgical resection of high-grade gliomas in eloquent regions guided by blood oxygenation level dependent functional magnetic resonance imaging, diffusion tensor tractography, and intraoperative navigated 3F ultrasound. *Minim Invasive Neurosurg*. 2009;52:17-24
10. Rasmussen IA, Jr., Lindseth F, Rygh OM, Berntsen EM, Selbekk T, Xu J, Nagelhus Hernes TA, Harg E, Haberg A, Unsgaard G. Functional neuronavigation combined with intra-operative 3F ultrasound: Initial experiences during surgical resections close to eloquent brain areas and future directions in automatic brain shift compensation of preoperative data. *Acta Neurochir (Wien)*. 2007;149:365-378
11. Lindseth F, Lovstakken L, Rygh OM, Tangen GA, Torp H, Unsgaard G. Blood flow imaging: An angle-independent ultrasound modality for intraoperative assessment of flow dynamics in neurovascular surgery. *Neurosurgery*. 2009;65:149-157; discussion 157
12. Reinertsen I, Jakola AS, Friderichsen P, Lindseth F, Solheim O, Selbekk T, Unsgard G. A new system for 3F ultrasound-guided placement of cerebral ventricle catheters. *Int J Comput Assist Radiol Surg*. 2012;7:151-157

13. Solheim O, Selbekk T, Lovstakken L, Tangen GA, Solberg OV, Johansen TF, Cappelen J, Unsgard G. Intracellar ultrasound in transsphenoidal surgery: A novel technique. *Neurosurgery*. 2010;66:173-185; discussion 185-176
14. Jakola AS, Gulati S, Weber C, Unsgard G, Solheim O. Postoperative deterioration in health related quality of life as predictor for survival in patients with glioblastoma: A prospective study. *PLoS One*. 2011;6:e28592
15. Jakola AS, Unsgard G, Solheim O. Quality of life in patients with intracranial gliomas: The impact of modern image-guided surgery. *J Neurosurg*. 2011;114:1622-1630
16. Solheim O, Selbekk T, Jakola AS, Unsgard G. Ultrasound-guided operations in unselected high-grade gliomas--overall results, impact of image quality and patient selection. *Acta Neurochirurgica*. 2010;152:1873-1886
17. Bamber JC. Ultrasonic attenuation in fresh human tissues. *Ultrasonics*. 1981;19:187-188
18. Kremkau FW, Barnes RW, McGraw CP. Ultrasonic attenuation and propagation speed in normal human brain. *J Acoust Soc Am*. 1981;70:29-38
19. Strowitzki M, Brand S, Jenderka KV. Ultrasonic radio-frequency spectrum analysis of normal brain tissue. *Ultrasound in Medicine & Biology*. 2007;33:522-529
20. Attenborough K. Waves and sound. In: Postema M, ed. *Fundamentals of medical ultrasonics*. New York: Spon Press; 2011.
21. Dussik KT. Über die möglichkeit, hochfrequente mechanische schwingungen als diagnostisches hilfsmittel zu verwerten. *Z Neurol Psychiatr*. 1942;174:153-168
22. Woo J. A short history of the development of ultrasound in obstetrics and gynecology. 2006;2012
23. Ballantine HT, Jr., Bolt RH, Hueter TF, Ludwig GD. On the detection of intracranial pathology by ultrasound. *Science*. 1950;112:525-528
24. French LA, Wild JJ, Neal D. Detection of cerebral tumors by ultrasonic pulses; pilot studies on postmortem material. *Cancer*. 1950;3:705-708
25. Wild JJ, Reid JM. Application of echo-ranging techniques to the determination of structure of biological tissues. *Science*. 1952;115:226-230
26. Chandler WF, Knake JE, McGillicuddy JE, Lillehei KO, Silver TM. Intraoperative use of real-time ultrasonography in neurosurgery. *Journal of Neurosurgery*. 1982;57:157-163
27. Rubin JM, Mirfakhraee M, Duda EE, Dohrmann GJ, Brown F. Intraoperative ultrasound examination of the brain. *Radiology*. 1980;137:831-832
28. Voorhies RM, Engel I, Gamache FW, Jr., Patterson RH, Jr., Fraser RA, Lavyne MH, Schneider M. Intraoperative localization of subcortical brain tumors: Further experience with B-mode real-time sector scanning. *Neurosurgery*. 1983;12:189-194
29. Aaslid R, Markwalder TM, Nornes H. Noninvasive transcranial doppler ultrasound recording of flow velocity in basal cerebral arteries. *Journal of neurosurgery*. 1982;57:769-774
30. Woydt M, Perez J, Meixensberger J, Krone A, Soerensen N, Roosen K. Intraoperative colour-duplex-sonography in the surgical management of cerebral AV-malformations. *Acta Neurochirurgica*. 1998;140:689-698

31. Bartels E, Bittermann HJ. Transcranial contrast imaging of cerebral perfusion in stroke patients following decompressive craniectomy. *Ultraschall Med.* 2004;25:206-213
32. He W, Jiang XQ, Wang S, Zhang MZ, Zhao JZ, Liu HZ, Ma J, Xiang DY, Wang LS. Intraoperative contrast-enhanced ultrasound for brain tumors. *Clin Imaging.* 2008;32:419-424
33. Holscher T, Ozgur B, Singel S, Wilkening WG, Mattrey RF, Sang H. Intraoperative ultrasound using phase inversion harmonic imaging: First experiences. *Neurosurgery.* 2007;60:382-386; discussion 386-387
34. Hansen R, Angelsen BA. Surf imaging for contrast agent detection. *IEEE Trans Ultrason Ferroelectr Freq Control.* 2009;56:280-290
35. Wells PNT, Liang HD. Medical ultrasound: Imaging of soft tissue strain and elasticity. *J R Soc Interface.* 2011;8:1521-1549
36. Bishop J, Poole G, Leitch M, Plewes DB. Magnetic resonance imaging of shear wave propagation in excised tissue. *J Magn Reson Imaging.* 1998;8:1257-1265
37. Muller M, Gennisson JL, Deffieux T, Tanter M, Fink M. Quantitative viscoelasticity mapping of human liver using supersonic shear imaging: Preliminary in vivo feasibility study. *Ultrasound in Medicine & Biology.* 2009;35:219-229
38. Davies G, Koenen M. Acoustic radiation force impulse elastography in distinguishing hepatic haemangiomas from metastases: Preliminary observations. *Br J Radiol.* 2011;84:939-943
39. Manduca A, Oliphant TE, Dresner MA, Mahowald JL, Kruse SA, Amromin E, Felmlee JP, Greenleaf JF, Ehman RL. Magnetic resonance elastography: Non-invasive mapping of tissue elasticity. *Medical Image Analysis.* 2001;5:237-254
40. Zhang L, Yang KH, King AI. Comparison of brain responses between frontal and lateral impacts by finite element modeling. *J Neurotrauma.* 2001;18:21-30
41. Brands DW, Peters GW, Bovendeerd PH. Design and numerical implementation of a 3-d non-linear viscoelastic constitutive model for brain tissue during impact. *J Biomech.* 2004;37:127-134
42. Kruse SA, Rose GH, Glaser KJ, Manduca A, Felmlee JP, Jack CR, Jr., Ehman RL. Magnetic resonance elastography of the brain. *Neuroimage.* 2008;39:231-237
43. Green MA, Bilston LE, Sinkus R. In vivo brain viscoelastic properties measured by magnetic resonance elastography. *NMR Biomed.* 2008;21:755-764
44. Venkatesh SK, Yin M, Glockner JF, Takahashi N, Araoz PA, Talwalkar JA, Ehman RL. MR elastography of liver tumors: Preliminary results. *AJR Am J Roentgenol.* 2008;190:1534-1540
45. Angelsen BAJ. Anisotropic tissue, shear waves and uniaxial stress. *Ultrasound imaging.* Trondheim: Emantec AS; 2000:4-132.
46. von Gierke H, Oestreicher H, Franke E, Parrack H, von Wittern W. Physics of vibrations in living tissues. *J Appl Physiol.* 1952;4:886-900
47. Dickinson RJ, Hill CR. Measurement of soft tissue motion using correlation between a-scans. *Ultrasound in medicine & biology.* 1982;8:263-271
48. Wilson LS, Robinson DE. Ultrasonic measurement of small displacements and deformations of tissue. *Ultrason Imaging.* 1982;4:71-82

49. Lerner RM, Huang SR, Parker KJ. "Sonoelasticity" images derived from ultrasound signals in mechanically vibrated tissues. *Ultrasound in medicine & biology*. 1990;16:231-239
50. Ophir J, Cespedes I, Ponnekanti H, Yazdi Y, Li X. Elastography: A quantitative method for imaging the elasticity of biological tissues. *Ultrasound Imaging*. 1991;13:111-134
51. Selbekk T, Bang J, Unsgaard G. Strain processing of intraoperative ultrasound images of brain tumours: Initial results. *Ultrasound in Medicine & Biology*. 2005;31:45-51
52. Souchon R, Rouvière O, Gelet A, Detti V, Srinivasan S, Ophir J, Chapelon JY. Visualisation of hifu lesions using elastography of the human prostate in vivo: Preliminary results. *Ultrasound in Med. & Biol.* 2003;29:1007-1015
53. Bae U, Dighe M, Dubinsky T, Minoshima S, Shamdasani V, Kim Y. Ultrasound thyroid elastography using carotid artery pulsation: Preliminary study. *J Ultrasound Med.* 2007;26:797-805
54. Hiltawsky KM, Krüger M, Starke C, Heuser L, Ermert H, Jensen A. Freehand ultrasound elastography of breast lesions: clinical results. *Ultrasound in Med. & Biol.* 2001;27:1461-1469
55. Salomon G, Kollerman J, Thederan I, Chun FK, Budaus L, Schlomm T, Isbarn H, Heinzer H, Huland H, Graefen M. Evaluation of prostate cancer detection with ultrasound real-time elastography: A comparison with step section pathological analysis after radical prostatectomy. *Eur Urol.* 2008;54:1354-1362
56. Emelianov SY, Rubin JM, Lubinski MA, Skovoroda AR, O'Donnell M. Elasticity imaging of the liver: Is a hemangioma hard or soft? *Proceedings of the 1998 IEEE Ultrasonics Symposium*. 1998;7:1749-1752
57. Nightingale K, Soo MS, Nightingale R, Trahey G. Acoustic radiation force impulse imaging: In vivo demonstration of clinical feasibility. *Ultrasound in Medicine and Biology*. 2002;28:227-235
58. Zhai L, Polascik TJ, Foo WC, Rosenzweig S, Palmeri ML, Madden J, Nightingale KR. Acoustic radiation force impulse imaging of human prostates: Initial in vivo demonstration. *Ultrasound in Medicine and Biology*. 2012;38:50-61
59. Tozaki M, Isobe S, Fukuma E. Preliminary study of ultrasonographic tissue quantification of the breast using the acoustic radiation force impulse (ARFI) technology. *European Journal of Radiology*. 2011;80:E182-E187
60. Gallotti A, D'Onofrio M, Romanini L, Cantisani V, Pozzi Mucelli R. Acoustic radiation force impulse (ARFI) ultrasound imaging of solid focal liver lesions. *Eur J Radiol.* 2012;81:451-455
61. Bercoff J, Tanter M, Fink M. Supersonic shear imaging: A new technique for soft tissue elasticity mapping. *Ieee Transactions on Ultrasonics Ferroelectrics and Frequency Control*. 2004;51:396-409
62. Bavu E, Gennisson JL, Couade M, Bercoff J, Mallet V, Fink M, Badel A, Vallet-Pichard A, Nalpas B, Tanter M, Pol S. Noninvasive in vivo liver fibrosis evaluation using supersonic shear imaging: A clinical study on 113 hepatitis c virus patients. *Ultrasound in Medicine and Biology*. 2011;37:1361-1373
63. Athanasiou A, Tardivon A, Tanter M, Sigal-Zafrani B, Bercoff J, Eux TD, Gennisson JL, Fink M, Neuenschwander S. Breast lesions: Quantitative

- elastography with supersonic shear imaging-preliminary results. *Radiology*. 2010;256:297-303
64. Tanter M, Touboul D, Gennisson JL, Bercoff J, Fink M. High-resolution quantitative imaging of cornea elasticity using supersonic shear imaging. *Ieee Transactions on Medical Imaging*. 2009;28:1881-1893
  65. Parker KJ, Dooley MM, Rubens DJ. Imaging the elastic properties of tissue: The 20 year perspective. *Physics in Medicine and Biology*. 2011;56:R1-R29
  66. Paulson OB, Gjerris F, Sørensen PS. *Klinisk neurologi og neurokirurgi*. København: FADL's Forlag Aktieselskab; 2004.
  67. Kleihues P, Cavenee WK. Pathology and genetics of tumours of the nervous system. *World health organization classification of tumours*. 2000
  68. Sanai N, Berger MS. Glioma extent of resection and its impact on patient outcome. *Neurosurgery*. 2008;62:753-764; discussion 264-756
  69. Stummer W, Reulen HJ, Meinel T, Pichlmeier U, Schumacher W, Tonn JC, Rohde V, Opperl F, Turowski B, Woiciechowsky C, Franz K, Pietsch T. Extent of resection and survival in glioblastoma multiforme: Identification of and adjustment for bias. *Neurosurgery*. 2008;62:564-576; discussion 564-576
  70. Jakola AS, Myrnes KS, Kloster R, Torp SH, Lindal S, Unsgard G, Solheim O. Comparison of a strategy favoring early surgical resection vs a strategy favoring watchful waiting in low-grade gliomas. *Jama*. 2012:1-8
  71. Schicho K, Figl M, Seemann R, Donat M, Pretterklieber ML, Birkfellner W, Reichwein A, Wanschitz F, Kainberger F, Bergmann H, Wagner A, Ewers R. Comparison of laser surface scanning and fiducial marker-based registration in frameless stereotaxy. Technical note. *J Neurosurg*. 2007;106:704-709
  72. Woerdeman PA, Willems PW, Noordmans HJ, Tulleken CA, van der Sprenkel JW. Application accuracy in frameless image-guided neurosurgery: A comparison study of three patient-to-image registration methods. *J Neurosurg*. 2007;106:1012-1016
  73. Letteboer MMJ, Willems PWA, Viergever MA, Niessen WJ. Brain shift estimation in image-guided neurosurgery using 3-d ultrasound. *Ieee Transactions on Biomedical Engineering*. 2005;52:268-276
  74. Reinges MHT, Nguyen HH, Krings T, Hutter BO, Rohde V, Gilsbach JM. Course of brain shift during microsurgical resection of supratentorial cerebral lesions: Limits of conventional neuronavigation. *Acta Neurochirurgica*. 2004;146:369-377
  75. Roberts DW, Hartov A, Kennedy FE, Miga MI, Paulsen KD. Intraoperative brain shift and deformation: A quantitative analysis of cortical displacement in 28 cases. *Neurosurgery*. 1998;43:749-758
  76. Lindseth F, Lango T, Bang J, Nagelhus Hernes TA. Accuracy evaluation of a 3d ultrasound-based neuronavigation system. *Comput Aided Surg*. 2002;7:197-222
  77. Koivukangas J, Louhisalmi Y, Alakuijala J, Oikarinen J. Ultrasound-controlled neuronavigator-guided brain surgery. *J Neurosurg*. 1993;79:36-42
  78. Hata N, Dohi T, Iseki H, Takakura K. Development of a frameless and armless stereotactic neuronavigation system with ultrasonographic registration. *Neurosurgery*. 1997;41:608-613
  79. Jodicke A, Deinsberger W, Erbe H, Kriete A, Boker DK. Intraoperative three-dimensional ultrasonography: An approach to register brain shift using

- multidimensional image processing. *Minimally Invasive Neurosurgery*. 1998;41:13-19
80. Grønningsæter Å, Kleven A, Ommedal S, Årseth TE, Lie T, Lindseth F, Langø T, Unsgård G. Sonowand, an ultrasound-based neuronavigation system. *Neurosurgery*. 2000;47:1373-1380
  81. Hirschberg H, Unsgaard G. Incorporation of ultrasonic imaging in an optically coupled frameless stereotactic system. *Acta Neurochir Suppl. (Wien)*. 1997;68:75-80
  82. Unsgaard G, Rygh OM, Selbekk T, Muller TB, Kolstad F, Lindseth F, Hernes TA. Intra-operative 3D ultrasound in neurosurgery. *Acta Neurochir (Wien)*. 2006;148:235-253; discussion 253
  83. Lindseth F, Lango T, Bang J, Nagelhus Hernes TA. Accuracy evaluation of a 3D ultrasound-based neuronavigation system. *Computer aided surgery : official journal of the International Society for Computer Aided Surgery*. 2002;7:197-222
  84. Rygh O. 3D ultrasound-based neuronavigation in neurosurgery - a clinical evaluation. *Department of Neuroscience*. 2008
  85. Gulati S, Jakola AS, Johannesen TB, Solheim O. Survival and treatment patterns of glioblastoma in the elderly: A population-based study. *World Neurosurg*. 2011
  86. Gulati S, Jakola AS, Nerland US, Weber C, Solheim O. The risk of getting worse: Surgically acquired deficits, perioperative complications, and functional outcomes after primary resection of glioblastoma. *World Neurosurg*. 2011;76:572-579
  87. Jakola AS, Gulati S, Nerland US, Solheim O. Surgical resection of brain metastases: The prognostic value of the graded prognostic assessment score. *J Neurooncol*. 2011;105:573-581
  88. Jakola AS, Sorlie A, Gulati S, Nygaard OP, Lydersen S, Solberg T. Clinical outcomes and safety assessment in elderly patients undergoing decompressive laminectomy for lumbar spinal stenosis: A prospective study. *BMC Surg*. 2010;10:34
  89. Gulati S. Surgical resection of high-grade gliomas. *Department of Laboratory Medicine*. 2012
  90. Solheim O. Ultrasound guided surgery in patients with intracranial tumours. *Department of Neuroscience*. 2011
  91. Le Roux PD, Berger MS, Wang K, Mack LA, Ojemann GA. Low grade gliomas: Comparison of intraoperative ultrasound characteristics with preoperative imaging studies. *J Neurooncol*. 1992;13:189-198
  92. Woydt M, Krone A, Becker G, Schmidt K, Roggendorf W, Roosen K. Correlation of intra-operative ultrasound with histopathologic findings after tumour resection in supratentorial gliomas - a method to improve gross total tumour resection. *Acta Neurochirurgica*. 1996;138:1391-1398
  93. Chacko AG, Kumar NK, Chacko G, Athyal R, Rajshekhar V. Intraoperative ultrasound in determining the extent of resection of parenchymal brain tumours - a comparative study with computed tomography and histopathology. *Acta Neurochirurgica*. 2003;145:743-748; discussion 748

94. Knauth M, Aras N, Wirtz CR, Dorfler A, Engelhorn T, Sartor K. Surgically induced intracranial contrast enhancement: Potential source of diagnostic error in intraoperative MR imaging. *AJNR. American journal of neuroradiology*. 1999;20:1547-1553
95. Duck FA. *Physical properties of tissue*. London: Academic Press; 1990.
96. Scholz M, Noack V, Pechlivanis I, Engelhardt M, Fricke B, Linstedt U, Brendel B, Ing D, Schmieder K, Ermert H, Harders A. Vibrography during tumor neurosurgery. *J Ultrasound Med*. 2005;24:985-992
97. Uff CE, Garcia L, Fromageau J, Dorward N, Bamber JC. Real-time ultrasound elastography in neurosurgery. *IEEE International Ultrasonics Symposium Proceedings*. 2009:467-470
98. Krouskop TA, Wheeler TM, Kallel F, Garra BS, Hall T. Elastic moduli of breast and prostate tissues under compression. *Ultrason Imaging*. 1998;20:260-274
99. Børstad TK. Intraoperative ultrasound strain imaging of brain tumours. *Department of Engineering Cybernetics*. 2011



# Paper I





● *Original Contribution*

## STRAIN PROCESSING OF INTRAOPERATIVE ULTRASOUND IMAGES OF BRAIN TUMOURS: INITIAL RESULTS

TORMOD SELBEKK,\* JON BANG\* and GEIRMUND UNSGAARD†

\*SINTEF Health Research, Trondheim, Norway; and †Department of Neurosurgery, University Hospital of Trondheim, and Norwegian University of Science and Technology, Trondheim, Norway

(Received 30 June 2004; revised 16 September 2004; accepted 22 September 2004)

**Abstract**—The purpose of the study was to investigate a method for strain calculation and its ability to discriminate between brain tumour and normal brain. During surgery of a low-grade astrocytoma and a metastasis, we acquired ultrasound (US) radiofrequency (RF) data with a hand-held probe at the dura mater. Using cross-correlation and phase-sensitive processing, we quantified the tissue displacements between consecutive US images and, subsequently, the local strain. In the elastograms, the tumour lesions were associated with lower strain levels than those found in the surrounding normal tissue. For both investigated cases, the strain images showed good agreement with the B-mode images. However, the results also indicated that the tumour interpretation might be different in the two modalities. An important finding was that the tissue motion caused by arterial pulsation is sufficient for generating elastograms. Requiring no specialised equipment or changes to acquisition procedures, strain data can be obtained as easily as conventional US imaging. (E-mail: Tormod.Selbekk@sintef.no) © 2005 World Federation for Ultrasound in Medicine & Biology.

**Key Words:** Intraoperative ultrasound, Elastography, Strain imaging, Brain tumours, Neurosurgery.

### INTRODUCTION

Ultrasound (US) strain imaging can be used to investigate the elastic properties of biologic tissue. Various methods for calculation of local strain and elastic parameters have previously been described (D'hooge et al. 2000; Gao et al. 1996; Ophir et al. 2000; Ophir et al. 2001). The processing algorithms are often evaluated using synthetic US data, or the US data might be acquired in an ex vivo laboratory experiment. However, these data may not be representative for data acquired from live biologic tissue and it may, therefore, be difficult to conclude about the in vivo performance of the algorithms.

In a clinical context, US strain imaging has previously been applied in cardiac examinations (D'hooge et al. 2002; Heimdal et al. 1998; Kiraly et al. 2003; Konofagou et al. 2002; Pellerin et al. 2003; Varghese et al. 2003) and for identification of lesions in, for example, breast (Garra et al. 1997; Hall et al. 2003; Hiltawsky et al. 2001), prostate (Souchon et al. 2003) and liver (Emelianov et al. 1998). To our knowledge, US strain imaging of the human brain has not been covered in any

previous article. However, conventional US imaging is established in brain surgery for image-guided resection of tumours and vascular lesions (Unsgaard et al. 2002a; Unsgaard et al. 2002b; Woydt et al. 2002). Conventional B-mode US images can usually discriminate solid tumour from normal brain. One possible exception is irradiated or recurrent tumours, where the presence of gliosis might impair the US imaging of the tumour margins (Hammoud et al. 1996; LeRoux et al. 1989). Strain imaging might provide additional information to aid in distinguishing the tissues, because the echogenicity and stiffness of tissue are, in general, uncorrelated (Ophir et al. 1999). It is possible that strain images might have a different sensitivity to differences in tumour malignancy or the degree of tumour cell infiltration than conventional B-mode images, which could provide complementary information about tissue pathology. Previous investigations have shown significantly lower strain levels in tumours than in surrounding normal tissue (Emelianov et al. 1998; Hiltawsky et al. 2001; Souchon et al. 2003).

In this article, we investigate strain processing on US RF data acquired during brain tumour surgery. Our hypothesis was that strain imaging could be used to distinguish between solid tumour and normal brain. We also hypothesised that the pulsation of the brain caused

Address correspondence to: Tormod Selbekk, SINTEF Health Research, Trondheim NO-7465 Norway. E-mail: Tormod.Selbekk@sintef.no

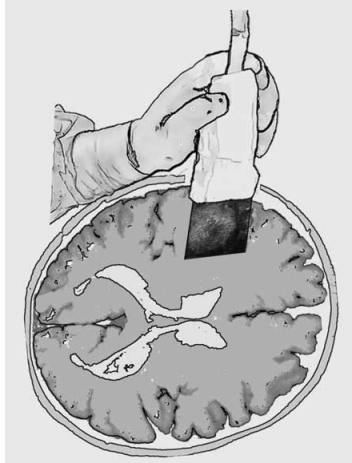


Fig. 1. The acquisition of US RF-data using a hand-held 10-MHz probe placed on intact dura mater. The probe was covered by a sterile condom and sterile gel was applied to ensure good acoustic coupling between the probe and the tissue.

by the normal arterial pressure variation provides sufficient tissue movement to enable quantification of strain.

The data were acquired with the US probe in a fixed position. We implemented an algorithm that uses cross-correlation and phase-sensitive processing for off-line strain calculation. The strain results were compared visually with the corresponding B-mode US images. We also recorded the ECG signal and compared it with the time development of the calculated strain.

## MATERIALS AND METHODS

### Data acquisition

The US data were acquired from two patients during brain surgery of, respectively, a metastasis and a low-grade

astrocytoma. The US RF data sets were acquired using a System FiVe scanner (GE Vingmed, Horten, Norway) and a 10-MHz flat linear-array probe. Figure 1 shows schematically the positioning of the probe during data acquisition. The data were acquired after craniotomy, but before opening the dura mater. The US probe, covered by a sterile condom, was gently positioned at the dura mater, using sterile gel to ensure a good acoustic coupling with minimal applied force. Thus, the probe positioning did not cause any significant deformation of the dura mater. When a satisfying cross-sectional image of the tumour was obtained, the probe was kept in a fixed position during data acquisition (3 to 4 s). The surgeon held the probe by hand, supported at the wrist to minimise artificial probe movements. The data were subsequently transferred to a computer for off-line processing.

The data-acquisition parameters are listed in Table 1.

### Processing of time shift and strain

The RF data processing was done in Matlab (The MathWorks Inc., Natick, MA). The processing scheme is presented in Fig. 2.

Tissue displacements are associated with changes in the US travel time between consecutive images. This change in travel time was found by the correlation technique for time shift estimation described by Simon et al. (1998). The motivation for using this method was that it is well suited for detecting tissue displacements with low velocities and small amplitudes, which can be expected in the brain. The time shift  $dt$  is found by inspection of the phase properties of the correlation function. The cross-correlation product of two identical analytical signals with zero time shift ( $dt = 0$ ) will have a zero-crossing of the phase at zero lag (i.e., at the maximum amplitude of the correlation function). A finite  $dt$  between the signals will

Table 1. Data acquisition parameters

	Metastasis	Low-grade astrocytoma
Ultrasound probe	FLA 10-MHz, 192 elements	FLA 10-MHz, 192 elements
Probe footprint (mm)	49 × 13	49 × 13
RF centre frequency (MHz)	8	8
Frame rate (fps)	46.2	37.1
RF, sampling frequency (MHz)	20	20
RF frames	79	79
B-mode start depth rel. probe (mm)	0.0	0.0
B-mode, height × width (mm)	35 × 32	40 × 32
RF start depth rel. probe (mm)	2.0	0.3
RF, height × width (mm)	30 × 32	38 × 32
RF samples	776	984
RF traces	174	174
RF bits (signed integer)	16	16
RF pixel size, vertical × horizontal (mm)	0.04 × 0.18	0.04 × 0.18
Estimated image thickness at focus (mm)	0.8	0.8
Simultaneous ECG	No	Yes

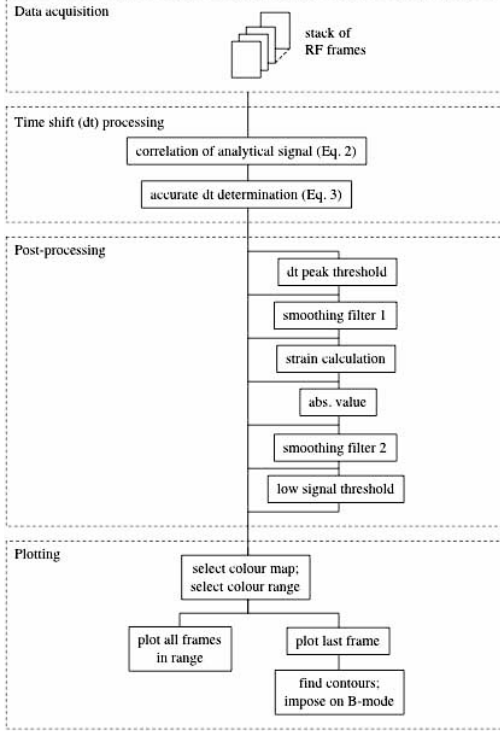


Fig. 2. Flow chart showing processing of time shift between consecutive RF frames, postprocessing options and plotting options. The postprocessing options may be applied independently of each other; however, the active options will occur in the displayed order.

cause the position of the correlation maximum to deviate from zero lag, shifting the zero-crossing of the correlation function's phase accordingly. The value of  $dt$ , therefore, corresponds to the shift of the phase's zero-crossing from zero lag. By assumption, the traces from subsequent US frames are nearly identical, justifying this procedure.

Equations (1) through (3) are taken from the article by Simon *et al.* (1998). First, we constructed an analytical signal  $\hat{r}$  from the RF traces:

$$\hat{r}(m, n, k) = r(m, n, k) - j \cdot [r(m, n, k) * h(m)] \quad (1)$$

where  $r(m, n, k)$  is the RF signal at sample  $m$  of trace  $n$  in frame  $k$ ,  $h(m)$  is an FIR Hilbert transformer, and the symbol  $*$  represents convolution along the “ $m$ ” direction. The complex cross-correlation at lag  $q$  between frames  $k$  and  $k + 1$  was then found from:

$$\hat{\gamma}(m, n; q, 0) = \sum_{m'=-M}^M \sum_{n'=-N}^N \hat{r}(m + m', n + n', k) \cdot \hat{r}^*(m + m' + q, n + n', k + 1). \quad (2)$$

Notice that the cross-correlation only works along the traces, with zero lag in the “ $n$ ” (lateral) direction. The superscript  $*$  denotes complex conjugation, and  $M$  and  $N$  define the evaluation window for  $\hat{\gamma}(m, n; q, 0)$ . In our processing, we used a window size of 1 trace and 17 samples (0.68 mm) for the metastasis and 1 trace and 11 samples (0.44 mm) for the low-grade astrocytoma. The correlation algorithm requires a certain window size to perform accurately. However, a long window will tend to reduce the correlation algorithm's ability to detect local displacements, and this may complicate the detection of local strain variations. The applied window sizes were selected based on visual inspection of the calculated strain.

At sufficiently high frame rates, the tissue movements between consecutive images will be smaller than one sample. We assumed that this was the case for our data (see the Discussion section for verification). As mentioned above, the time shift can be determined from the position of the correlation function's phase zero-crossing. We therefore found the time shift  $dt$  with sub-sample accuracy by interpolating phase values at lag  $-1$ ,  $0$  and  $+1$ :

$$dt(m, n) = \frac{-2 \cdot \angle \hat{\gamma}(m, n; 0, 0)}{\angle \hat{\gamma}(m, n; 1, 0) - \angle \hat{\gamma}(m, n; -1, 0)} T_{\text{samp}}, \quad (3)$$

where  $\angle \hat{\gamma}(m, n; q, 0)$  is the phase of the cross-correlation function at lag  $q$ , and  $T_{\text{samp}}$  is the sampling time along the beam. Note that eqn (3) has a sign change compared to the formula in Simon *et al.* (1998). This sign change is necessary to obtain negative time shifts for movements toward the probe, and agrees with the corresponding derivation found in Loupas *et al.* (1995).

Strain was found by differentiation along the axial direction:

$$\varepsilon(m, n) = \frac{dt(m + 1, n) - dt(m, n)}{T_{\text{samp}}}. \quad (4)$$

In our processing, we implemented the options to remove anomaly peaks in the calculated  $dt$  values and also the option to filter the  $dt$  values before strain estimation. Figure 2 shows the order of these processing options.

#### Postprocessing

The visual appearance of the results may depend significantly on factors like postprocessing filtering, thresholding and colour scale. We have therefore implemented several postprocessing options that may be used to enhance

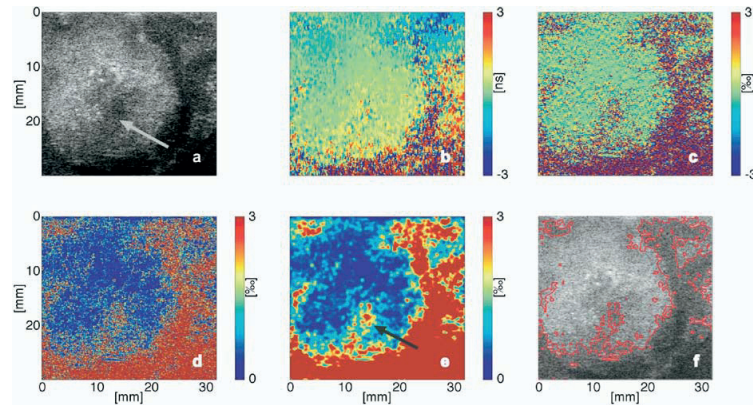


Fig. 3. US image of a metastasis tumour and display of results from successive processing steps. (a) RF data; (b) calculated time shift between the image in (a) and its predecessor; (c) axial component of the local strain; (d) magnitude of the axial strain component; (e) previous image smoothed by a Gaussian profile filter; and (f) contour at approximately 2% overlaid on the original RF data. The arrows in (a) and (e) indicate a region with lower echogenicity/higher strain than the surrounding tumour.

various image features. Figure 2 presents all options that were implemented for algorithm development and testing. Some of them proved to give significant image enhancement, as shown in the Results and Discussion sections.

### RESULTS

Figure 3 displays the results of various processing steps, on a selected frame of the US RF data acquired from the metastasis. This frame was selected in a period where the  $dt$  results indicated relatively low tissue motion. The original RF image is shown in Fig. 3a. This image is subject to the following processing: estimation of time shift, eqns (1) to (3), Fig. 3b; strain calculation by differentiation, eqn (4), Fig. 3c; and postprocessing by rectification, Fig. 3d; and smoothing, Fig. 3e. The 2-D smoothing filter had a window size of  $0.8 \times 0.8$  mm and a bell-shaped (Gaussian) profile in both directions, with width defined by the parameter  $\sigma = 0.2$  mm. Figure 3f shows the same RF data as in Fig. 3a, with an overlaid contour that was extracted from Fig. 3e at the yellow strain level (approx. 2%).

Figure 4 shows an US tissue image of the low-grade astrocytoma and the corresponding strain results. The strain values were rectified and smoothed equivalent to the data shown in Fig. 3e. However, a logarithmic colour scale was used for plotting because this gave slightly better overall contrast than a linear scale.

Figure 5a shows the calculated travel time differences, eqn (3), over an image sequence of 75 frames (approximately 2.1 s) from the low-grade astrocytoma. We observe that, in the central region of the images, the calculated time shifts vary in both magnitude and polarity throughout the

sequence. We also observe that, in all of the calculated results, there are some high-amplitude events in the lower left part of the image. This area is associated with very low signal amplitudes in the RF data (see Fig. 4a). In Fig. 5b, every fourth image of the calculated time shifts is plotted together with the ECG curve that was recorded simultaneously with the US data. The position along the ECG time axis is indicated by the mark below each image. The figure shows that the images with high tissue displacement values are repeating with a periodicity similar to the periodicity of the ECG signal.

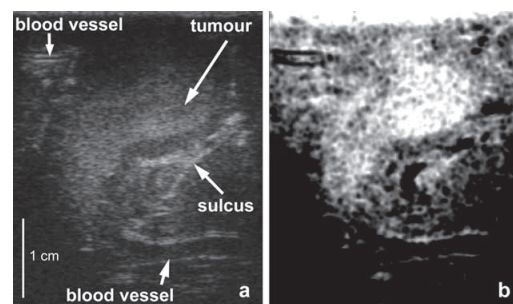


Fig. 4. (a) US B-mode image of a low-grade astrocytoma, cropped to the RF image size. The arrows indicate the tumour and various anatomical structures. (b) Strain (rectified and smoothed) derived from the RF data, plotted with a logarithmic grey-scale mapping (dark areas corresponding to high strain values). The image size is  $38 \times 32$  mm.

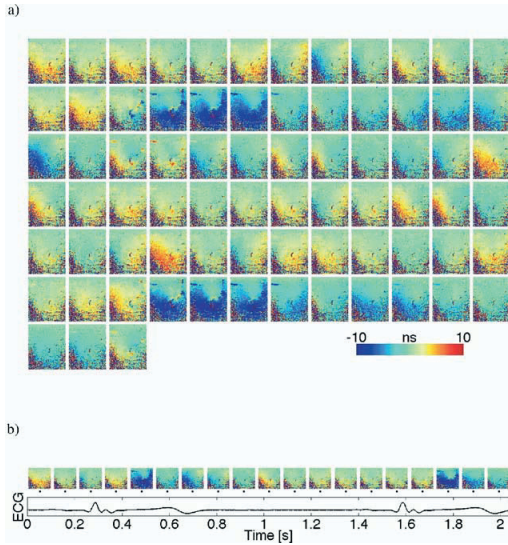


Fig. 5. (a) Changes in  $dt$  processed from a low-grade astrocytoma during approximately 1.5 cardiac cycles. The 75 frames captured at 37.1 fps are shown in sequence (left-right; then top-bottom). In (b), every fourth frame is positioned along the time axis for comparison to the simultaneously recorded ECG signal. The dimension of each image is the same as in Fig. 4 ( $38 \times 32$  mm).

## DISCUSSION

### Data acquisition

The US data were acquired with the hand-held US probe kept motionless on the dura mater. The validity of this procedure can be verified by the results shown in Fig. 5. In this figure, large time shifts (blue) follow shortly after the QRS complex of the ECG signal. Thus, the largest tissue velocities are associated with the systole. Similarly, the smaller time shifts (green and yellow) seem to correspond to the diastole. Furthermore, the periodicity observed in the calculated  $dt$  values seem to have a good correlation with the heart cycle found in the ECG curve. In both cases, the periodicity appears to be approximately 1.3 s. There is a certain lag between the QRS complex and the large strain magnitudes. One reason for this is that the QRS complex is a feature of the heart's electrical currents and does not coincide with the contraction of the left ventricle. Furthermore, there will be a delay of the pressure pulse between the heart and the brain.

A repeating pattern in the calculated time shifts was also observed for the metastasis, with a periodicity of about 1.0 s. However, for these measurements, the ECG signal was not recorded.

These observations strongly indicate that the time shifts are caused by internal pressure variation due to the

arterial blood flow. This implies that the brain does not need to be excited by any external force (e.g., by manual palpation or mechanical devices) to enable calculation of displacements and, thus, strain. A couple of measurements (not presented) were performed by gently and slowly pushing the brain surface with the US probe. Axial motion of the probe by only a few millimetres led to significant degradation of the results. Time shifts larger than a depth sample,  $T_{\text{samp}}$ , in magnitude will invalidate the assumptions for the processing, as discussed in the next section. This may be one of the main reasons for the poor results when applying external compression. Furthermore, the decorrelation effect due to lateral and out-of-plane motion is expected to increase with increased tissue compression (Varghese and Ophir 1997).

### Processing and visualisation

It should be emphasised that our choice of processing algorithm was guided by the expected dynamic characteristics of the tissue motion. In particular, the small amplitudes and relatively low velocities favoured the use of other techniques than those generally used in, for example, cardiac applications.

A basic assumption in the time-shift processing algorithm is that the maximum change in travel time  $dt_{\text{max}}$  between adjacent US frames is less than the depth sampling time  $T_{\text{samp}}$ . This corresponds to a maximum axial tissue velocity  $v_{\text{max}}$  defined by:

$$v_{\text{max}} = dz / T_{\text{fps}}, \quad (5)$$

where  $dz$  is the depth sampling interval, and  $T_{\text{fps}}$  is the time lapse between the US frames (inverse of frame rate). We used a frame rate of 37 frames/s or higher and a typical sampling interval of 0.04 mm. The maximum (axial) tissue velocity that can be handled by the algorithm is thus  $\approx 1.5$  mm/s. Reported values for pulsation-induced velocities in various parts of the brain parenchyma are 0.4 to 1.3 mm/s (Feinberg and Mark 1987), 1.0 to 1.5 mm/s (Greitz *et al.* 1992), 1.5 to 2.0 mm/s (Poncelet *et al.* 1992), less than 1 mm/s (Maier *et al.* 1994) and around 1 mm/s (Wirestam *et al.* 1997). All these groups applied noninvasive magnetic resonance (MR) imaging techniques.

Figure 5 shows that the magnitude of the tissue displacement varies considerably during a heart cycle. For the low-grade astrocytoma, we calculated the median time shift over an image area ( $50 \times 20$  pixels) selected in the normal brain tissue between the sulcus and the lower blood vessel (Fig. 4a). The most extreme value was  $-12$  ns, occurring during the systole (at about 0.5 and 1.8 s in Fig. 5b). This corresponds to a (axial) tissue velocity of  $-0.34$  mm/s, which is reasonable compared to the values cited above. In the diastolic period, the median time shift was up to  $+3$  ns, corresponding to  $0.09$  mm/s.

The strain algorithm implies that only one strain component (axial in the US image) is processed and visualised. However, the actual motion of the brain takes place in three dimensions. The lateral and out-of-plane motion components will, therefore, not be calculated. Furthermore, this motion causes a decorrelation between the axial traces that are compared in the cross-correlation, eqn (2). This decorrelation may degrade the time shift estimates. Kallel and Ophir (1997) have shown that the decorrelation effect decreases with increased sample volume dimensions. The sampling volume corresponding to one pixel is larger laterally (0.18 mm) and perpendicularly to the image plane (estimated to 0.8 mm at focus) than axially (0.04 mm). Assuming velocities of the magnitudes mentioned above ( $\sim 1$  mm/s  $\approx 0.025$  mm/frame) in the lateral and perpendicular directions, the tissue displacements during  $T_{\text{fps}}$  will be significantly smaller than the respective sample volume dimensions. We therefore expect the decorrelation effect due to such motion to be small.

The correlation result may also degrade because of reduced signal-to-noise ratio (SNR) of the input data. This may yield less accuracy in  $dt$  values within the algorithm's valid output range ( $\pm 1$  sample =  $\pm 50$  ns) and increased amounts of extreme values falling outside this range. To investigate the latter effect, the percentage of  $dt$  values with magnitude less than  $T_{\text{samp}}$  was calculated in various parts of the images, over areas of size  $50 \times 20$  pixels. For the low-grade astrocytoma, we selected areas in the bottom left corner, inside the assumed tumour lesion and between the sulcus and the lower-situated blood vessel (Fig. 4a), and found that typically about 60%, 100% and 100%, respectively, of the calculated  $dt$  values were less than 50 ns. This indicates that the calculated  $dt$  results in the lower left corner of the image may be severely affected by the low signal amplitudes (low SNR) seen in this part of the input data. For the metastasis, we selected similar areas within and below the suspected tumour lesion (Fig. 3), in which the corresponding percentages were calculated to be about 100% and 93%, respectively. These results indicate that low signal amplitude may only be a minor problem in the metastasis case. Because the acquisition gain is, in general, adjusted to provide B-mode images with visible structures in both the lesion and the normal tissue, the signal level should normally be sufficient for correlation analysis.

For the present acquisition method, the results may be vulnerable to error sources introducing artificial relative motion, such as unintentional hand or probe movements. However, for the two cases investigated, we did not find evidence of significant influence from such error sources.

We evaluated the postprocessing options shown in Fig. 2 with respect to improved visualisation of the strain differences between normal brain and tumour. Of these options, we found that rectification and subsequent smoothing (filter 2) of the calculated strain improved the

visualisation of the tumour margins, and also enabled contour tracking (Fig. 3). We expect the strain magnitude in tumour to be lower than in the surrounding normal brain, based on reported results from studies on other organs (Emelianov et al. 1998; Hiltawsky et al. 2001; Souchon et al. 2003). The rectification will not alter the magnitudes of the calculated strain; thus, local differences in strain level are preserved. The smoothing filter might reduce the resolution of the strain image. We can assume that the resolution before filtering is approximately half a wavelength ( $\lambda/2 \approx 0.1$  mm) axially and equal to the beam width ( $\sim 0.2$  mm) laterally, neglecting the effect of the correlation window size. The width of the bell-shaped filter is about  $2 \cdot \sigma = 0.4$  mm in both directions. Considering the filtering process as a convolution, we obtain an estimated resolution in the elastograms of approximately  $0.41 \times 0.45$  mm.

Other tumours may require other processing options and parameter settings than those applied for these two cases.

We have also addressed the effect of averaging the strain results over several frames. Averaging could reduce scattered noise seen in some of the calculated elastograms, but the differences from a single image were generally not substantial. However, these matters should be further investigated using data from a larger number of clinical cases.

#### Clinical considerations

The results such as Figs. 3e and 4b indicate that the implemented processing method is able to detect spatial strain variations in the brain. The strain levels in the assumed tumour lesions are lower than those found in the surrounding normal tissue.

The strain image of the metastasis gives a similar outline of the lesion as in the US RF data (Fig. 3f). Furthermore, in the RF data (Fig. 3a), we observe a region within the tumour (indicated by arrow) with reduced echogenicity compared with the rest of the lesion. In the strain image (Fig. 3e), this region is associated with higher strain values, thus indicating softer tissue.

The low-grade astrocytoma is not as well delineated in the US B-mode image (Fig. 4a) as is the metastasis. However, this is mainly related to the difference in pathology between the tumours. Glial tumours, such as low-grade astrocytomas, are known to be diffuse infiltrating tumours, whereas metastases are usually not. In the strain image of the low-grade astrocytoma (Fig. 4b), anatomical structures such as the sulcus and blood vessels can be recognised. The imaging of the lesion is quite similar in both of the imaging modalities. However, in the strain image, the tumour region may be interpreted as extending slightly more to the surface (upper image edge) than is apparent from the B-mode image.

It should be noted that our interpretations are based

on the US images only, and are not confirmed by histopathological data.

### CONCLUSIONS

We have demonstrated strain processing and visualisation of brain tumours based on intraoperative US data acquired before opening the dura mater. The investigated cases were a low-grade astrocytoma and a metastasis. The data were collected with a hand-held probe and processed off-line with a cross-correlation technique.

The results show that the pulsation of the brain caused by the normal systole/diastole arterial pressure variation is sufficient for reliable strain calculation. This means that the surgeon only needs to hold the probe in a fixed position for a few seconds and the data acquisition thus implies no changes to equipment or procedures normally applied during US-guided neurosurgery.

In the strain images, the brain tumours were associated with lower strain magnitude than the surrounding normal tissue. The strain imaging of the tumours showed overall good qualitative correspondence with the B-mode images; however, we also noticed smaller areas where the strain data might indicate tumour, whereas the conventional US did not. For the two cases investigated, rectification and subsequent smoothing of the strain images enhanced the visualisation of the tumour borders.

We conclude that vascular pulsation is sufficient for generation of elastograms of the brain and that this imaging modality can be used for tumour detection. However, further work is needed to evaluate the possible clinical benefits of this technique.

*Acknowledgements*—This work was financed by the Norwegian Ministry of Health and Social Affairs through the National Centre of Competence-3D Ultrasound in Surgery and by SINTEF Health Research.

### REFERENCES

- D'hooge J, Heimdal A, Jamal F, et al. Regional strain and strain rate measurements by cardiac ultrasound: Principles, implementation and limitations. *Eur J Echocardiogr* 2000;1:154–170.
- D'hooge J, Bijnens B, Thoen J, et al. Echocardiographic strain and strain-rate imaging: A new tool to study regional myocardial function. *IEEE Trans Med Imaging* 2002;21:1022–1030.
- Emelianov SY, Rubin JN, Lubinski MA, Skovoroda AR, O'Donnell M. Elasticity imaging of the liver: Is a hemangioma hard or soft? *IEEE Ultrason Symp* 1998;2:1749–1752.
- Feinberg DA, Mark AS. Human brain motion and cerebrospinal fluid circulation demonstrated with MR velocity imaging. *Radiology* 1987;163:793–799.
- Gao L, Parker KJ, Lerner RM, Levinson SF. Imaging of the elastic properties of tissue—A review. *Ultrasound Med Biol* 1996;22:959–977.
- Garra BS, Cespedes EI, Ophir J, et al. Elastography of breast lesions: Initial clinical results. *Radiology* 1997;202:79–86.
- Greitz D, Wirestam R, Franck A, et al. Pulsatile brain movement and associated hydrodynamics studied by magnetic resonance phase imaging. *Neuroradiology* 1992;34:370–380.
- Hall TJ, Zhu Y, Spalding CS. In vivo real-time freehand palpation imaging. *Ultrasound Med Biol* 2003;29:427–435.
- Hammoud MA, Ligon BL, ElSouki R, et al. Use of intraoperative ultrasound for localizing tumors and determining the extent of resection: A comparative study with magnetic resonance imaging. *J Neurosurg* 1996;84:737–741.
- Heimdal A, Støylen A, Torp H, Skjerpe T. Real-time strain rate imaging of the left ventricle by ultrasound. *J Am Soc Echocardiogr* 1998;11:1013–1019.
- Hiltawsky KM, Krüger M, Starke C, et al. Freehand ultrasound elastography of breast lesions: Clinical results. *Ultrasound Med Biol* 2001;27:1461–1469.
- Kallel F, Ophir J. Three-dimensional tissue motion and its effect on image noise in elastography. *IEEE Trans Ultrason Ferroelec Freq Control* 1997;44:1286–1296.
- Kiraly P, Kapusta L, Thijssen JM, Daniels O. Left ventricular function in congenital valvar aortic stenosis assessed by ultrasound tissue-velocity and strain-rate techniques. *Ultrasound Med Biol* 2003;29:615–620.
- Konofagou EE, D'hooge J, Ophir J. Myocardial elastography—A feasibility study in vivo. *Ultrasound Med Biol* 2002;28:475–482.
- LeRoux PD, Berger MS, Ojemann GA, Wang K, Mack LA. Correlation of intraoperative ultrasound tumour volumes and margins with preoperative computerized tomography scans. An intraoperative method to enhance tumour resection. *J Neurosurg* 1989;71:691–698.
- Loupas T, Powers JT, Gill RW. An axial velocity estimator for ultrasound blood flow imaging, based on a full evaluation of the Doppler equation by means of a two-dimensional autocorrelation approach. *IEEE Trans Ultrason Ferroelec Freq Control* 1995;42:672–688.
- Maier SE, Hardy CJ, Jolesz FA. Brain and cerebrospinal fluid motion: Real-time quantification with M-mode MR imaging. *Radiology* 1994;193:477–483.
- Ophir J, Alam SK, Garra B, et al. Elastography: Ultrasonic estimation and imaging of the elastic properties of tissues. *Proc Instn Mech Eng* 1999;213:203–233.
- Ophir J, Garra B, Kallel F, et al. Elastographic imaging. *Ultrasound Med Biol* 2000;26(Suppl. 1):S23–S29.
- Ophir J, Kallel F, Varghese T, et al. Elastography. *C R Acad Sci Paris IV-Phys* 2001;2:1193–1212.
- Pellerin D, Sharma R, Elliott P, Veyrat C. Tissue Doppler, strain, and strain rate echocardiography for the assessment of left and right systolic ventricular function. *Heart* 2003;89(Suppl. 3):9–17.
- Poncelet BP, Wedeen VJ, Weisskopf RM, Cohen MS. Brain parenchyma motion: Measurement with cine echo-planar MR imaging. *Neuroradiology* 1992;185:645–651.
- Simon C, VanBaren P, Ebbini ES. Two-dimensional temperature estimation using diagnostic ultrasound. *IEEE Trans Ultrason Ferroelec Freq Control* 1998;45:1088–1099.
- Souchon R, Rouvière O, Gelet A, et al. Visualisation of HIFU lesions using elastography of the human prostate in vivo: Preliminary results. *Ultrasound Med Biol* 2003;29:1007–1015.
- Unsgaard G, Gronningsaeter A, Ommedal S, Nagelhus Hernes TA. Brain operations guided by real-time two-dimensional ultrasound: New possibilities as a result of improved image quality. *Neurosurgery* 2002a;51:402–412.
- Unsgaard G, Ommedal S, Muller T, Gronningsaeter A, Nagelhus Hernes TA. Neuronavigation by intraoperative three-dimensional ultrasound: Initial experience during brain tumor resection. *Neurosurgery* 2002b;50:804–812.
- Varghese T, Ophir J. A theoretical framework for performance characterization of elastography: The strain filter. *IEEE Trans Ultrason Ferroelec Freq Control* 1997;44:164–172.
- Varghese T, Zagzebski JA, Rahko P, Breburda CS. Ultrasonic imaging of myocardial strain using cardiac elastography. *Ultrason Imaging* 2003;25:1–16.
- Wirestam R, Salford LG, Thomsen C, et al. Quantification of low-velocity motion using a navigator-echo supported MR velocity-mapping technique: Application to intracranial dynamics in volunteers and patients with brain tumours. *Magn Reson Imaging* 1997;15:1–11.
- Woydt M, Horowski A, Krauss J. Three-dimensional intraoperative ultrasound of vascular malformations and supratentorial tumors. *J Neuroimaging* 2002;12:28–34.



# Paper II





● *Original Contribution*

## TISSUE MOTION AND STRAIN IN THE HUMAN BRAIN ASSESSED BY INTRAOPERATIVE ULTRASOUND IN GLIOMA PATIENTS

TORMOD SELBEKK,<sup>\*†‡</sup> REIDAR BREKKEN,<sup>\*†‡</sup> OLE SOLHEIM,<sup>\*†§</sup> STIAN LYDERSEN,<sup>†</sup>  
TORIL A. N. HERNES,<sup>\*†‡</sup> and GEIRMUND UNSGAARD<sup>\*†§</sup>

<sup>\*</sup>National Centre for 3D Ultrasound in Surgery, St. Olavs Hospital, Trondheim, Norway; <sup>†</sup>SINTEF, Trondheim, Norway; <sup>‡</sup>Norwegian University of Science and Technology, Trondheim, Norway; and <sup>§</sup>St. Olav University Hospital, Trondheim, Norway

(Received 19 August 2008; revised 24 March 2009; in final form 11 May 2009)

**Abstract**—The objective of the study was to investigate tissue motion and strain imposed by cardiovascular pulsation in pathologic and normal brain parenchyma, as quantified from *in vivo* ultrasound data. Ultrasound acquired during surgery of 16 patients with glial tumors was retrospectively processed and analyzed. The tissue velocity was quantified at depths of 1 cm, 2 cm and 3 cm from brain cortex to investigate spatial dependency with depth. Comparison of strain and velocity in tumor and adjacent normal parenchyma was performed by selecting two regions-of-interest in the hyperechoic tumor and two regions in the low-echogenic areas interpreted as mainly normal tissue with some degree of tumor cell infiltration. The absolute maximum tissue velocity is seen to increase with increasing depths in 14 of 16 cases (87.5%). The maximum tissue velocities in the four regions close to the ultrasound visible tumor border are not statistically different ( $p = 0.163$  to  $p = 0.975$ ). The strain magnitudes are significantly higher in the regions with expected normal brain parenchyma than in regions with expected glial tumor tissue, both for the two regions being closest to the tumor border ( $p = 0.0004$ ) and for the two regions further away from the tumor border ( $p = 0.0009$ ). We conclude that the velocity of the brain parenchyma imposed by arterial pulsation during a cardiac cycle is generally increasing with increasing depth from cortex. The maximum velocity appears to be similar in regions with expected normal brain and tumor tissue, thus, does not seem to be affected by pathology. Strain magnitude is, however, a suitable parameter for discrimination of glial tumor and normal brain parenchyma. (E-mail: Tormod.Selbekk@sintef.no) © 2010 World Federation for Ultrasound in Medicine & Biology.

**Key Words:** Ultrasound, Strain, Elasticity, Brain, Tumor, Neurosurgery.

### INTRODUCTION AND LITERATURE

Ultrasound (US) is an established image modality in brain surgery, and may be used for guidance and resection control in surgery of neurologic tumors, (Kolstad et al. 2006; Sun and Zhao 2007; Unsgaard et al. 2006). Differentiation between normal and tumor tissue using conventional US imaging may be challenging in the presence of gliosis or edema (Hammoud et al. 1996). Glial tumors are diffusely infiltrating and it is known that tumor cells will be present outside the US visible tumor border (Kelly et al. 1987; Unsgaard et al. 2005). The surgeon frequently aims to perform a gross total tumor resection, however, fear of new neurologic deficits will often reduce resection grades when tumor borders are not clearly visible. It

would, therefore, be desirable to have a peroperative diagnostic imaging modality that in a quantifiable manner could distinguish between solid tumor masses, tumor infiltrated tissue, normal tissue with gliosis or edema and normal brain parenchyma.

MRI has previously been used to investigate the tissue velocity in brain parenchyma (Greitz et al. 1992; Maier et al. 1994; Poncelet et al. 1992). The major part of these investigations has been conducted in healthy subjects. However, Wirestam et al. (1997) used MRI to estimate tissue velocity in a meningioma and two astrocytomas and found the velocity to be low compared with normal tissue during the entire cardiac cycle. If the tissue velocity is different in normal brain and tumor this could potentially be used to discriminate the tissues.

Strain quantifies the relative deformation in an object that is exposed to stress. Stiff tissue will have lower strain than soft tissue when exposed to the same stress. Tumors are often stiffer than normal parenchyma and strain may

Address correspondence to: Tormod Selbekk, M.Sc., SINTEF Health Research, NO-7465 Trondheim, Norway. E-mail: Tormod.Selbekk@sintef.no

represent a suitable parameter for differentiation of tumor and normal tissue. The conventional B-mode US images are resulting from differences in acoustic impedance whereas the strain imaging is related to the deformation of tissue. US strain imaging may, therefore, provide complementary information to B-mode.

In a clinical context, US strain imaging is reported used in tumor identification and for cardiac or vascular applications (Brekken *et al.* 2006; de Korte and van der Steen 2002; Heimdal *et al.* 1998; Hiltawsky *et al.* 2001). US strain imaging may provide information complementary to B-mode about tissue pathology, however, the qualitative interpretation of the strain images are still prone to interobserver variability (Burnside *et al.* 2007; Regner *et al.* 2006). The use of US strain imaging in neurosurgery was first reported in a paper describing a method for strain processing of intraoperative US data (Selbekk *et al.* 2005). Strain imaging was successfully demonstrated in two cases of brain tumors, using a processing technique that could calculate small tissue deformations in the brain imposed by the arterial pulsation. Later articles by Scholz *et al.* (2005, 2007) described a technique called vibrography in which the brain cortex was excited by a vibrating device and demonstrated its ability for imaging of brain tumors. These articles suggest that US imaging of tissue stiffness might be beneficial for diagnostics in brain tumor surgery. However, quantitative comparison of strain and tissue velocity between normal tissue and pathologic tissue has not been reported.

The objective of the present study was to investigate tissue velocity and strain in brain parenchyma imposed by the cardiovascular pulsation, using a previously described method for processing of intraoperative US data. First, we investigated whether or not the velocity of the brain parenchyma varies with depth. Second, we assessed if velocity or strain is able to discriminate between regions with assumed tumor tissue and tumor-adjacent regions with presumably mainly normal brain tissue.

## MATERIALS AND METHODS

### Patients

US imaging is routinely used during brain tumor surgery at St. Olavs University Hospital. We have analyzed US radio-frequency (RF) data acquired during surgery of 16 patients with glial tumors, in the period from January 2004 till March 2007 at St. Olav Hospital (Trondheim, Norway). The Regional Research Ethics Committee of Central Norway approved the retrospective study. The committee waived the use of written informed consent.

The US RF-data was acquired after craniotomy but on intact dura using a conventional scanner (System FiVe, GE Vingmed, Horten, Norway), with the hand-held

draped US probe (10 MHz flat linear array) kept as motionless as possible during acquisition (Fig. 1). The RF-sequences covered at least one cardiac cycle in time for all 16 cases; Electrocardiography (ECG) data was recorded in 12 cases. The clinical cases are summarized in Table 1.

### Signal processing

The US data was transferred to a computer for offline processing by methods implemented in MatLab (The MathWorks Inc., Natick, MA, USA). The first step in the signal processing was determining the tissue displacements  $ds$  between consecutive US frames. The velocity of the parenchyma was then estimated by using the frame rate period,  $T_{FPS}$  in the relation:

$$v = \frac{ds}{T_{FPS}} \quad (1)$$

Strain was found by differentiation of the tissue displacement along the axial direction. The processing method is described in detail in Selbekk *et al.* (2005).



Fig. 1. Conceptual display showing a typical orientation of the flat linear probe on a coronal MR T1-weighted image slice. The major arteries supplying the brain are located on the skull base below the brain hemispheres. The paired carotid artery is segmented from MR-angio data and is shown in red. The basilar artery and vertebral arteries are volume rendered in white.

Table 1. The cases investigated, with histopathology and WHO-grade and the maximum cross-section of the tumor

Operation No.	Histopathology, WHO-grade	tumor diameter $\varnothing_{\max}$ [mm]
1	Astrocytoma, grade II	31
2	Astrocytoma, grade IV	42
3	Astrocytoma, grade I	53
4	Astrocytoma, grade IV	45
5	Astrocytoma, grade IV	35
6	Astrocytoma, grade II	7
7	Astrocytoma, grade IV	60
8	Astrocytoma, grade II	50
9	Astrocytoma, grade II	50
10	Astrocytoma, grade IV	30
11	Astrocytoma, grade IV	37
12	Astrocytoma, grade III	24
13	Astrocytoma, grade II	65
14	Oligodendroglioma, grade II	66
15	Astrocytoma, grade IV	22
16	Astrocytoma, grade III	43

#### Tissue velocity vs. depth

The median tissue velocity was calculated at three different depths of 1 cm, 2 cm and 3 cm using a region size of  $7 \times 15$  beams/samples. (Fig. 2a). The selected regions were usually localized close to the lateral midpoint of the US image, irrespective of image findings (tumor/normal).

Next, the maximum velocity magnitude following the systolic heart cycle (as seen in the ECG curve) was noted, as well as the time range  $T_{RV}$  between the occurrence of the R-wave in the ECG curve and the occurrence of the maximum magnitude in the velocity curves. The

maximum velocity in a time interval of minimum one second was used in cases with missing ECG.

#### Tissue velocity and strain in regions with expected tumor and expected normal tissue

To analyze the tissue velocity and strain in tumor and normal brain we selected four regions-of-interest (ROIs) in the US RF-data; two in expected normal tissue and two in expected tumor tissue. The calculation areas ( $7 \times 21$  beams/samples) were located at equal depths, symmetric about the tumor border seen in the US image (Fig. 2b). The ROIs outside the solid tumor mass (in expected normal tissue) are annotated N1 and N2, while the ROIs in the tumor mass are annotated T1 and T2. The median tissue velocity calculated for the ROIs were plotted vs. time and the absolute maximum velocity during a heart cycle was observed.

The strain magnitude vs. time was quantified in the same ROIs (size and location) as used when calculating tissue velocity. The average strain magnitude for the whole time sequence covering a single cardiac cycle (or minimum 1 s if no ECG data were recorded) was calculated for each ROI and compared statistically.

#### Statistical methods

Maximum velocity and average strain magnitude between the four regions (N1, N2, T1, T2) were compared using the nonparametric paired Wilcoxon signed rank test, as data was not normally distributed. The receiver operating characteristic (ROC) curve for the strain magnitudes

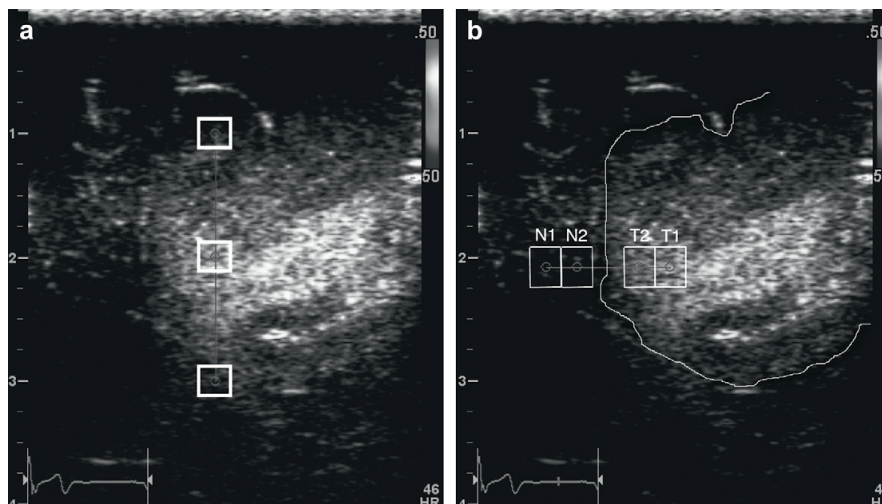


Fig. 2. Ultrasound B-mode image of a patient with low grade glioma showing the calculation windows at 1 cm, 2 cm and 3 cm depth for estimation of tissue velocity (a). Corresponding example showing the selected region-of-interests for analysing tissue velocity and strain in presumably normal brain (N1, N2) and presumably pathologic (hyperechoic) tissue (T2, T1) (b). The interpretation of the tumor border is overlaid as a contour.

was calculated using the ultrasound B-mode images as the gold standard, *i.e.*, assuming isoechoic areas (N1 + N2) to be normal tissue and hyperechoic regions (T1 + T2) to represent tumor tissue.

Normalized strain magnitude was calculated in each of the four regions by normalizing the data for each patient with respect to the value in region N1. These normalized values were normally distributed (approximately), as verified by visual inspection of Q-Q plots. The 95% confidence interval for the normalized strain magnitudes was, therefore, calculated assuming the normal distribution. Analyses were performed in SPSS 16 for Mac.

## RESULTS

The processing of the images was successfully performed in all cases, and strain magnitude images of the tumors could be obtained (Fig. 3).

### *Tissue velocity vs. depth*

The median tissue velocity was calculated for ROIs at depths of 1 cm, 2 cm and 3 cm (Fig. 2a) and displayed along with the ECG data if present. For each depth the maximum velocity magnitude ( $|V_{max}|$ ) was found, as well as the time period ( $T_{RV}$ ) between the R-wave in the ECG curve and the maximum peak velocity (Fig. 4). The RF-data acquisition window covered all three depths in 8 of the 16 patients only, and the ECG signal was acquired in 12 patients. The median velocity for the increasing depths was 0.48 mm/s, 0.76 mm/s and 1.05 mm/s, respectively, while the median time from the R-wave of the ECG-curve to the maximum tissue velocity was 0.19 s (1 cm), 0.17 s (2 cm) and 0.16 s (3 cm) (Table 2). The maximum tissue velocity increases with depth in 14 of 16 cases (87.5%), decreases with depth in one

case (6.25%) and is the largest at 2 cm depth in one case (6.25%) (Fig. 5).

### *Tissue velocity and strain in regions with expected tumor and expected normal tissue*

The tissue movements and strain was investigated in pairs of two ROIs, found at similar depths inside and outside the tumor borders as seen in the ultrasound image (Fig. 6). The depths of the ROIs for these analyses vary from patient to patient. The velocities are not directly comparable between cases, as we have found that tissue velocity can vary with depth. However, the median tissue velocity for the measurements in regions N1 and N2 was 0.82 mm/s ( $N = 30$ ), with range [0.15, 2.89] (Table 3). For the measurements in regions T1 and T2 the median velocity was 0.75 mm/s ( $N = 32$ ) with range [0.20, 2.49].

Comparing the velocities of the four investigated areas (T1, T2, N1, N2) using the paired nonparametric Wilcoxon signed rank test we find that the velocities are not significantly different ( $p = 0.163$  to  $p = 0.975$ ).

The strain magnitude values range from 1.46% to 24.04% for the ROIs in expected normal tissue (N1, N2) with a median of 9.52% ( $N = 30$ ) (Table 4). For the ROIs in expected tumor tissue (T1, T2) the values range from 0.60% to 9.64%, with a median value of 1.30% ( $N = 32$ ).

Differences in strain magnitude were statistically significant between regions N1 and N2 ( $p = 0.0157$ ), regions T1 and T2 ( $p = 0.0013$ ), regions N2 and T2 ( $p = 0.0004$ ), and regions N1 and T1 ( $p = 0.0009$ ).

The relative differences between the regions were evaluated by calculating the mean and the 95% confidence interval of the normalized strain magnitude levels (Fig. 7). The mean normalized strain level in T2 and T1 are approximately 28% and 22% respectively of the strain level

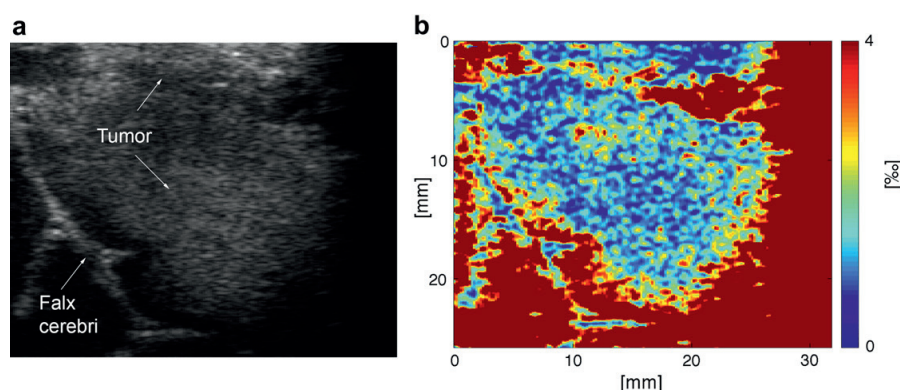


Fig. 3. Intraoperative ultrasound image (RF) of a glioblastoma (a) and the corresponding strain magnitude image (b).

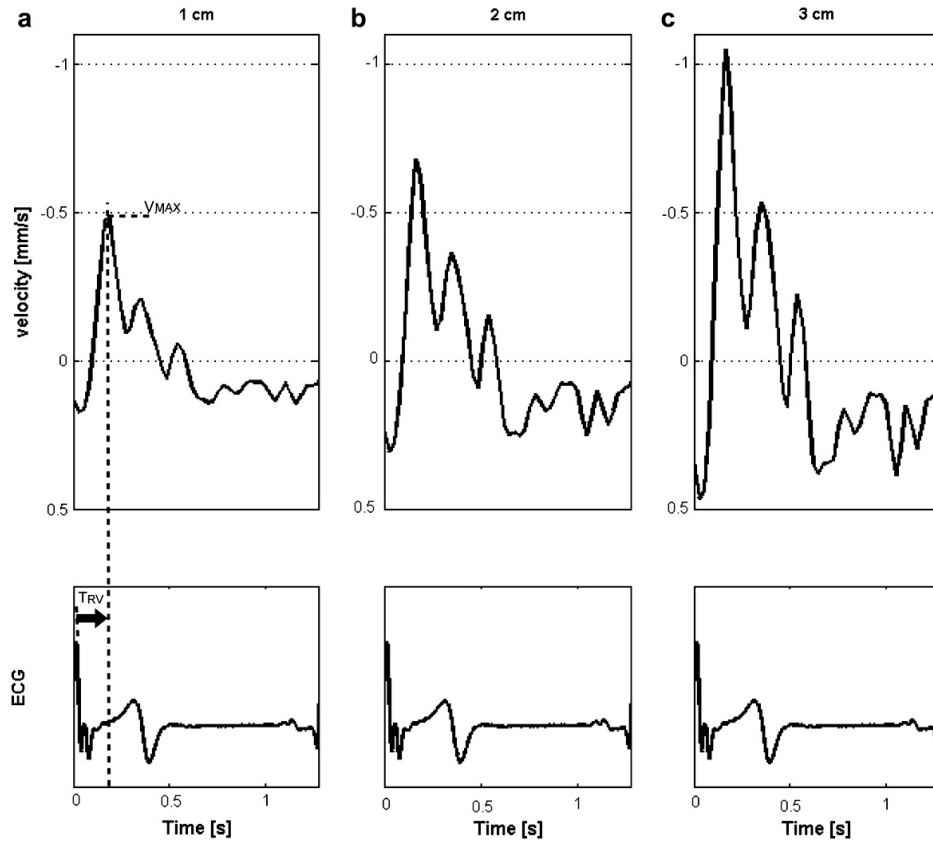


Fig. 4. Calculated tissue velocity vs. time during a cardiac cycle (ECG curve in bottom row) for ROI at 1 cm (a), 2 cm (b) and 3 cm (c) depths in a patient with low grade glioma (see Fig. 2a). The determination of the time period  $T_{RV}$  and velocity  $V_{max}$  is indicated in a.

observed in region N1. The mean normalized strain level in region N2 is approximately 83% of the normalized strain level in N1.

The ROC curve for the strain magnitudes was calculated, and the area under the ROC-curve was 0.912 (Fig. 8).

## DISCUSSION AND SUMMARY

### *Tissue velocity vs. depth*

Analyses of the velocity at depths of 1 cm, 2 cm and 3 cm show that the velocity increases with depth in 14 of the 16 patients. The time interval  $T_{RV}$  between the R-wave to the maximum peak velocity decreases with depth. The pulsations of the major arteries (carotid arteries, basilar artery) located at the base below the brain hemispheres (Fig. 1) is likely to generate an excitation of the adjacent brain parenchyma, which will propagate toward the brain surface with a certain time delay and decay in velocity

amplitude. Although the limited number of measurements should be kept in mind (especially for the time delay measurements), the results may imply that the major arteries supplying the brain significantly influence the motion of the brain parenchyma.

The regions used for analyzing velocity vs. depth covered both hyperechoic tumor regions and isoechoic regions with presumably normal tissue. The possible effect of tissue pathology is not accounted for in these analyses, which could potentially have influenced the estimates. However, our later analyses of tissue velocity in both hyperechoic and isoechoic regions at equal depths did not establish any significant velocity differences. This suggests that the velocity of the brain parenchyma increases with increasing depth, irrespective of echogenicity and thereby pathology.

Tissue motion in brain has also been previously investigated using noninvasive imaging methods. Greitz et al. (1992) investigated brain movements during a cardiac

Table 2. Velocity magnitude  $|V_{\max}|$  for ROI at depths of 1 cm, 2 cm, and 3 cm from the probe surface, with time  $T_{RV}$  between maximum in ECG-curve (R-wave) and absolute maximum in the velocity curves

Operation	Depth 1 cm		Depth 2 cm		Depth 3 cm	
	$ V_{\max} $ [mm/s]	$T_{RV}$ [s]	$ V_{\max} $ [mm/s]	$T_{RV}$ [s]	$ V_{\max} $ [mm/s]	$T_{RV}$ [s]
1	0.48	0.17	0.68	0.15	1.05	0.15
2	0.46	-	0.60	-	0.76	-
3	0.22	0.22	0.73	0.19	1.15	0.19
4	0.10	-	0.29	-	0.62	-
5	0.28	0.21	0.60	0.16	0.66	0.16
6	-	-	1.17	0.20	1.44	0.20
7	0.27	0.30	0.68	0.30	-	-
8	0.38	0.26	0.67	0.28	-	-
9	0.72	0.21	1.01	0.21	-	-
10	0.56	0.17	2.51	0.17	-	-
11	0.48	-	0.60	-	-	-
12	1.98	0.14	2.51	0.11	2.07	0.11
13	0.52	0.11	0.79	0.13	-	-
14	1.49	0.11	1.32	0.11	0.69	0.11
15	1.50	0.14	1.86	0.12	-	-
16	0.27	0.36	0.81	0.35	1.09	0.36
<b>Median</b>	0.48	0.19	0.76	0.17	1.05	0.16

A dash indicates that no RF-data was recorded at this depth, or no ECG recorded.

cycle using MR phase imaging. The arterial expansion was found to cause the major part of the measured brain movements. The caudal and anterior motions were found to increase toward the foramen magnum and toward the midline. Wirestam *et al.* (1997) used MR technology to quantify the intracranial tissue motion in volunteers and in three patients with brain tumors. The maximal caudal velocities were observed in the central parts of the brain, and ranged from 0.5 mm/s–1.5 mm/s with a mean of 0.94 mm/s. Another finding of this study was that the tissue velocity within the tumor mass was low during the entire cardiac cycle. Other reported values for pulsation-induced velocities found by MR analysis of various parts of the brain parenchyma are 0.4–1.3 mm/s (Feinberg and Mark 1987), 1.5–2.0 mm/s (Poncelet *et al.* 1992) and less than 1 mm/s (Maier *et al.* 1994).

Although our data are acquired after craniotomy and the displacement is calculated only in the axial direction of

the ultrasound image, we find that our calculated tissue velocities are comparable to those previously reported.

#### *Tissue velocity and strain in regions with expected tumor and expected normal tissue*

In the calculated velocity vs. time curves a repeating pattern was observed for the cardiac cycles and a peak velocity could be found (Fig. 6). The strain magnitude curves did not have the same temporal variation, but seem to have some deviation around a given strain level.

Assuming that the hyperechoic areas in the ultrasound image represent tumor tissue and the isoechoic areas are mainly associated with normal tissue, our results show that the maximum tissue velocity observed during a cardiac cycle is not affected by pathology.

The strain magnitudes averaged over a cardiac cycle in time are substantially different in the hyperechoic tumor tissue and in isoechoic regions with presumably normal tissue. However, the strain magnitude levels in the two hyperechoic tumor regions are also significantly different, which is also the case for the two regions with expected normal tissue.

The differences in strain magnitude observed in the regions with similar echogenicity might be explained by the diffuse infiltrating nature of glial tumors, but the presence of edema or gliosis could influence the strain magnitude. The tumor cell density is higher in the central parts of the tumor than in the periphery. In a study comparing the histopathology and US image findings for biopsies sampled at the tumor border zone seen in the US image, the presence of tumor cells was found beyond the hyperechoic area (Unsgaard *et al.* 2005). In our analysis, we should expect the highest density of neoplastic cells in the region located most centrally in the tumor mass (ROI T1). Assuming that the strain magnitude is related to the density of neoplastic cells, we should expect the strain magnitude levels to be lowest in the T1 region and highest in N1. This can be evaluated in our measurements by normalizing the strain levels with respect to N1 and calculate the average for all cases in a given ROI and its 95% confidence interval (Fig. 7).

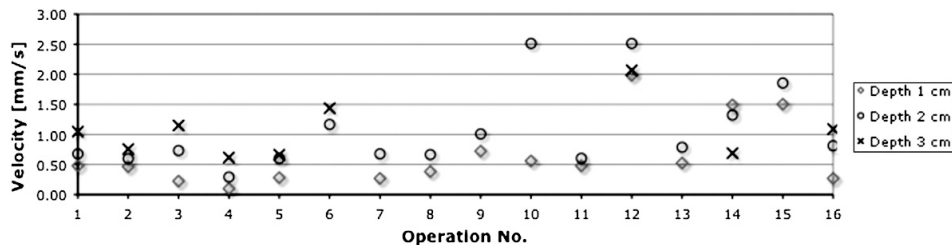


Fig. 5. The absolute maximum tissue velocity for ROIs at 1 cm, 2 cm and 3 cm depth for the investigated cases. The RF data covered all three depths in 8 of the 16 cases only.

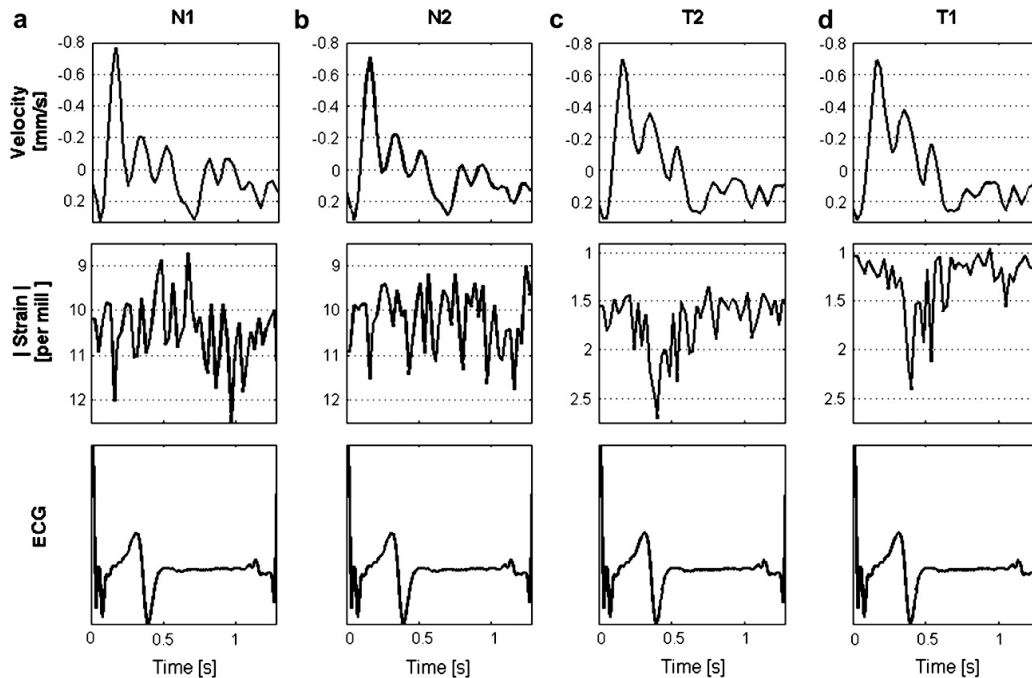


Fig. 6. Calculated tissue velocity vs. time (top row), strain magnitudes vs. time (middle row) and the ECG-signal (bottom row) for regions N1 (column a), N2 (column b), T2 (column c), T1 (column d) for a patient with low grade glioma (see Fig. 2b).

The average normalized strain magnitude in region N2 (closer to the border) is slightly lower than in N1, which may be explained by a higher degree of tumor cell infiltration. The average normalized strain level in region T2 is much lower than in N2 but slightly higher than in T1 that is located more centrally in the tumor. It seems that the normalized strain values vary with the distance to the ultrasound visible tumor border. It would have been interesting to analyze regions even further away from the border, in the presumably normal tissue, to see if the strain magnitudes would continue to increase or stabilize at a certain level. However, in the initial data acquisition, the emphasis was on the close proximity of the tumor border and the US RF window was selected accordingly.

The variation in normalized strain levels could be related to the tumor cell density but other factors as *e.g.*, edema formation may also influence the strain magnitudes. Edema formation is not to be expected in patients with low-grade glioma (WHO grade I-II). The strain magnitude levels between the 4 ROIs for this patient group still seem to adhere to the same variations as observed for the other patients (Table 4). It is, therefore, a sound hypothesis that the observed variation in normalized strain magnitude between the ROIs is proportional to the degree of tumor cell infiltration. However, this

hypothesis needs to be investigated in designated studies comparing strain magnitudes and histopathology.

ROC curves are often used to assess the diagnostic accuracy of a specific test, often using histopathology as the gold standard. In this context the ROC curve in Figure 8 shows the ability of strain magnitude to predict the regions with expected solid tumor and regions with presumably normal or infiltrated tissue as seen in the ultrasound B-mode image, rather than the diagnostic accuracy of the strain measurements. The ROC curve is composed of corresponding values of sensitivity and 1-specificity, estimated by letting the cut point vary over all possible strain magnitude values. For example, if a threshold of 3.4% is chosen, then 26 of the 32 regions labeled T1 or T2 would be classified as tumor (*i.e.*, having a strain magnitude less than 3.4% as can also be counted from Table 4), giving a sensitivity of  $26/32 = 0.81$ . Further, 24 of the 30 regions labeled N1 or N2 would be classified as normal (*i.e.*, having a strain magnitude larger than 3.4%), giving a specificity of 0.80.

The area under the ROC curve (0.912) is the probability that a randomly chosen non-tumor B-mode region (isoechoic) has higher strain magnitude than a randomly chosen tumor B-mode region (hyperechoic). An area above 0.90 is considered as outstanding discrimination

Table 3. Maximum velocity magnitude for ROIs in presumably normal tissue (N1, N2) and in tumor tissue (T1, T2)

No.	Maximum magnitude of velocity [mm/s]			
	N1	N2	T2	T1
1	0.77	0.71	0.70	0.69
2	0.52	0.54	0.70	0.74
3	1.48	1.44	1.13	1.10
4	0.48	0.52	0.37	0.20
5	0.54	0.51	0.39	0.35
6	0.95	1.02	1.26	1.24
7	0.90	0.93	0.99	1.01
8	0.38	0.45	0.44	0.47
9	0.51	0.54	0.57	0.54
10	0.27	0.15	0.53	0.90
11	0.88	0.87	0.76	0.62
12	2.05	2.22	2.16	2.06
13	0.97	1.10	1.20	1.22
14	2.89	2.77	2.49	2.32
15		1.04	0.77	0.78
16		0.59	0.54	0.40

In two cases only one ROI could be selected in normal tissue.

(Hosmer and Lemeshow 2000). This should imply that a small strain magnitude is most likely associated with hyperechoic tumor region in the B-mode image and a large strain magnitude is most likely associated with an isoechoic region with presumably normal or infiltrated tissue. The effect of using a given strain magnitude threshold to predict hyper- or isoechoic areas in the B-mode images of 16 gliomas of various tumor grading is shown in the ROC-curve. To further explore the potential diagnostics benefits the quantitative strain measurements and B-mode image findings should have been compared with histopathology, which is not available for our data.

Table 4. Average strain magnitude for ROIs in presumably normal tissue (N1, N2) and in tumor tissue (T1, T2)

No.	Strain magnitude ‰			
	N1	N2	T2	T1
1	10.51	10.22	1.72	1.28
2	16.79	18.06	9.64	8.36
3	23.53	10.94	1.22	0.82
4	24.04	6.74	1.48	1.00
5	11.99	11.84	2.51	1.42
6	8.88	6.81	4.33	2.66
7	11.21	7.51	1.31	0.88
8	6.60	3.74	1.22	0.99
9	11.90	10.15	5.79	4.25
10	1.46	1.47	0.64	0.60
11	1.87	2.69	0.89	0.87
12	23.20	17.64	4.16	3.07
13	3.82	3.07	0.86	0.76
14	5.92	5.41	1.90	1.01
15		2.25	0.79	1.03
16		16.09	1.59	1.42

In two cases only one ROI could be selected in normal tissue.

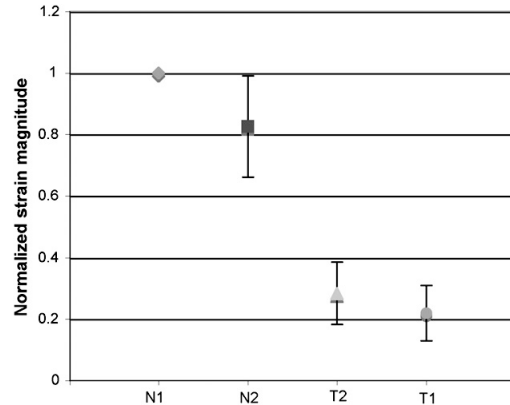


Fig. 7. Mean normalized (with respect to N1) strain magnitude value in region N1, N2, T2, T1 and the 95% confidence interval of the mean ( $n = 14$ ).

Differences in the calculated maximum velocity magnitudes in region N1, N2, T1 and T2 are not statistically significant. Thus, the maximum tissue velocity observed in the hyperechoic tumor mass is not significantly different from observations in the isoechoic areas assumed to be normal tissue.

#### Limitations of the study

In the analyses hyperechoic areas in the US image are interpreted as tumor tissue and isoechoic areas are interpreted as normal tissue. These categories are coarse and

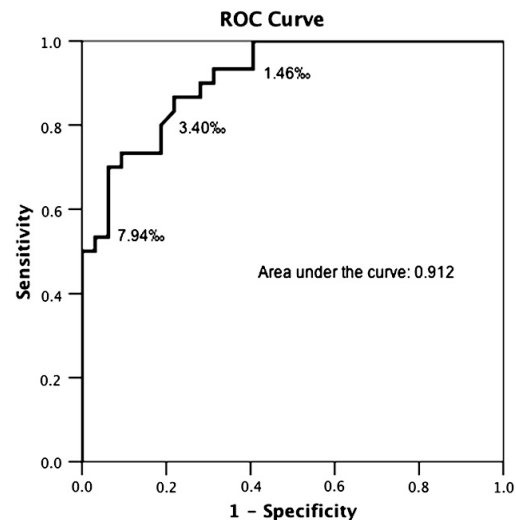


Fig. 8. The ROC curve for the strain magnitude values, using the ultrasound B-mode images as the gold standard.

are not verified by histopathologic examinations. Glial tumors with high malignancy may have regions, especially peripherally, with lower malignancy. For diffuse infiltrating glial tumors there will be scattered tumor cells beyond the tumor border identified in the ultrasound image (Unsgaard et al. 2005). However, the hyperechoic regions should be associated with a substantially higher density of neoplastic cells than the isoechoic regions. Our selected regions (ROI) should therefore be representative for areas consisting of mainly normal tissue and areas with mainly tumor tissue.

The tissue movement in the brain is in general three-dimensional. The parameters reported in this article are calculated in the axial plane of the ultrasound image only. This implies that only one component of the tissue movement and strain is detected by the processing. The direction of the component is defined by the orientation of the hand-held ultrasound probe relative to the patient. Therefore, the results do not necessarily represent the true maximum of either velocity or strain occurring during a cardiac cycle.

### CONCLUSIONS

The ultrasound assessment of *in vivo* pulsatile tissue motion in brain shows that the velocity magnitude is spatially varying and generally increasing with depth.

The velocity of the parenchyma was analyzed on both sides of the ultrasound visible tumor border. There were no significant differences in tissue velocity between hyperechoic regions interpreted as mainly tumor tissue and isoechoic regions interpreted as mainly normal tissue. The strain magnitudes in regions interpreted as tumor are, on the other hand, significantly lower than strain levels in regions interpreted as mainly normal brain parenchyma. There are also significant differences in strain level between regions located within tissue with similar echogenicity. These differences are not as large as differences observed between regions with different echogenicity. Regions located close to the ultrasound visible tumor border have significantly different strain levels compared with regions located more centrally within the given tissue. This may be addressed to the diffuse infiltrating nature of the glial tumors and the variance in tumor cell density of the tissues. We conclude that ultrasound strain imaging along with conventional B-mode images may contribute as a useful tool for discrimination of tumor and normal brain tissue in surgery of glial tumors.

*Acknowledgements*—This work was financed by the Norwegian Ministry of Health and Social Affairs through the National Centre for 3D Ultrasound in Surgery and by SINTEF Health Research. The authors acknowledge their former colleague Dr. Jon Bang's work for implementation in MatLab some of the algorithms used in the strain processing.

### REFERENCES

- Brekken R, Bang J, Ødegård A, Aasland J, Hernes TA, Myhre HO. Strain estimation in abdominal aortic aneurysms from 2-D ultrasound. *Ultrasound Med Biol* 2006;32:33–42.
- Burnside ES, Hall TJ, Sommer AM, Hesley GK, Sisney GA, Svensson WE, Fine JP, Jiang JJ, Hangiandreou NJ. Differentiating benign from malignant solid breast masses with US strain imaging. *Radiology* 2007;245:401–410.
- de Korte CL, van der Steen AFW. Intravascular ultrasound elastography: An overview. *Ultrasonics* 2002;40:859–865.
- Feinberg DA, Mark AS. Human-brain motion and cerebrospinal-fluid circulation demonstrated with MR velocity imaging. *Radiology* 1987;163:793–799.
- Greitz D, Wirestam R, Franck A, Nordell B, Thomsen C, Ståhlberg F. Pulsatile brain movement and associated hydrodynamics studied by magnetic resonance phase imaging. *Neuroradiology* 1992;34:370.
- Hammoud MA, Ligon BL, ElSouki R, Shi WM, Shomer DF, Sawaya R. Use of intraoperative ultrasound for localizing tumors and determining the extent of resection: A comparative study with magnetic resonance imaging. *J Neurosurg* 1996;84:737–741.
- Heimdal A, Stoylen A, Torp H, Skjaerpe T. Real-time strain rate imaging of the left ventricle by ultrasound. *J Am Soc Echocardiogr* 1998;11:1013–1019.
- Hiltawsky KM, Krüger M, Starke C, Heuser L, Ermer H, Jensen A. Free-hand ultrasound elastography of breast lesions: Clinical results. *Ultrasound Med Biol* 2001;27:1461–1469.
- Hosmer DW, Lemeshow S. *Applied logistic regression*. Wiley series in probability and statistics. New York: John Wiley & Sons, Inc.; 2000.
- Kelly PJ, Dumas-Dupport C, Kispert DB, Kall BA, Scheithauer BW, Illig JJ. Imaging-based stereotaxic serial biopsies in untreated intracranial glial neoplasms. *J Neurosurg* 1987;66:865–874.
- Kolstad F, Rygh OM, Selbekk T, Unsgaard G, Nygaard OP. Three-dimensional ultrasonography navigation in spinal cord tumor surgery. Technical note. *J Neurosurg Spine* 2006;5:264.
- Maier SE, Hardy CJ, Jolesz FA. Brain and cerebrospinal-fluid motion - Real-time quantification with M-mode MR-imaging. *Radiology* 1994;193:477–483.
- Poncellet BP, Wedeen VJ, Weisskoff RM, Cohen MS. Brain parenchyma motion - Measurement with cine echo-planar MR imaging. *Radiology* 1992;185:645–651.
- Regner DM, Hesley GK, Hangiandreou NJ, Morton MJ, Nordland MR, Meixner DD, Hall TJ, Farrell MA, Mandrekar JN, Harmsen WS, Charboneau JW. Breast lesions: Evaluation with US strain imaging - Clinical experience of multiple observers. *Radiology* 2006;238:425–437.
- Scholz M, Lorenz A, Pesavento A, Brendel B, Khaled W, Engelhardt M, Pechlivanis I, Noack V, Harders A, Schmieder K. Current status of intraoperative real-time vibrography in neurosurgery. *Ultraschall Med* 2007;28:493–497.
- Scholz M, Noack V, Pechlivanis I, Engelhardt M, Fricke B, Linstedt U, Brendel B, Ing D, Schmieder K, Ermer H, Harders A. Vibrography during tumor neurosurgery. *J Ultrasound Med* 2005;24:985–992.
- Selbekk T, Bang J, Unsgaard G. Strain processing of intraoperative ultrasound images of brain tumours: Initial results. *Ultrasound Med Biol* 2005;31:45–51.
- Sun H, Zhao JZ. Application of intraoperative ultrasound in neurological surgery. *Min Invasive Neurosurg* 2007;50:155–159.
- Unsgaard G, Rygh OM, Selbekk T, Müller TB, Kolstad F, Lindseth F, Hernes TAN. Intra-operative 3D ultrasound in neurosurgery. *Acta Neurochirurgica* 2006;148:235–253.
- Unsgaard G, Selbekk T, Müller TB, Ommedal S, Torp SH, Myhr G, Bang J, Nagelhus Hernes TA. Ability of navigated 3D ultrasound to delineate gliomas and metastases - Comparison of image interpretations with histopathology. *Acta Neurochirurgica* 2005;147:1259–1269.
- Wirestam R, Salford LG, Thomsen C, Brockstedt S, Persson BRR, Ståhlberg F. Quantification of low-velocity motion using a navigator-echo supported MR velocity-mapping technique: Application to intracranial dynamics in volunteers and patients with brain tumors. *Mag Reson Imaging* 1997;15:1–11.



# Paper III



RESEARCH ARTICLE

Open Access

# Comparison of contrast in brightness mode and strain ultrasonography of glial brain tumours

Tormod Selbekk<sup>1,2\*</sup>, Reidar Brekken<sup>1,2</sup>, Marit Indergaard<sup>2</sup>, Ole Solheim<sup>2,3</sup> and Geirmund Unsgård<sup>2,3</sup>

## Abstract

**Background:** Image contrast between normal tissue and brain tumours may sometimes appear to be low in intraoperative ultrasound. Ultrasound imaging of strain is an image modality that has been recently explored for intraoperative imaging of the brain. This study aims to investigate differences in image contrast between ultrasound brightness mode (B-mode) images and ultrasound strain magnitude images of brain tumours.

**Methods:** Ultrasound radiofrequency (RF) data was acquired during surgery in 15 patients with glial tumours. The data were subsequently processed to provide strain magnitude images. The contrast in the B-mode images and the strain images was determined in assumed normal brain tissue and tumour tissue at selected regions of interest (ROI). Three measurements of contrast were done in the ultrasound data for each patient. The B-mode and strain contrasts measurements were compared using the paired samples t- test.

**Results:** The statistical analysis of a total of 45 measurements shows that the contrasts in the strain magnitude images are significantly higher than in the conventional ultrasound B-mode images ( $P < 0.0001$ ).

**Conclusions:** The results indicate that ultrasound strain imaging provides better discrimination between normal brain tissue and glial tumour tissue than conventional ultrasound B-mode imaging. Ultrasound imaging of tissue strain therefore holds the potential of becoming a valuable adjunct to conventional intraoperative ultrasound imaging in brain tumour surgery.

**Keywords:** Ultrasound, Elastography, Elastogram, Strain, Brain, Neurosurgery, Brain tumours, Image contrast

## Background

Prior to modern neuroimaging, the neurosurgeon could detect pathological tissue by palpating the suspected areas of the brain during surgery. The tumour would be felt as a region with different elasticity compared to the surrounding normal brain, as such tumours most often have a firmer consistency than normal tissue. Even today when an operating microscope is used, the surgeon may palpate the tissue using the surgical instruments in order to find areas of the brain with differences in tissue hardness. This manual inspection of tissue hardness may aid to identify remaining tumour tissue that may be difficult to detect with direct visualisation using the operating microscope. Ultrasound imaging can also be used for the assessment

of tissue hardness through imaging of *strain* in the tissue. Assuming that the stress applied to the tissue is uniform, the calculated and displayed strain values should in ideal circumstances be proportional to the modulus of elasticity (Young's modulus) of the tissues. The imaging technique is therefore often also referred to as *ultrasound elastography* and the corresponding images are often called *elastograms*.

Several research groups have investigated the use of ultrasound elastography in imaging brain tumours [1-3]. However, the clinical benefit of ultrasound strain imaging compared to conventional ultrasound imaging is still to be determined. The publications so far have shown only a few example images of brain tumours and have mainly demonstrated that it is feasible to generate elastograms of brain tumours. The measurements and display of strain require some form of displacement of the tissue, which means that internal or external forces need to act on the organ. Previous studies have demonstrated strain images (elastograms) generated by the internal displacements in

\* Correspondence: tormod.selbekk@sintef.no

<sup>1</sup>Department of Medical Technology, SINTEF, Olav Kyrres gate 9, Trondheim, Norway

<sup>2</sup>Faculty of Medicine, Norwegian University of Science and Technology, Olav Kyrres gate 9, Trondheim, Norway

Full list of author information is available at the end of the article

the brain parenchyma caused by arterial pulsation, or generated by the use of either a mechanical shaker device or manual palpation to induce tissue displacements [1-3]. Quantitative assessments of ultrasound strain images of brain tumours have been performed in one study, which used the natural pulsation of the brain parenchyma to generate strain images. The study concluded that strain magnitudes of brain tumours are significantly lower than the strain magnitudes of normal brain tissue [4]. However, quantitative comparisons between ultrasound *strain images* and conventional *brightness mode images* have not been published so far.

The clinical performance of ultrasound strain imaging has been evaluated more thoroughly in breast tumours. In a study by Burnside *et al.*, the use of ultrasound strain imaging in combination with ultrasound B-mode imaging led to a higher area under the receiver operating characteristics (ROC) curve than by using ultrasound B-mode images alone [5].

A few ultrasound machines have implemented the option of calculating the *strain ratio* between strain levels in assumed tumour and in assumed normal tissue. This has resulted in several recent papers on the use of strain ratio (also referred to as *strain index*) for diagnostic purposes. One study compared the performance of B-mode images, strain images and strain ratio in differentiating benign and malignant tumours in a group of 227 women with focal breast lesions [6]. The authors concluded that B-mode images provided the highest sensitivity, but the strain images and strain ratio provided higher specificity. In another study Cho *et al.* compared the diagnostic performance of ultrasound B-mode sonography and strain rate in differentiation of malignant and benign breast masses and found no significant difference in the area under the ROC curve [7].

These and other studies indicate that ultrasound strain imaging may to some extent provide an improvement in diagnostics of some tumours compared to using conventional ultrasound alone. It might be asked what features of strain imaging do account for an increase in diagnostic performance compared to conventional B-mode imaging. Ultrasound is able to produce B-mode images with high spatial and temporal resolution, but the contrast resolution may be limited compared to other imaging techniques like Magnetic Resonance Imaging (MRI) or Computed Tomography (CT). The difference in brightness intensity between the lesion to diagnose and the normal tissue may in some cases appear to be low, thus having a poor contrast resolution. An improved image contrast would probably lead to improved diagnostics of these low-contrast lesions. It could be speculated that the ultrasound strain images might possess a higher image contrast than conventional ultrasound. The imaging of strain is related to other properties of tissue than the

generation of ultrasound B-mode images, and therefore holds the potential to provide unique information about tissue pathology [8].

It is therefore of clinical interest to make comparisons of attributes like image contrast between the two modalities, to assess potential differences in imaging of lesions.

In this study we have processed and analysed ultrasound data acquired during surgery of glial tumours in order to compare the image contrast in conventional ultrasound images (B-mode) versus the image contrast in ultrasound strain images. We have performed a quantitative comparison of image contrast between ultrasound strain images generated by the natural pulsation of the brain parenchyma and the corresponding B-mode images. The measurements of image contrast have been performed in the peripheral parts of the tumour, covering the transition from cancerous tissue towards more normal brain tissue. The hypothesis of the study was that the contrast between tumour and normal tissue is higher in the ultrasound strain images than in the ultrasound B-mode images.

## Methods

Regional Research Ethics Committee of Central Norway approved the study protocol and the use of previously acquired ultrasound data in this retrospective study. The anonymous ultrasound data used in this study has been acquired with the patient's informed consent as a part of a prior study.

### Data acquisition

Ultrasound radiofrequency (RF) data was acquired during surgery of 15 glial tumours. The patients were diagnosed by histopathology. Eight patients had low-grade glioma (WHO-grade I and II) and 7 patients had high-grade astrocytoma (WHO grade III & IV). The data were acquired after craniotomy with the 10 MHz flat linear probe (System FiVE, GE Vingmed, Horten, Norway) kept motionless on intact dura. An engineer (TS) adjusted the settings of the ultrasound scanner (power, gain, time gain control-TGC) prior to acquisition, aiming to provide ultrasound B-mode images with a homogenous appearance but avoiding brightness saturation. The acquired data covered at least one cardiac cycle in time.

### Strain processing

The axial strain was calculated by differentiation of time delays that were estimated by processing of the ultrasound RF-data. The time delays were calculated by implementing in Matlab (MathWorks, Natic, MA, USA) a method initially suggested by Cabot [9], which has been further refined for time delay estimation in later publications [10,11]. The strain processing of the RF-

data is described in details in an earlier publication from our research group [1].

#### Performing the measurements

The B-mode and strain magnitude images were analysed with measuring methods implemented in Matlab. For each dataset a total of three measurements of contrast for both strain and B-mode were done at three different locations in the images. That is, a different location in the image was selected for each measurement. All three measurements for a given tumour were done at the same image frame, i.e. at the same point in time. With reference to the B-mode images, the measurements were performed in the hyperechoic tumour and the surrounding isoechoic regions presumably representing normal brain tissue.

The procedure for obtaining the contrast measurements is illustrated in Figure 1. After import and strain processing of the ultrasound data, the B-mode image was displayed. As a first step, the operator (MI) identified the tumour border as seen in the ultrasound B-

mode images, and selected one position (using the mouse) on the border for contrast measurement. The B-mode intensity and strain magnitude were subsequently plotted along the lateral direction for the given depth, with a cross mark (X) indicating the lateral position of the point selected by the operator (Figure 1C-D). The plotted strain magnitudes and B-mode intensity were calculated by averaging the values over an area of approx.  $1 \text{ mm}^2$  in the images.

The second step of the measurements was to calculate the contrast between expected cancerous tissue and normal tissue for both image modalities. The calculation was based on the local minimum and maximum values found closest to the cross mark (X) in the respective plotted curves, i.e. the local extrema close to the tumour border as identified by the operator.

The maximum allowable lateral range for the amplitude picking was defined with the aid of a low-pass (LP) filtered version of the curves (shown as a light grey step-wise curve in Figure 1C-D), in order to increase the

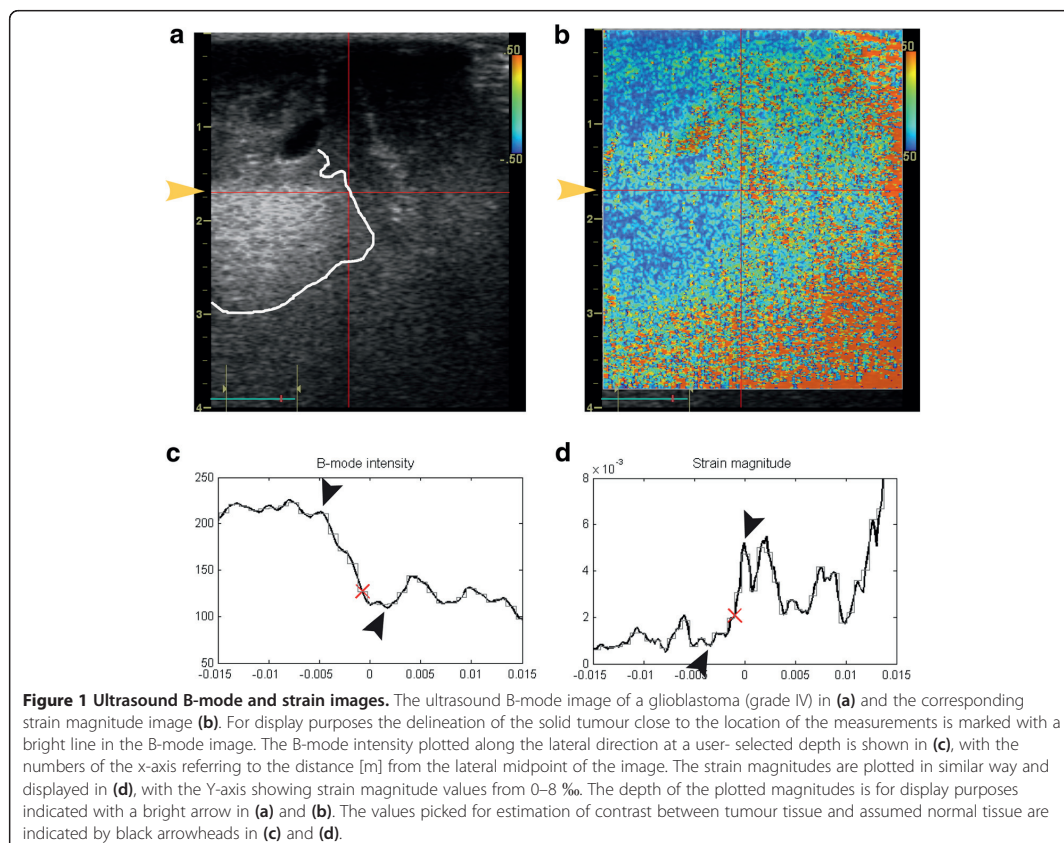


**Table 1 Strain and B-mode contrast**

Glioma grading	Dataset No.	Average strain magnitude contrast ( $\sigma$ )	Average B-mode contrast ( $\sigma$ )
low-grade glioma	1	0.55 (0.11)	0.43 (0.20)
	2	0.56 (0.27)	0.61 (0.20)
	3	0.57 (0.08)	0.27 (0.04)
	4	0.58 (0.19)	0.46 (0.13)
	5	0.51 (0.04)	0.32 (0.06)
	6	0.64 (0.12)	0.36 (0.07)
	7	0.66 (0.25)	0.35 (0.12)
	8	0.84 (0.04)	0.56 (0.11)
high-grade glioma	9	0.58 (0.22)	0.31 (0.06)
	10	0.48 (0.21)	0.24 (0.09)
	11	0.58 (0.11)	0.25 (0.19)
	12	0.50 (0.07)	0.29 (0.06)
	13	0.69 (0.17)	0.42 (0.08)
	14	0.65 (0.17)	0.60 (0.12)
	15	0.60 (0.03)	0.44 (0.24)
All data		0.60 (0.16)	0.39 (0.16)

The average and standard deviation ( $\sigma$ ) of the three contrast measurements obtained for each patient.

robustness towards minor amplitude deviations. The valid lateral range was between the first minimum and first maximum values for the LP-curve found locally around the user-selected position (marked X) of the tumour border as seen in the ultrasound images. The local extrema of the original and unfiltered curves within this lateral range were found by manual inspection, and used for the calculation of contrast. Thus, the contrast was calculated by selecting one extremum value in the tumour and a second extremum value in the supposedly normal brain tissue. The contrast between the assumed

normal tissue and the tumour tissue for the two image modalities was calculated as

$$C = \frac{|A_1 - A_2|}{A_1 + A_2} \quad (1)$$

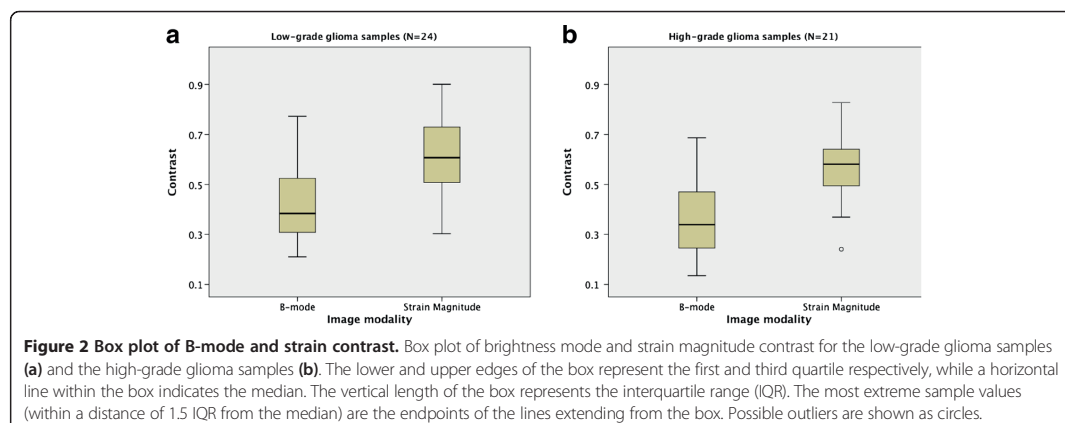
where  $A_1$  and  $A_2$  are the respective local minimum and maximum values for strain magnitude or brightness intensity observed across the tumour border as depicted by ultrasound. A value of  $C = 0$  means no difference in contrast between areas of tumour and areas of assumed normal brain tissue.

### Statistics

The differences in contrast between ultrasound strain and B-mode were statistically analysed using the paired samples t-test (SPSS Statistics, v 19.0, IBM corporation, NY, USA), using a significance level  $\alpha = 0.05$ . Normal quantile plots (Q-Q plots) were used for assessment of the sample populations' probability distribution. The independent samples t-test was used to investigate differences in contrast between the subgroups of low-grade and high-grade gliomas for a given image modality.

### Results

For each glial tumour (15 cases) three analyses of contrast were done on ultrasound strain magnitude and B-mode images, giving a total of 45 measurements for each modality. The measurements were performed at depths between 0.7 and 3.0 cm, with the average measurement depth being 1.9 cm for the 45 samples. Table 1 shows the average contrast and standard deviation of the three measurements performed for each patient. The average contrast is higher for the strain magnitude than for the B-mode intensity in all cases except one with a low-grade glioma. Box plot of the strain and B-mode contrast measurements is shown for the subgroups of low-grade and high-grade gliomas (Figure 2).



The difference in contrast between the two image modalities was statistically investigated for all contrast measurements of the tumours ( $N = 45$ ), and for the measurements in the subgroups low-grade gliomas ( $N_l = 24$ ) and high-grade gliomas ( $N_h = 21$ ). The normal probability distributions of the sample populations were confirmed by inspection of Q-Q-plots. For the glial tumours as a whole the contrasts between tumour and presumably normal tissue in the strain images were significantly higher than the corresponding contrast in the B-mode images ( $P < 0.0001$ ). For the subgroup of patients with high-grade gliomas the contrast in the strain images were significantly higher than the contrast in the B-mode images ( $P < 0.0001$ ), and the same was observed for the subgroup with low-grade gliomas ( $P < 0.0001$ ).

There was not a significant difference in contrast between the two subgroups' low-grade and high-grade gliomas, neither for the strain images ( $P = 0.49$ ) nor the B-mode images ( $P = 0.25$ ).

### Discussion

In this study we have performed measurements of strain magnitude and brightness intensity across the ultrasound depicted border of glial tumours, with subsequent analysis of differences in contrast between the image modalities. The results of the analyses show a significantly higher contrast between tumour tissue and presumed normal tissue in the strain images, as compared to the B-mode images. From Table 1 we observe that the mean contrast for all B-mode measurements is 0.39 while it is 0.60 for the strain magnitude measurements, which is 54 % higher. One interpretation of the results could be that ultrasound strain imaging should be the preferred image modality to use during surgery of brain tumours, since the strain images provide better discrimination (higher contrast) between the tumour tissue and the normal brain tissue. However, in a clinical setting there are still several key issues to solve before the surgeons can use ultrasound strain imaging as a practical tool for identification of the resectable tumour tissue. With the processing parameters applied in this study the strain images generally appear noisier than the conventional B-mode images. This is partly introduced by the processing of the data where e.g. the differentiation of the calculated time delays in the axial direction typically introduces strain values with alternating polarity and a spiking appearance in the strain image. The processing is also prone to decorrelation of the echo signal due to low signal levels (hypoechoic regions in the B-mode image) or "out of plane" tissue motion causing loss of temporally coherent signals. This may cause the processing to produce false results with abnormally high strain values. Also, our method for estimation of time delays assumes that the delay is smaller than the sampling time  $T_s$ , i.e. that the tissue velocity is low compared to the

number of frames acquired per second. If this assumption is not met the processing may produce incorrectly high strain values.

In our processed strain images we have indeed seen that noise can be present in parts of the image. This is typically seen in regions with low intensity in the B-mode image, for example when imaging homogenous tissue like the brain stem and deeper white brain matter that appear hypoechoic compared to other brain tissue. However, our measurements are intentionally performed in the transition zone from tumour to presumed normal brain tissue. In this short distal range we expect the data to be least influenced by noise, with the B-mode intensity ranging from the hyperechoic tumour to the isoechoic areas with presumed normal tissue. The inspection of the strain magnitude curves did not indicate any abrupt change of signal level within the spatial distance analysed, as could be expected if the strain processing produced invalid results.

It can be argued that the measurements performed in the transition zone from tumour to normal tissue impose a selection bias for the contrast analysis. This is the region that is of interest to the surgeon, but it is also the region where we should expect the strain images to be least affected by noise. The contrast measurements are only valid for analysis of image contrast between glial tumour tissue and adjacent normal tissue. It should not be interpreted to represent differences in contrast resolution between the image modalities in general.

The methodology for the analysis of image contrast in the peripheral parts of tumour involves a subjective assessment of the approximate position of the depicted tumour border and manual reading of the displayed strain magnitude and brightness curves. Even if the implemented method of analysis is not fully automatic, the measurements were obtained by following a standardized procedure, as outlined in the Methods section. Quantitative image quality measures will usually imply some subjective decisions about where to perform the analysis in the image. It is therefore difficult to establish a method without some kind of manual intervention. However, the calculation of additional measures like e.g. the contrast-to-noise ratio (CNR), or signal-to-noise ratio (SNR) would increase the robustness of the image assessment and should be considered in future studies [12]. It would also have been interesting to address intra- and interobserver variability of the measurements, which was not performed in this study.

As discussed above there are different factors that may have affected the measurements. However, we have found the obtained measurements to be quite robust and we believe that the differences in contrast found between ultrasound strain magnitude and B-mode intensity should represent actual differences between the image modalities.

Ultrasound strain imaging in brain surgery is a quite novel approach and we have not found other studies performing a similar comparison between strain images and conventional B-mode images. It is therefore difficult to compare our results with previous findings. Some studies have however explored the use of strain ratio for diagnostic purposes, but the similar ratio for B-mode intensity has not been reported. The strain ratio is a quantitative index but should not be considered as an objective *diagnostic* parameter as its value may be heavily dependent on which regions are selected for comparison and is therefore prone to variations between observers and within the patient population, which has also been pointed out by others [13]. It should be noted that the contrasts calculated in our study are not intended to serve a diagnostic purpose; the sole purpose is the pairwise comparison between the ultrasound modalities.

The *diagnostic value* of ultrasound strain imaging of brain tumours has not been assessed in this study. This would require a comparison between image findings and histology, which was not available for the current study. Glial tumours are diffuse infiltrating and tumour cells are likely to be present also beyond the border zone seen in the ultrasound B-mode image [14]. Scattered tumour cells are likely to be present in the isoechoic regions interpreted to be mainly normal brain tissue, but to a substantially less extent than in the hyperechoic regions. The calculated contrasts should therefore represent differences in magnitude (strain/brightness) between areas in the brain predominated by glial tumour cells and areas predominated by normal brain cells, respectively.

The results obtained should provide a rationale for further technical developments and investigations of methods for real-time intraoperative ultrasound strain imaging of brain tumours. The ultrasound strain magnitude images possess a higher contrast between tumour and normal brain tissue in the peripheral parts of the tumour than the conventional B-mode images. This suggests that the surgeon may use imaging of strain to improve detection of remaining tumour towards the end of surgery, compared to using conventional ultrasound imaging alone.

## Conclusions

Off-line processing of ultrasound RF-data to yield strain magnitude images has been performed on *in vivo* data acquired during brain tumour surgery. The strain magnitude images have a significantly higher contrast between normal tissue and tumour tissue than conventional B-mode images. We conclude that for glial brain tumours, ultrasound imaging of strain holds the potential to become a valuable adjunct to conventional brightness mode imaging. However, the practical aspects of acquisition and

display of strain images in real time as well as evaluation of diagnostic value must be addressed in future studies.

## Competing interests

The authors declare that they have no competing interests.

## Authors' contributions

TS contributed to the study design, acquisition of data, data analyses and drafting of manuscript, RB contributed to the study design and implementation of the strain processing methods and measurements method in Matlab, MI performed the measurements and contributed to the statistical analyses and drafting of manuscript, OS contributed to data acquisition and drafting of manuscript and GU contributed to the study design, acquisition of data and drafting of manuscript. All authors read and approved the final manuscript.

## Acknowledgements

The study has been financed by the regional health authorities in central Norway through the financing of the National Centre for 3D ultrasound in Neurosurgery, the independent research institute SINTEF and the MI Lab and Department of Circulation and Medical Imaging, Norwegian University of Science and Technology, Trondheim, Norway. We acknowledge our former colleague Dr Jon Bang for implementation in Matlab some of the algorithms used in the strain processing.

## Author details

<sup>1</sup>Department of Medical Technology, SINTEF, Olav Kyrres gate 9, Trondheim, Norway. <sup>2</sup>Faculty of Medicine, Norwegian University of Science and Technology, Olav Kyrres gate 9, Trondheim, Norway. <sup>3</sup>Department of Neurosurgery, St. Olav University Hospital, Olav Kyrres gate 9, Trondheim, Norway.

Received: 25 August 2011 Accepted: 23 May 2012

Published: 23 May 2012

## References

1. Selbekk T, Bang J, Unsgaard G: **Strain processing of intraoperative ultrasound images of brain tumours: initial results.** *Ultrasound Med Biol* 2005, **31**(1):45–51.
2. Scholz M, Noack V, Pechlivanis I, Engelhardt M, Fricke B, Linstedt U, Brendel B, Ing D, Schmieder K, Ermet H, Harders A: **Vibrography during tumor neurosurgery.** *J Ultrasound Med* 2005, **24**(7):985–992.
3. Uff CE, Garcia L, Fromageau J, Dorward N, Bamber JC: **Real time ultrasound elastography in neurosurgery.** *Proceedings of the IEEE International Ultrasonics Symposium 2009*, 467–470.
4. Selbekk T, Brekken R, Solheim O, Lydersen S, Hernes TAN, Unsgard G: **Tissue motion and strain in the human brain assessed by intraoperative ultrasound in glioma patients.** *Ultrasound Med Biol* 2010, **36**(1):2–10.
5. Burnside ES, Hall TJ, Sommer AM, Hesley GK, Sisney GA, Svensson WE, Fine JP, Jiang J, Hangiandreou NJ: **Differentiating benign from malignant solid breast masses with US strain imaging.** *Radiology* 2007, **245**(2):401.
6. Thomas A, Degenhardt F, Farrokh A, Wojcinski S, Slowinski T, Fischer T: **Significant differentiation of focal breast lesions: calculation of strain ratio in breast sonoelastography.** *Acad Radiol* 2010, **17**(5):558–563.
7. Cho N, Moon WK, Kim HY, Chang JM, Park SH, Lyou CY: **Sonoelastographic strain index for differentiation of benign and malignant nonpalpable breast masses.** *J Ultrasound Med* 2010, **29**(1):1–7.
8. Wells PNT, Liang HD: **Medical Ultrasound: imaging of soft tissue strain and elasticity.** *J R Soc Interface* 2011, **8**(64):1521–1549.
9. Cabot RC: **A note on the application of Hilbert transform to time delay estimation.** *IEEE Trans. Acoust. Speech Signal Processing* 1981, **29**:607–609. ASSP.
10. Loupas T, Powers JT, Gill RW: **An axial velocity estimator for ultrasound blood flow imaging, based on a full evaluation of the Doppler equation by means of a two-dimensional autocorrelation approach.** *IEEE Trans Ultrason Ferroelect Freq Control* 1995, **42**:672–688.
11. Simon C, VanBaren P, Ebbini ES: **Two-dimensional temperature estimation using diagnostic ultrasound.** *IEEE Trans Ultrason Ferroelect Freq Control* 1998, **45**:1088–1099.
12. Varghese T, Ophir J: **An analysis of elastographic contrast-to-noise ratio.** *Ultrasound Med Biol* 1998, **24**:915–924.

13. Kagoya R, Monobe H, Tojima H: **Utility of elastography for differential diagnosis of benign and malignant thyroid nodules.** *Otolaryngol Head Neck Surg* 2010, **143**(2):230–234.
14. Unsgaard G, Selbekk T, Müller TB, Ommedal S, Torp SH, Myhr G, Bang J, Hernes TAN: **Ability of navigated 3D ultrasound to delineate gliomas and metastases - comparison of image interpretations with histopathology.** *Acta Neurochir* 2005, **147**(12):1259–1269.

doi:10.1186/1471-2342-12-11

**Cite this article as:** Selbekk *et al.*: Comparison of contrast in brightness mode and strain ultrasonography of glial brain tumours. *BMC Medical Imaging* 2012, **12**:11.

**Submit your next manuscript to BioMed Central  
and take full advantage of:**

- Convenient online submission
- Thorough peer review
- No space constraints or color figure charges
- Immediate publication on acceptance
- Inclusion in PubMed, CAS, Scopus and Google Scholar
- Research which is freely available for redistribution

Submit your manuscript at  
[www.biomedcentral.com/submit](http://www.biomedcentral.com/submit)





# Paper IV



## Clinical Article

# Ability of navigated 3D ultrasound to delineate gliomas and metastases – comparison of image interpretations with histopathology

G. Unsgaard<sup>1,2,4</sup>, T. Selbekk<sup>3,4</sup>, T. Brostrup Müller<sup>1,4</sup>, S. Ommedal<sup>3,4</sup>, S. H. Torp<sup>2,5</sup>,  
G. Myhr<sup>2,6</sup>, J. Bang<sup>3,4</sup>, and T. A. Nagelhus Hernes<sup>2,3,4</sup>

<sup>1</sup> Department of Neurosurgery, St. Olav University Hospital, Trondheim, Norway

<sup>2</sup> The Norwegian University of Science and Technology, Trondheim, Norway

<sup>3</sup> SINTEF Health Research, Trondheim, Norway

<sup>4</sup> National Centre for 3D ultrasound in Surgery, St. Olav University Hospital, Trondheim, Norway

<sup>5</sup> Department of Pathology and Medical Genetics and of Laboratory Medicine, St. Olav University Hospital, Trondheim, Norway

<sup>6</sup> MR Centre, St. Olav University Hospital, Trondheim, Norway

Received May 19, 2004; accepted July 14, 2005; published online September 19, 2005

© Springer-Verlag 2005

## Summary

**Background.** The objective of the study was to test the ability of a 3D ultrasound (US) based intraoperative imaging and navigation system to delineate gliomas and metastases in a clinical setting. The 3D US data is displayed as reformatted 2D image slices. The quality of the displayed 3D data is affected both by the resolution of the acquired data and the reformatting process. In order to investigate whether or not 3D US could be used for reliable guidance in tumour surgery, a study was initiated to compare interpretations of imaged biopsy sites with histopathology. The system also enabled concomitant comparison of navigated preoperative MR with histopathology.

**Method.** Eighty-five biopsies were sampled between 2–7 mm from the tumour border visible in the ultrasound images. Biopsies were collected from 28 operations (7 low-grade astrocytomas, 8 anaplastic astrocytomas, 7 glioblastomas and 6 metastases). Corresponding cross-sections of preoperative MR T1, MR T2 and intraoperative US were concomitantly displayed, steered by the biopsy forceps equipped with a positioning sensor. The surgeons' interpretation of the images at the electronically indicated biopsy sites were compared with the histopathology of the samples.

**Findings.** The ultrasound findings were in agreement with histopathology in 74% (n = 31) for low-grade astrocytomas, 83% (n = 18) for anaplastic astrocytomas, 77% (n = 26) for glioblastomas and 100% (n = 10) for metastases. Excluding irradiated patients, the results for glioblastomas improved to 80% concurrence (n = 20). As expected tumour cells were found in biopsies outside the US visible tumour border, especially in low-grade gliomas. Navigated 3D US have a significantly better agreement with histopathology than navigated MR T1 for low-grade astrocytomas.

**Conclusion.** Reformatted images from 3D US volumes give a good delineation of metastases and the solid part of gliomas before starting the resection. Navigated 3D US is at least as reliable as navigated 3D MR to delineate gliomas and metastases.

**Keywords:** Brain tumour surgery; biopsies; histopathology; intraoperative imaging; magnetic resonance imaging; three-dimensional ultrasound imaging.

## Introduction

The use of intraoperative imaging may lead to a more complete resection of infiltrating tumours [2, 12, 14, 19, 22, 24] with the possibility for increased patient survival time [20, 25]. However, aggressive surgery may also increase the risk of inflicting neurological injury. The self-evident criterion for an intraoperative imaging system is that it provides imaging quality sufficient to discriminate between tumour and normal brain, but also between tumour and non-tumour pathology, such as oedema.

Several authors have previously reported the benefits of 2D US for intraoperative imaging and guidance in brain surgery [1, 4, 5, 8, 9, 13, 16, 21, 23]. Woydt *et al.* [26] and LeRoux *et al.* [15] compared ultrasound images of gliomas with histopathology, and concluded that intraoperative US could improve gross total resection. It is challenging to use 2D US to precisely localize and resect tumour tissue, because the instrument must always be visualized in the ultrasound plane [23].

We have previously reported our initial experience with an intraoperative imaging system based on 3D US [24]. This system makes it possible to follow the progression of the tumour resection and to identify, localize and remove residual tumour tissue. It also, of course, makes it possible to identify biopsy sites in the images.

As we were starting to use the system more and more in daily clinical practice, we felt it was important to have an evaluation of the ability of the 3D US system to delineate the tumour in a clinical setting. Good concurrence has been found between the delineation of a tumour by MR and 2D US [16]. The spatial resolution of the US beam is, however, lower in the elevation direction (thickness of the plane) than in the radial and lateral direction. This could lead to an unclear border of the lesion in reformatted 3D US. The present study was initiated to investigate whether the images from the 3D US imaging system provide the surgeon with sufficient information to do a safe delineation of the margins of gliomas and metastases during the operation.

This was done by comparing the biopsy sites in reformatted images from intraoperative US and preoperative MR volumes with histopathology prior to tumour resection.

## Materials and methods

### Clinical material

Patients with tumours located in the supratentorial region of the brain were included. The tumours were deep-seated with a diameter of 2–5 cm. Superficial tumours (depth less than 2 cm) were excluded because the probe was not optimal in the nearfield. Table 1 summarizes the patient characteristics for the 28 operations performed during a 3 year study period. The patients were informed about the methodology and accepted to be included in the study.

A total of 139 biopsies in 28 operations (27 patients) were acquired prior to the start of the resection (Table 2). We have chosen to analyze the 85 biopsies located in the border-zone, i.e. biopsies within 2–7 mm from the ultrasound tumour border. This border-zone was arbitrarily chosen for the following reasons: Biopsies located within 2 mm from the detected tumour border were excluded from

Table 1. Patient characteristics

	Low-grade astrocytoma	Anaplastic astrocytoma	Glioblastoma multiforme	Metastasis
No. of operations	7	8	7	6
Sex				
– Female/Male	4/3	5/3	2/5	3/3
Age [yrs]				
– Average	44	50	61	64
– Range	23–59	33–67	49–73	49–81
Prev. treatment				
– Surgery	2	1	2	0
– Radiation therapy	1	0	2	0

the analyses due to imaging accuracy of the SonoWand system (1.4 mm) [17] and the size of the biopsy forceps (3 mm). On the other hand, biopsies located more than 7 mm from the border were thought not to challenge the ability of 3D US to detect tumour tissue.

### Preoperative preparations and planning

Preoperative 3D MR examinations were performed using a clinical Picker Edge 1.5T unit (Marconi, Cleveland, USA) ( $n = 26$ ). Scan parameters for the T2 sequence were 3D FSE TR 3177/TE 95, NEX 3. In total 120 slices of 1.5 mm thickness were acquired without interslice gap in 10 subvolumes. A 3D T1-weighted sequence (RF-FAST TR13/TE 4.4, flip angle 30, NEX 1, matrix  $192 \times 256$ ) was performed after the injection of Gadolinium-DTPA-BMA (Omniscan<sup>®</sup>, Amersham Health, Oslo, Norway). Slice thickness was 1.5 mm without interslice gap, 110 slices were acquired. At the time of the study our MR department could not offer 3D FLAIR images, which would have been more optimal especially for the low-grade astrocytomas. Two of the MR examinations were performed using a 1.5T Siemens Symphony scanner (Siemens, Erlangen, Germany) with similar settings.

Before MR scanning, five self-adhesive fiducial markers were attached to the patient's head in a fixed pattern. The 3D MR volumes were registered to the patient on the operating table. The accuracy of the patient registration was estimated by a root mean square value and by pointing at anatomical landmarks. When the obtained accuracy was found to be satisfactory (error less than 2 mm by anatomical landmarks), the surgeon used the system to plan the surgical procedures.

Table 2. Summary of the biopsies collected in the study

	Low-grade astrocytoma	Anaplastic astrocytoma	Glioblastoma multiforme	Metastasis	Total
No. of operations	7	8	7	6	28
No. of biopsies	45	40	40	14	139
Biopsies per case					
– Average	6.4	5.0	5.7	2.3	
– Range	4–12	2–8	2–8	1–4	
No. of biopsies with distance to tumour edge					
– Less than 2 mm	5	12	6	1	24
– Between 2–7 mm	31	18	26	10	85
– Greater than 7 mm	9	10	8	3	30

*Intraoperative 3D ultrasound imaging*

A system integrating US imaging with neuronavigation to form a 3D US based intraoperative imaging system, have been employed in this study (SonoWand, MISON A/S, Trondheim, Norway). The system is able to track the position of US probes, pointers and surgical instruments like biopsy forceps and ultrasonic surgical aspirators (Fig. 1) [3, 7, 24]. The biopsy forceps were calibrated within a few seconds by positioning the tip of the instrument at a fixed position on the reference frame. The ultrasound examinations were performed with a 4–8 MHz phased array probe with a footprint of 15×21 mm. The 3D US volumes were acquired on intact dura by tilting the handheld US probe for 15–20 sec, thus accumulating a set of 2D US sector scans that were merged with the corresponding positioning data into a 3D volume (Fig. 2A). The

average accuracy of the navigated US images measured in the laboratory is 1.4 mm [17].

Image quality is of crucial importance for image guided surgery. The US image quality is related to the spatial resolution (the ability to resolve targets), which in the 2D US scan plane is mainly determined by the frequency of the probe used. The radial resolution (along the beam) equals approximately the transmitted pulse length and the lateral resolution (normal to the beam) equals the beam width (width of the main lobe at the focus). For a typical all-round probe like a 5 MHz phased array probe the radial and lateral resolution is approximately 0.5, and 1.0 mm respectively. In addition, the image plane itself has a certain width that varies with the depth. This is the elevation resolution (normal to the scan-plane) and is less than 2.0 mm for the above probe at the optimal depth

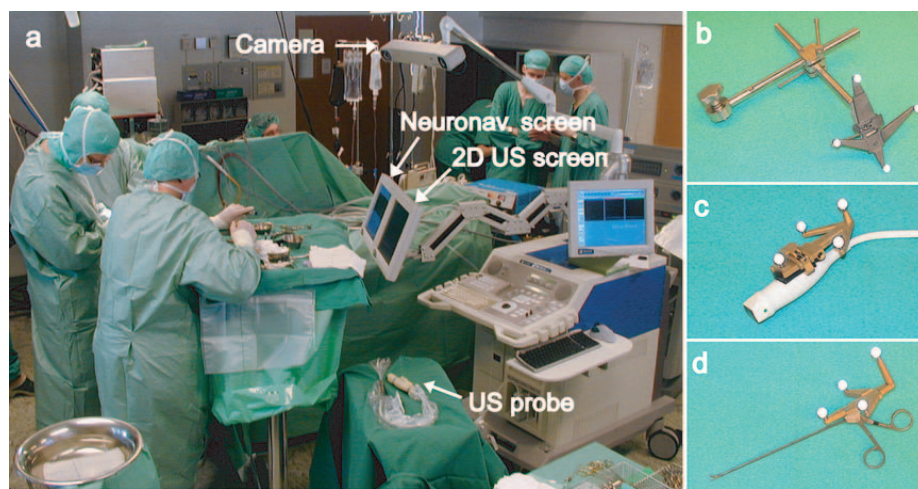


Fig. 1. (a) Prototype version of the ultrasound neuronavigation system in the operating room with the optical camera unit seen in the middle of the picture. The ultrasound probe covered with sterile drape is seen lying on a table in front of the system. Closeups of (b) the patient reference frame, (c) the ultrasound probe, and (d) the biopsy forceps are shown to the right

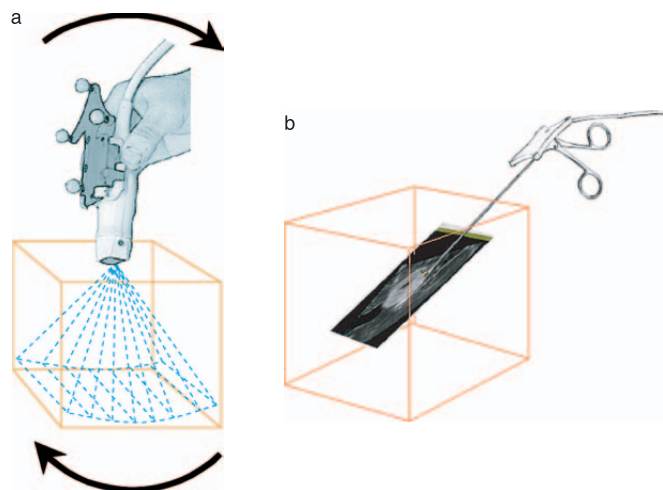


Fig. 2. The acquisition of a 3D ultrasound volume is illustrated in (a), where a volume is built from a set of 2D ultrasound scans with known spatial positions. The volume is acquired by tilting and/or translating the handheld ultrasound probe equipped with a positioning sensor. The “anyplane” view is illustrated in (b) where a single reformatted image slice is selected based on the direction and rotation of the navigation tool. The tip position of the instrument equipped with a positioning sensor is electronically marked in the image slice

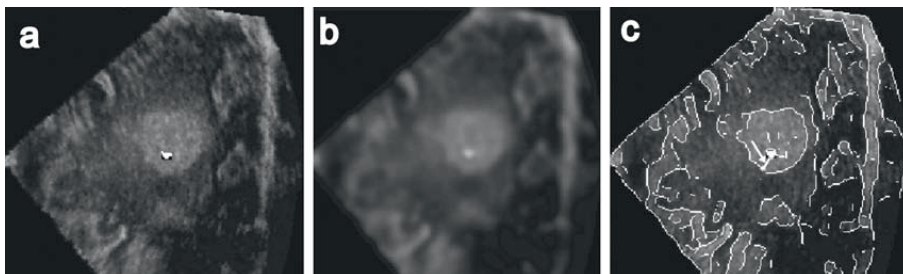


Fig. 3. Ultrasound image slice of a metastasis (a), after smoothing the image with a median filter (b) and the original data with the edges detected by the Sobel method overlaid (c). A thin bright line (see white arrow in c) indicates the calculated shortest distance of 3.9 mm between the biopsy position (marked with an triangle in the original image) and the detected tumour border

range. The resolution in the extracted image slices will vary according to the resolution in the radial, lateral and elevation direction.

Several display methods were available. For this study we used a single reformatted image, where the image plane is selected based on the direction and rotation of the surgical instrument (Fig. 2B). The system will concomitantly display reformatted cross sections of MR T1 and MR T2 corresponding to the reformatted ultrasound images. This display technique, named “anyplane view” [7, 24], was used in all biopsy samplings.

#### Image-guided biopsy sampling

The surgeon used the biopsy forceps to acquire 3 to 8 samples after a small opening in the dura but prior to any resection, using the “anyplane” ultrasound display for guidance. Biopsies were collected close to the tumour border visualized by the anyplane cross sections through 3D US volumes. The tip of the biopsy forceps was electronically marked in the 3D US cross sections and the corresponding 3D MR T1 and T2 cross sections. Just when the biopsy forceps were closed around the sample, a graphical screen dump was performed in order to document the biopsy position in all three imaging modalities. The biopsies, usually of 2–3 mm in diameter, were prepared for histopathological evaluations either by frozen sections or by paraffin sections.

#### Image interpretation and analysis

The surgeon (GU) interpreted the biopsy sites in the reformatted MR T1, MR T2 and US images as either “tumour” or “not tumour”. To test inter observer variability the US images were evaluated by another senior neurosurgeon (TBM) with less experience in US imaging and the MR images by a senior neuroradiologist (GM). The image evaluations were performed without prior knowledge as to histopathology. In some of the operations included in the study only one of the MR volumes (T1-weighted or T2-weighted) were available.

To measure the distance between biopsy position and tumour border, it was necessary to introduce a mathematical tool. In each US image the tumour borders were estimated by an edge detection algorithm, which analyzed the gradient of the gray-scale intensity in the ultrasound images, using the Sobel method implemented in Matlab 5.2 (Mathworks, Natick, MA). To smoothen the ultrasound images, they were pre-processed by applying a 2D median filter with a Hamming profile. The pre-processing suppressed speckle and high frequent noise, thus improving the output of the edge detection algorithm (Fig. 3). The shortest distance between the tip of the biopsy forceps and the detected border was calculated.

#### Histopathological analysis

A senior neuropathologist (SHT) examined the biopsies according to the WHO 2000 classification scheme [11]. All histopathological analyses were performed without prior knowledge of the image information. In the project database, the histopathological results were classified as “tumour”, or “not tumour”. Diagnoses classified as “not tumour” included oedema, gliosis and normal brain tissue. If the histopathological analysis revealed even scattered tumour cells in the tissue, the biopsy was categorized as “tumour”.

For each patient, the type of tumour was classified according to biopsies in the central part of the tumour.

## Results

#### Comparison of image findings and histopathology

Biopsies were sampled with various distances to the tumour border as seen in the ultrasound images (examples are shown in Figs. 4–7). The rate of concurrence between histopathology (“gold standard”) and image interpretation are listed in Table 3 and shown graphically in Fig. 8. There were no complications (haemorrhage, infection) related to the biopsy collection.

The agreement between US interpretation and histopathology was 74% ( $n = 31$ ) for low-grade gliomas, 83% ( $n = 18$ ) for anaplastic gliomas and 77% ( $n = 26$ ) for glioblastomas. For metastases the concurrence was 100% ( $n = 10$ ).

The sensitivity, specificity, positive and negative predictive values for US image interpretations compared to histopathology are shown in Table 4. The low negative predictive value especially for low grade gliomas (20%), but also for anaplastic gliomas and glioblastomas indicate that most of the disagreement for gliomas was due to tumour cells found in biopsies outside the US interpreted tumour border. This disagreement seems to be due mainly to well known biological factors with infiltration of tumour cells into the neighbouring brain tissue.

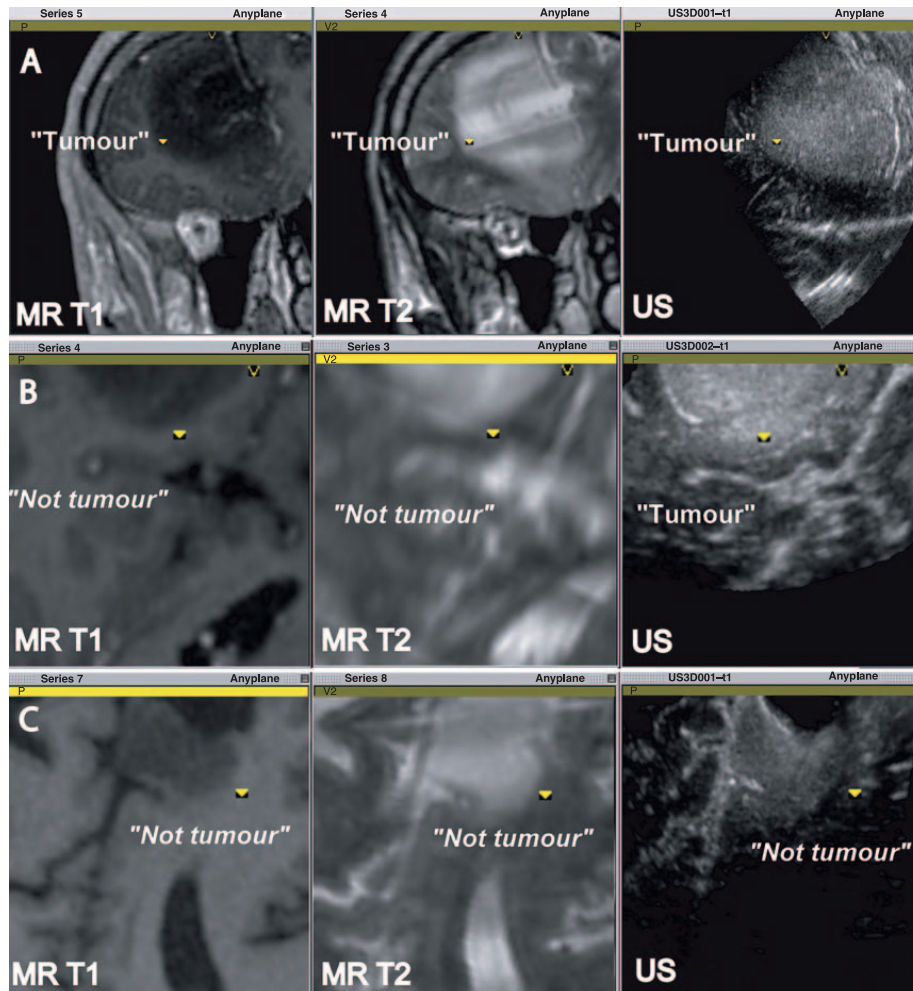


Fig. 4. Preoperative T1-weighted and T2-weighted MR images and intraoperative US images of three different low-grade astrocytomas as displayed on the intraoperative imaging system during biopsy sampling. The biopsy sites are indicated as a bright triangles in the images. The neurosurgeon's interpretation ("tumour" or "not tumour") of the images at the indicated biopsy position is written in each image slice. If written in *Italic* the interpretation of the neurosurgeon does not match the histopathology. The histopathology of the biopsies documented in the images in row A, B, and C was low-grade astrocytoma ("tumour") in all three cases

Even though comparison between the navigated US and the navigated MR was not the main objective of the study the system provides us with those data, and we think it is important to present them to help validate our interpretation of the US results.

For low-grade astrocytoma (Fig. 4) the degree of agreement between MR T1, MR T2, and US findings and histopathology were 35% ( $n = 31$ ), 59% ( $n = 27$ ), and 74% ( $n = 31$ ), respectively.

For anaplastic astrocytoma (Fig. 5) the findings in the MR T1, MR T2, and US images agreed with the histopathology in 69% ( $n = 13$ ), 79% ( $n = 14$ ), and 83% ( $n = 18$ ) of the cases, respectively.

In Fig. 5 it is shown that in a tumour classified as anaplastic astrocytoma by the central biopsies, the histopathological diagnosis of a border-zone biopsy was low-grade astrocytoma. In all lesions classified as anaplastic astrocytoma, low-grade astrocytoma was found

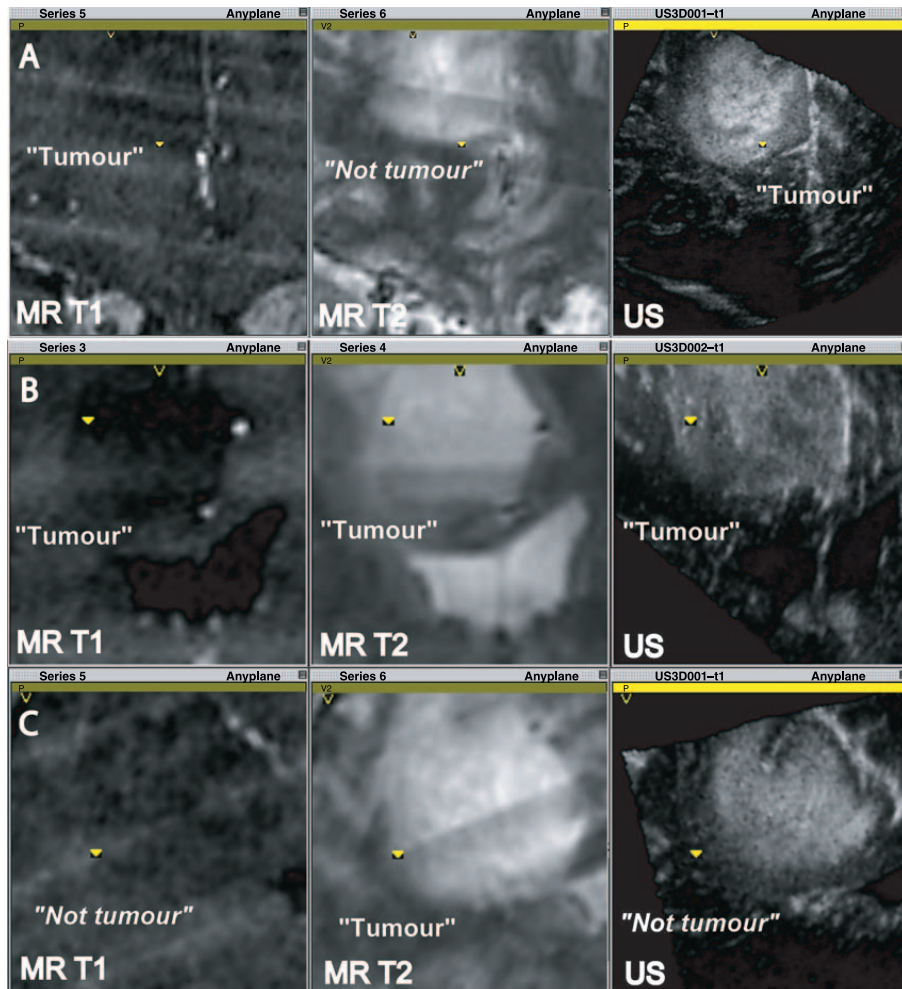


Fig. 5. Same as Fig. 4 but for anaplastic astrocytoma. For the biopsies shown in the images in row A, B and C the histopathology was low-grade astrocytoma ("tumour"). For the biopsy shown in the images in row C, the neuropathologist reported the presence of scattered tumour cells

in 9 of 14 border-zone biopsies (data not shown in Table).

For glioblastoma (Fig. 6) the results showed a concurrence rate between histopathology and findings in MR T1, MR T2 and US images of 65% ( $n=26$ ), 69% ( $n=16$ ) and 77% ( $n=26$ ), respectively. Of the ultrasound images that were not in agreement with histopathology, four of six were false positives (Tables 3, 4). Of these, two occurred in one patient (of two) with previous radiation therapy (Fig. 6B).

Excluding the two irradiated glioblastoma patients the MR T1, MR T2, and US findings agreed with histo-

pathology in 75% ( $n=20$ ), 73% ( $n=11$ ) and 80% ( $n=20$ ) of the cases, respectively.

Although the material for metastases is sparse (Fig. 7), the results show that the interpretation of the MR T1, MR T2 and US agreed with histopathology in 90% ( $n=10$ ), 86% ( $n=7$ ), and 100% ( $n=10$ ) of the cases, respectively.

Even though there is a tendency for US to give a slightly better rate of agreement with histopathology than MR, the only statistically significant value was between MR T1 and US for low-grade astrocytomas (McNemar's exact test  $P=0.005$ ).

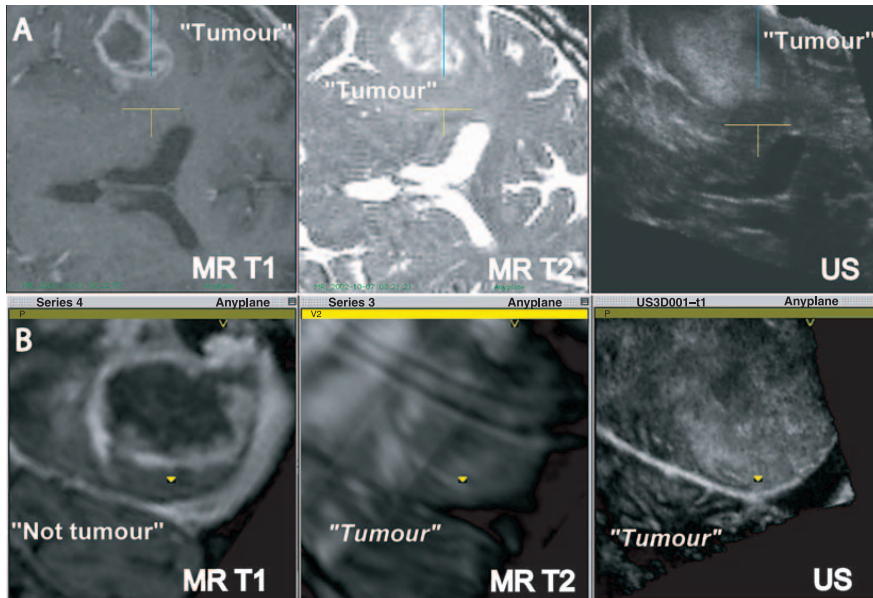


Fig. 6. Same as Fig. 4 but for glioblastoma multiforme. For the biopsy shown in the images in row A the biopsy site is at the endpoint of the vertical bar. The cross-hair was virtually extended by 10 mm in the images during biopsy sampling. The histopathology of the biopsy shown in row A was anaplastic astrocytoma ("tumour"). The images in row B documents a biopsy sampled in a patient with previous radiation therapy. The histopathology of the biopsy in B was gliosis ("not tumour")

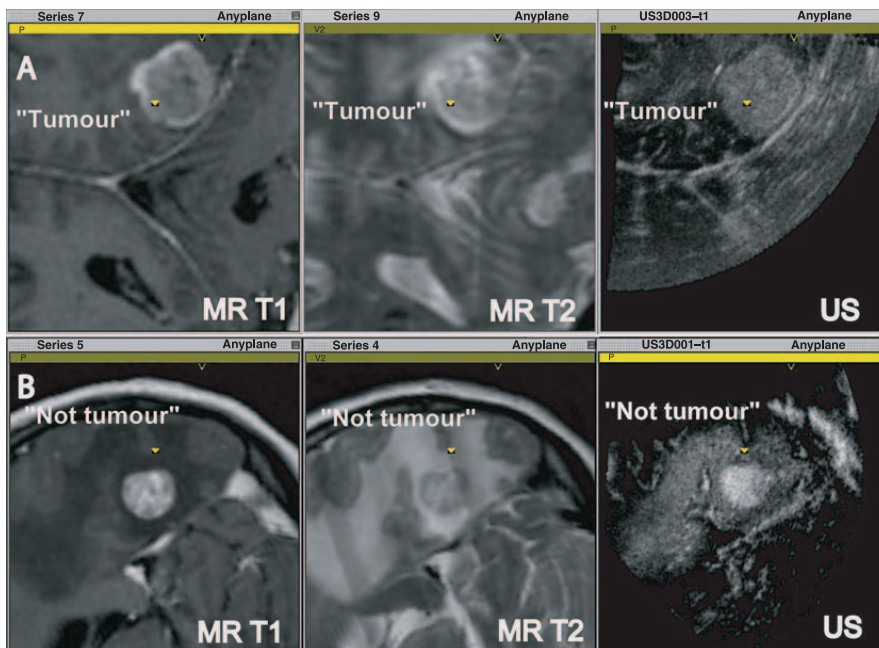


Fig. 7. Same as Fig. 4 but for metastasis. For the biopsy shown in the images in row A the histopathology was "tumour" (sarcom metastasis), while for the biopsy shown in the images in row B the histopathology was "not tumour"

Table 3. Comparison of image findings and histopathology for border-zone biopsies (2–7 mm)

Images	Histopath.	Low-grade		Anaplastic		Glioblastoma		Metastasis	
		Tumour	Not tumour	Tumour	Not tumour	Tumour	Not tumour	Tumour	Not tumour
3D UL	tumour	21	0	12	1	15	4	4	0
	not tumour	8	2	2	3	2	5	0	6
MR T1	tumour	9	0	6	0	10	2	4	1
	not tumour	20	2	4	3	7	7	0	5
MR T2	tumour	14	0	9	1	9	3	3	1
	not tumour	11	2	2	2	2	2	0	3

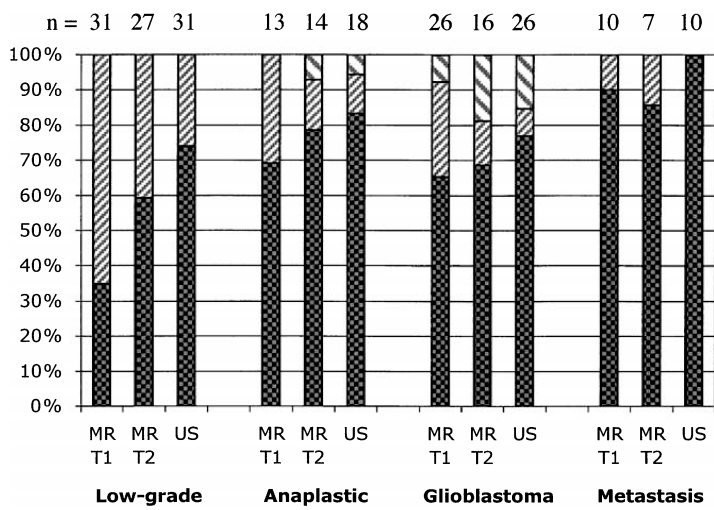


Fig. 8. The results of the comparison between image findings and histopathology for border-zone biopsies (2–7 mm) shown as a bar chart. Each bar describes the rate of agreement between histopathology and interpretation of the image at the biopsy site. False negative; biopsy sites with normal image and tumour histopathology. False positive; biopsy sites with tumour image and normal histopathology. The number of cases for each image modality and tumour classification is shown above each bar. False negative; False positive; Rate of agreement

Table 4. The sensitivity, specificity, positive predictive value (PPV) and negative predictive value (NPV) of the US image interpretations compared to histopathology

	Sensitivity (%)	Specificity (%)	PPV (%)	NPV (%)
Low-grade astrocytoma	72	100	100	20
Anaplastic astrocytoma	86	75	92	60
Glioblastoma multiforme	88	56	79	71
Metastasis	100	100	100	100

#### Image interpretation by different observers

The degree of match between interpretation of image and histopathology for the neuroradiologist was similar to the results obtained by the neurosurgeon. The Cohen's Kappa value for inter observer variability was 0.84 for MR T1 and 0.71 for MR T2. Two neurosurgeons interpreted the US images, one with a long experience of US and one with a shorter experience. For the two

neurosurgeons only 4 of 85 ultrasound images were interpreted differently, resulting in a Kappa value of 0.89.

#### Discussion

##### Delineation of tumour

Delineation of tumour borders in different imaging modalities will differ according to the physical properties of the imaging modality and the biology of the tissue. In US images, the echogenicity is related to the fluctuations in mass density and stiffness of the tissue. In MR images the source of information is the magnetic properties of the hydrogen nuclei in the tissue. Our results show that navigated US is just as good as navigated MR T2, and better than navigated MR T1 in detecting the tumour border as evaluated by histopathology. There is a possibility that a registration error and brain shift could impair the result for preoperative MR, although the study was

designed to minimize the influence of these sources of error.

It is well known that tumour cells infiltrate beyond the MR defined tumour borders [6, 10, 18]. As expected, that is the same for US, as shown by the false negative results, especially in low-grade astrocytomas. US, like MR, underestimates the extent of tumour cell infiltration, but it can certainly delineate the major component of the tumour where the overwhelming part of the tissue is tumour cells. The presence of scattered tumour cells in several of the biopsies where the US and MR images did not indicate tumour cells does not necessarily reduce the usefulness of intraoperative 3D US, because tissue with scattered tumour cells in normal tissue should usually not be resected, especially in eloquent areas.

Few biopsies with normal tissue were collected inside the US interpreted tumour border (high positive predictive value), indicating that navigated 3D US is a safe way of delineating the tumour in a clinical setting by not jeopardizing the normal brain tissue.

Metastases are mostly well circumscribed. The results for metastases show that no tumour cells were found in biopsies sampled beyond the tumour borders indicated in the ultrasound images.

Gliomas are known to be heterogeneous. Nine of 14 border zone biopsies of tumours classified as anaplastic astrocytoma (according to central biopsies) were diagnosed as low-grade astrocytoma (data not shown in Table). One interpretation could be that anaplastic astrocytoma has developed from the central part of a low-grade astrocytoma.

For glioblastoma multiforme, four of the US images indicating tumour were false positive. In a comparative study of tumour volumes estimated by intraoperative ultrasound and preoperative CT, LeRoux *et al.* reported that ultrasound tends to overestimate the tumour volume for recurrent and irradiated tumours and that the presence of gliosis may account for the increase in volume [14]. Also, Hammoud *et al.* [8] reported that US imaging of tumour margins for gliomas was impaired in patients with radiation-induced lesions. This radiation-induced gliosis usually contain few active neuronal elements. However, it is important to be aware of this limitation of ultrasound delineation of irradiated tumour during resection.

#### *Inter observer evaluation*

The independent evaluations of the findings in 3D US by two neurosurgeons gave very similar results for all

tumours investigated. The Kappa test showed a very good agreement, suggesting that the US evaluations are highly reproducible. Both neurosurgeons have experience in using US in brain tumour surgery. We are, however, convinced that the learning curve is steep and that devoted users will readily reach the same level of precision. The Kappa test for the independent evaluation of MR by the neurosurgeon and the neuroradiologist showed good agreement, excluding the possibility of bias by the neurosurgeon.

#### *Error sources*

A possible source of error is introduced by the methodology used to document the location of the biopsy sample. The graphical screen dump, performed manually on the intraoperative imaging system, should be done exactly at the time the biopsy is sampled. Any movements of the biopsy forceps between the time of sampling and the time of the screen dump might introduce an error in the biopsy position as shown in the MR and US images. Other error sources are the imaging accuracy of 3D ultrasound, which is in the order of 1.4 mm [17] and the size of the biopsy forceps (3 mm). To minimize the influence of these error sources, biopsies located less than 2 mm from the tumour border were excluded. In that way the uncertainty as to whether the biopsy is taken on the tumour side or the normal side of the border as visualized by ultrasound, is minimized.

Another source of error is the histopathology. The size of the biopsy samples was in the range of diameter 2–3 mm. Sources of failure regarding evaluations of small biopsies are: difficulties in malignancy grading of the tumour tissue, not representative biopsies, and difficulties of establishing a definite tumour diagnosis (i.e. gliosis vs. glioma). It is possible that using a smear technique instead of sections could reduce the histopathology error, but we had to stick to the technique that our neuropathologist was familiar with. Paraffin sections are superior to frozen sections in tumour diagnosis. However, in this study 32 (38%) of the border-zone biopsies were prepared as frozen sections, providing a basis for improved resection control.

An idea of the contribution of these sources of error to the final result could be derived from biopsies collected in the central part of the tumour more than 7 mm from the border. The concurrence rate should ideally be 100%, but it was found to be 94.7% (n = 19), giving an indirect quantification of the problems with the “gold standard”.

### Ethical aspects

The ethical aspect of intentional sampling of biopsies in the outer border of the tumour, as seen in the MR and US images, was given consideration. Biopsies from the outside of the US indicated tumour border were never sampled in eloquent areas. As a result fewer biopsies were collected on the outside than on the inside of the US visible tumour border. Most of the biopsies from the outside were also sampled on the route from the surface to the tumour. All together we never saw a haemorrhage or any other complication that could be related to biopsy sampling.

### Conclusions

In the present study we have compared the surgeons interpretation of the biopsy sites in reformatted US and MR images with histopathology. The biopsies were collected at the border of gliomas and metastases with equipment that enables concomitant navigation in preoperative registered 3D MR volumes and intraoperative acquired 3D ultrasound volumes. The results indicate that US, in the same way as MR, underestimates the extent of glioma cell infiltration, especially for low-grade gliomas. But it also shows that before starting the resection, reformatted 3D ultrasound is just as reliable as MR to localize and delineate metastases and the solid component of glial tumours. This result makes it reasonable to carry on with the 3D US technology, but it does not tell whether 3D US provides sufficient intraoperative information for the surgeon in the presence of resection artefacts. Another study is therefore under way to test the reliability of 3D ultrasound during and at the end of resection.

### Acknowledgement

This work was supported by a grant from the Research Council of Norway through the Strategic University Program in Medical Technology at the Norwegian University of Science and Technology (NTNU), and the Norwegian ministry of Health and Social Affairs through the National Center of Competence in 3D ultrasound. We also acknowledge a donation from the Fossum family. We wish to thank Stian Lydersen at the Norwegian University of Science and Technology for his valuable help and assistance with the statistical analysis.

### References

- Auer LM, Velthoven VV (1990) Intraoperative Ultrasound (US) Imaging. Comparison of pathomorphological findings in US and CT. *Acta Neurochir (Wien)* 104: 84–95
- Bohinski RJ, Kokkino AK, Warnick RE, Gaskill-Shibley MF, Kormos DW, Lukin RR, Tew JM (2001) Glioma resection in a shared-resource magnetic resonance operating room after optimal image-guided frameless stereotactic resection. *Neurosurgery* 48: 731–744
- Bonsanto MM, Staubert A, Wirtz CR, Tronnier V, Kunze S (2001) Initial experience with an ultrasound-integrated single-rack neuro-navigation system. *Acta Neurochir (Wien)* 143: 1127–1132
- Comeau RM, Sadikot AF, Fenster A, Peters TM (2000) Intraoperative ultrasound for guidance and tissue shift correction in image-guided neurosurgery. *Med Phys* 27: 787–800
- Di Lorenzo N, Esposito V, Lunardi P, Delfini R, Fortuna A, Cantore G (1991) A comparison of computerized tomography-guided stereotactic and ultrasound-guided techniques for brain biopsy. *J Neurosurg* 75: 763–765
- Earnest F, Kelly PJ, Scheithauer BW, Kall BA, Cascino TL, Ehman RL, Forbes GS, Axley PL (1988) Cerebral astrocytomas: histopathologic correlation of MR and CT contrast enhancement with stereotactic biopsy. *Radiology* 166: 823–827
- Grønningsæter Å, Kleven A, Ommedal S, Årseth TE, Lie T, Lindseth F, Langø T, Unsgård G (2000) SonoWand, an ultrasound-based neuronavigation system. *Neurosurgery* 47: 1373–1380
- Hammoud MA, Ligon BL, ElSouki R, Shi WM, Shomer DF, Sawaya R (1996) Use of intraoperative ultrasound for localizing tumors and determining the extent of resection: a comparative study with magnetic resonance imaging. *J Neurosurg* 84: 737–741
- Hata N, Dohi T, Iseki J, Takakura K (1997) Development of a frameless and armless stereotactic neuronavigation system with ultrasonographic registration. *Neurosurgery* 41: 608–614
- Kelly PJ, Dumas-Duport C, Kispert DB, Kall BA, Scheithauer BW, Illig JJ (1987) Imaging-based stereotactic serial biopsies in untreated intracranial glial neoplasms. *J Neurosurg* 66: 865–874
- Kleihues P, Cavenee WK (eds) (2000) *Pathology and Genetics of Tumours of the Nervous System: World Health Organization Classification of Tumours*, IARC Press. Lyon
- Knauth M, Wirtz CR, Tronnier VM, Aras N, Kunze S, Sartor K (1999) Intraoperative MR imaging increases the extent of tumor resection in patients with high-grade gliomas. *AJNR Am J Neuroradiol* 20: 1642–1646
- Koivukangas J, Louhisalmi Y, Alakujala Y, Oikarinen J (1993) Ultrasound-controlled neuronavigator-guided brain surgery. *J Neurosurg* 79: 36–42
- LeRoux PD, Berger MS, Ojemann GA, Wang K, Mack LA (1989) Correlation of intraoperative ultrasound tumour volumes and margins with preoperative computerized tomography scans. An intraoperative method to enhance tumour resection. *J Neurosurg* 71: 691–698
- LeRoux PD, Berger MS, Wang K, Mack LA, Ojemann GA (1992) Low grade gliomas: comparison of intraoperative ultrasound characteristics with preoperative imaging studies. *J Neuro-Oncol* 13: 189–198
- LeRoux PD, Winter TC, Berger MS, Mack LA, Wang K, Elliot JP (1994) A comparison between preoperative magnetic resonance and intraoperative ultrasound tumor volumes and margins. *J Clin Ultrasound* 22: 29–36
- Lindseth F, Langø T, Bang J, Nagelhus Hernes TA (2002) Accuracy evaluation of a 3D ultrasound-based neuronavigation system. *Comput Aided Surg* 7: 197–222
- Lunsford LD, Martinez AJ, Latchaw RE (1986) Magnetic resonance imaging does not define tumor boundaries. *Acta Radiol [Suppl]* 369: 154–156
- Martin AJ, Hall WA, Liu H, Pozza CH, Michel E, Casey SO, Maxwell RE, Truwitt CL (2000) Brain tumor resection: intraoperative monitoring with high-field-strength MR imaging-initial results. *Radiology* 215: 221–228
- Maurer M, Becker G, Wagner R, Woydt M, Hofmann E, Puls I, Lindner A, Krone A (2000) Early postoperative transcranial sono-

- graphy (TCS), CT, and MRI after resection of high grade glioma: evaluation of residual tumour and its influence on prognosis. *Acta Neurochir (Wien)* 142: 1089–1097
21. Regelsberger J, Lohmann F, Helmke K, Westphal M (2000) Ultrasound-guided surgery of deep seated brain lesions. *Eu J Ultras* 12: 115–121
  22. Schneider JP, Schulz T, Schmidt F, Dietrich J, Lieberenz S, Trantakis C, Seifert V, Kellermann S, Schober R, Schaffranietz L, Laufer M, Kahn T (2001) Gross-total surgery of supratentorial low-grade gliomas under intraoperative MR guidance. *Am J Neuro-radiol* 22: 89–98
  23. Unsgaard G, Gronningsaeter A, Ommedal S, Nagelhus Hernes TA (2002) Brain operations guided by real-time two-dimensional ultrasound: new possibilities as a result of improved image quality. *Neurosurgery* 51: 402–411
  24. Unsgaard G, Ommedal S, Muller T, Gronningsaeter A, Nagelhus Hernes TA (2002) Neuronavigation by intraoperative three-dimensional ultrasound: initial experience during brain tumor resection. *Neurosurgery* 50: 804–812
  25. Wirtz CR, Knauth M, Staubert A, Bonsanto MM, Sartor K, Kunze S, Tronnier VM (2000) Clinical evaluation and follow-up results for intraoperative magnetic resonance imaging in neurosurgery. *Neurosurgery* 46: 1112–1122
  26. Woydt M, Krone A, Becker G, Schmidt K, Roggendorf W, Roosen K (1996) Correlation of intra-operative ultrasound with histopathologic findings after tumour resection in supratentorial gliomas. *Acta Neurochir (Wien)* 138: 1391–1398

### Comment

The authors report on a correlative clinical series in which they operated 28 patients with a broad spectrum of pathologies and took altogether 85 biopsies from the surrounding area which they detected by 3D intraoperative ultrasound. By virtue of a biopsy forceps equipped with a positioning sensor, preoperative T1, T2 MR slices and ultrasound were simultaneously displayed to indicate the position of the biopsy and these images were interpreted (scored?) by the surgeon to be later correlated with histological findings.

This is an interesting technological study by a group which is very experienced in three-dimensional intraoperative ultrasound. A major problem with such studies which correlate images, subjective scoring and solid data like presence of cells in histological sections is that of parametrization. The major concession which has to be made is, that the whole study does not have any solid measurable data except the number of cells in the sections. All else is subjective and even in the MRI the definition of tumor vs boundary is highly divergent between different scoring individuals. The results are not surprising because low grade gliomas are very diffuse and are difficult to delineate already on the scans. With the high grade tumors, the boundary may be sharper and therefore “easier” to score on the MR and correspondingly in the US but as the authors admit, tumor cells were frequently also outside the areas scored as tumor. Metastases should be very well delineated and provide the best correlation and if it does not reach 100% it is due to the inaccuracy of the navigation systems (2mm) because even histologically the boundaries are very sharp. The question remains, why was this study done except than to verify the expertise of the single surgeon who did the operations? A true test would be to see if people with less experience would have the same results.

The study has its merit in illustrating that with 3D ultrasound, surgeons may have a very useful realtime guidance during surgery which is not affected by frameshift. This should be emphasized and put forward as a message, leaving out all statistics and percentages and significances because they relate to something which is not measured by any electrophysiological, biochemical or pharmacological method but based on a person-based rating scheme. The authors say already, that both, MR and US underestimate the infiltration and are mainly useful to delineate the major component of the tumors. That is what the real purpose is, stay close to the tumor, see it diminish during resection and get an estimate of radicality to not leave major parts behind. In that respect, US as presented here may be as good as intraoperative MRI which would be the real comparator because it is a realtime technique which is compared to the preoperative reference scans in the navigation computer.

*Manfred Westphal*  
Hamburg

Correspondence: Geirmund Unsgaard, St. Olav University Hospital, 7005 Trondheim, Norway. e-mail: geirmund.unsgard@medisin.ntnu.no



# Paper V



## Comparison of navigated 3D ultrasound findings with histopathology in subsequent phases of glioblastoma resection

Ola Morten Rygh · Tormod Selbekk ·  
Sverre Helge Torp · Stian Lydersen ·  
Toril Anita Nagelhus Hernes · Geirmund Unsgaard

Received: 11 November 2007 / Accepted: 22 June 2008 / Published online: 5 September 2008  
© Springer-Verlag 2008

### Abstract

**Objective** The purpose of the study was to compare the ability of navigated 3D ultrasound to distinguish tumour and normal brain tissue at the tumour border zone in subsequent phases of resection.

**Materials and methods** Biopsies were sampled in the tumour border zone as seen in the US images before and during surgery. After resection, biopsies were sampled in the resection cavity wall. Histopathology was compared with the surgeon's image findings.

**Results** Before resection, the tumour border was delineated by ultrasound with high specificity and sensitivity (both 95%). During resection, ultrasound had acceptable sensi-

tivity (87%), but poor specificity (42%), due to biopsies falsely classified as tumour by the surgeon. After resection, sensitivity was poor (26%), due to tumour or infiltrated tissue in several biopsies deemed normal by ultrasound, but the specificity was acceptable (88%).

**Conclusions** Our study shows that although glioblastomas are well delineated prior to resection, there seem to be overestimation of tumour tissue during resection. After resection tumour remnants and infiltrated brain tissue in the resection cavity wall may be undetected. We believe that the benefits of intraoperative ultrasound outweigh the shortcomings, but users of intraoperative ultrasound should keep the limitations shown in our study in mind.

O. M. Rygh  
Department of Radiology, St.Olav University Hospital,  
Trondheim, Norway

O. M. Rygh · S. H. Torp · G. Unsgaard  
Department of Neuroscience,  
Norwegian University of Science and Technology,  
Trondheim, Norway

T. Selbekk · T. A. N. Hernes  
SINTEF Health Research, Trondheim, Norway

O. M. Rygh · T. Selbekk · T. A. N. Hernes · G. Unsgaard  
National Centre for 3D Ultrasound in Surgery,  
St.Olav University Hospital, Trondheim, Norway

S. H. Torp  
Department of Pathology and Medical Genetics,  
St Olav University Hospital, Trondheim, Norway

S. Lydersen  
Unit for Applied Clinical Research,  
Department of Cancer Research and Molecular Medicine,  
Norwegian University of Science and Technology,  
Trondheim, Norway

G. Unsgaard  
Department of Neurosurgery,  
St.Olav University Hospital, Trondheim, Norway

T. A. N. Hernes  
Department of Circulation and Medical Imaging,  
Norwegian University of Science and Technology,  
Trondheim, Norway

S. H. Torp  
Section of Morphology, Department of Laboratory Medicine,  
Children's and Women's Health, Faculty of Medicine,  
Norwegian University of Science and Technology (NTNU),  
Trondheim, Norway

O. M. Rygh (✉)  
Vegmesterstien 17c, 7022 Trondheim, Norway  
e-mail: ola.rygh@ntnu.no

**Keywords** Brain tumour surgery · Biopsies · Histopathology · Intraoperative imaging · Neuronavigation · Three-dimensional ultrasound imaging

#### Abbreviations

US	ultrasound
3D	three dimensional
MHz	megahertz
PPV	positive predictive value
NPV	negative predictive value
ROC	receiver operating characteristics
AUC	area under curve

#### Background

In the surgical treatment of glioblastomas the goal is to perform the most complete resection possible without damaging normal tissue [2, 17]. Neuronavigation systems have become part of the routine tools assisting the surgeon in achieving this goal. Intraoperative imaging appears to be necessary to maintain accuracy of neuronavigation during subsequent stages of tumour resection [19, 25, 29]. To be of value, intraoperative imaging modalities must reliably discriminate between tumour and normal tissue in the subsequent stages of surgery. At present, the alternatives for intraoperative imaging in brain tumour surgery are MRI and ultrasound [10, 11, 20, 24, 31]. Although recognized to be useful for detecting residual tumour during resection [9, 30, 35, 36], it is not known how intraoperative factors affect the ability of ultrasound to delineate tumour. The aim of the present study was to assess the ability of intraoperative 3D ultrasound in neuronavigation to distinguish tumour and normal brain tissue in the tumour border zone, before, during and after resection.

#### Materials and methods

##### Patients and biopsies

Nineteen patients (four females and 15 males, average age 59, age range 45–83 years) with the final diagnosis of glioblastoma were included in the present study. The patients were included in the period 2003–2006. A total of 301 biopsies were acquired, 186 biopsies were included in this study. The study was approved by the Regional Research Ethics Committee in medicine in Mid-Norway and the patients signed an informed consent form before the operation.

##### Neuronavigation equipment and intraoperative 3D ultrasound imaging

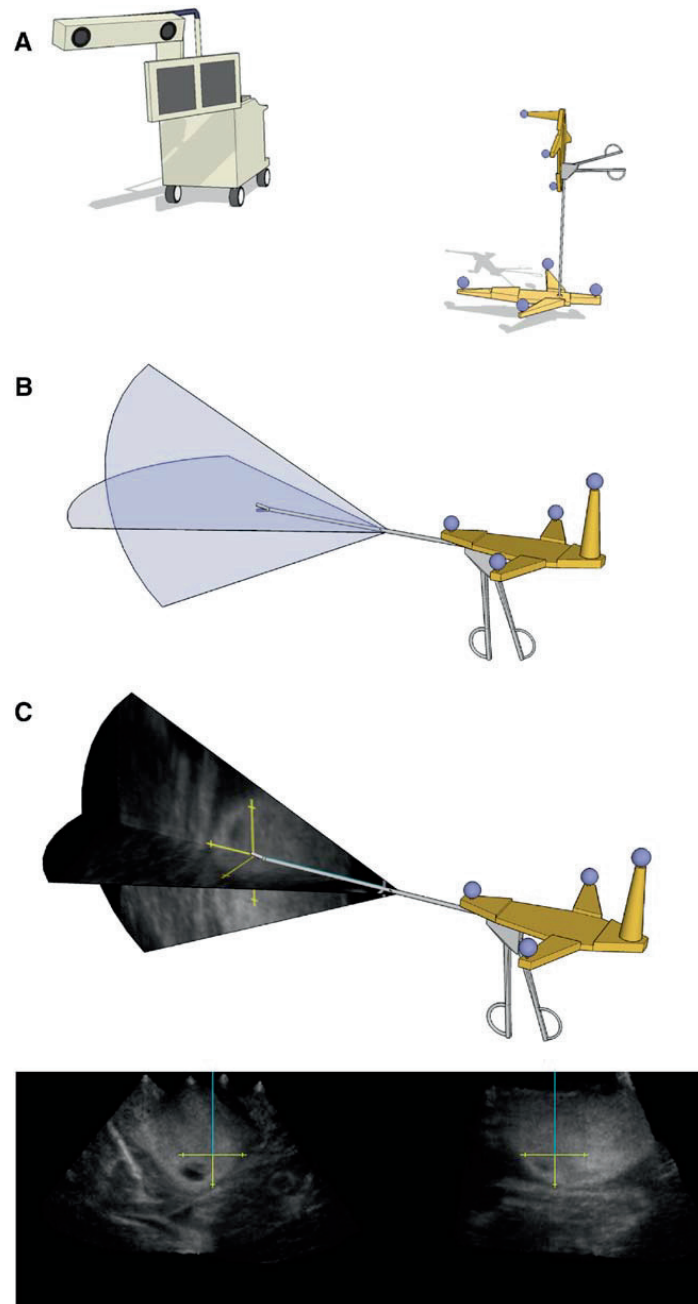
A 3D ultrasound based image guidance system was used; SonoWand<sup>®</sup>, equipped with a 5 MHz probe with tracking. The biopsy forceps used in the study was equipped with a tracking frame, which enabled image guided biopsies (Fig. 1). This system is described in further detail in other papers [8, 21, 37]. Preoperative MRI (T1 with contrast enhancement, T2 and FLAIR) was imported in the neuronavigation system and used for planning and anatomical orientation, but not during biopsy sampling. 3D ultrasound data was acquired immediately before biopsy sampling in each phase (Fig. 2). When a resection cavity had been created, the cavity was filled with saline before 3D ultrasound acquisition. The saline was removed afterwards.

##### Image-guided biopsy sampling and analysis

The biopsies were sampled in three different phases of resection; (1) After opening the dura, immediately before starting the resection. (2) After most resection had been performed, but with some residual tumour left. (3) After completed resection, having removed all detected/known residual tumour (either detected visually or by use of intraoperative ultrasound) except in eloquent areas. The biopsy forceps was calibrated to the navigation system by positioning the tip of the biopsy forceps at a reference point on the patient reference frame (Fig. 1.) The position and trajectory of the biopsy forceps was displayed on two perpendicular image slices on the neuronavigation unit, marking the biopsy site. The surgeon's assumption on whether the biopsy was sampled in tumour or normal tissue based on the ultrasound image findings was noted at the time of biopsy sampling. The surgeon classified the biopsies as "tumour", "tumour, uncertain", "normal uncertain" and "normal". Images (snapshots) from the neuronavigation system taken at the time of biopsy sampling were stored for further processing and analysis.

The biopsies were collected from the border-zone of the tumour, not further from the assumed tumour border in the US images (as judged by the surgeon) than 7 mm and not closer than 2 mm. After completed resection however, biopsies were only collected from the resection cavity wall. Before and during resection, two to four biopsies were collected in assumed solid tumour tissue, while one to three biopsies were sampled from assumed normal brain tissue. All biopsies included in the study were postoperatively controlled to ensure that they were sampled in the 2–7 mm distance from the tumour border as defined from the navigation images. Biopsies outside the 2–7 mm area of interest were excluded, and this was the most frequent reason for exclusion of biopsies. In cases of doubt, the

**Fig. 1** Biopsy sampling method. **a** The biopsy forceps is calibrated to the navigation system by positioning the tip of the forceps in a known reference point on the patient reference frame, in the shape of a small cone with a hole in the middle. **b** Two perpendicular planes are determined by the position and trajectory of the biopsy forceps. **c** The 3D ultrasound data volume is sliced in the two perpendicular planes, displayed on screen (*bottom*). The tip of the biopsy forceps is thus indicated in the two image planes, marking the site for biopsy sampling



screenshots were analyzed with an edge-detection algorithm (described elsewhere [38]). The shortest distance between the tip of the biopsy forceps and the detected border was then found. Biopsies where the pathologist

could not categorize the biopsy, for example, because of too small or traumatized biopsies, were also excluded.

The majority of biopsies (176 of 186 included biopsies) was fixed in buffered formalin and embedded in paraffin.

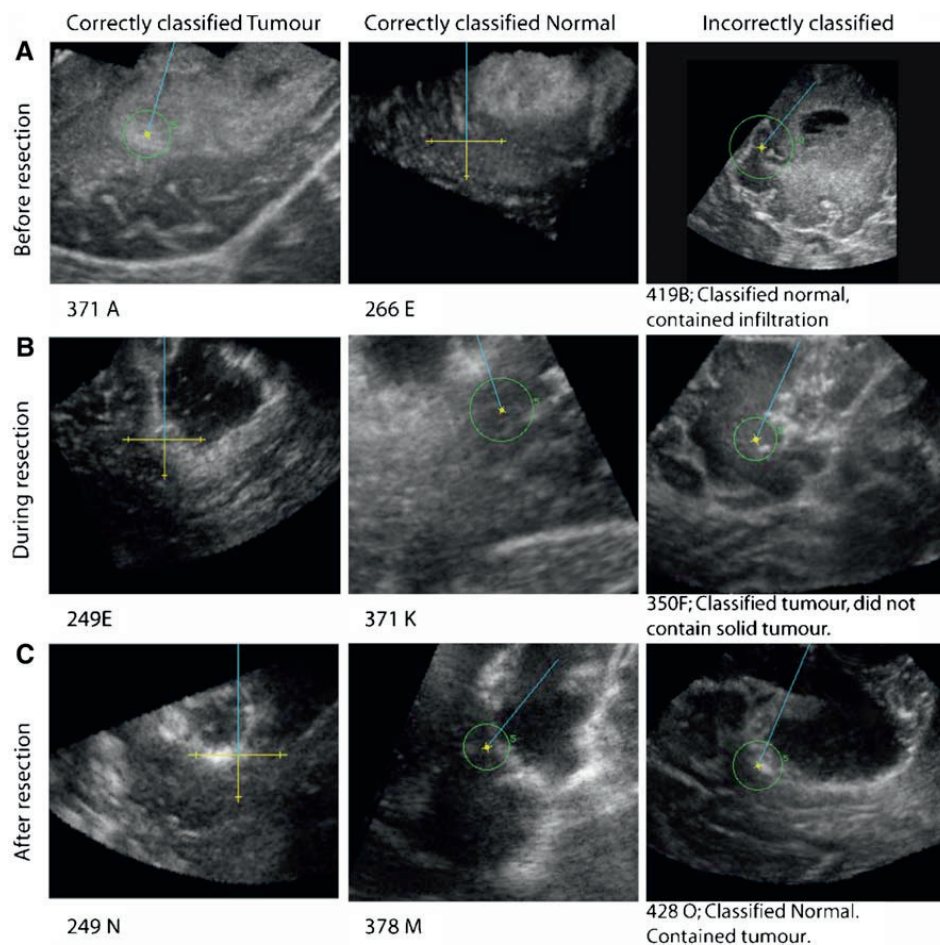


**Fig. 2** Biopsy examples. **a** Screenshots from biopsy sampling before resection. *Left:* Biopsy sampled from area interpreted as tumour, confirmed by histopathology. *Middle:* Biopsy sampled from site interpreted as normal, confirmed by histopathology. *Right:* Biopsy sampled from site interpreted as normal, histopathology showed infiltration. **b** Screenshots from biopsy sampling during resection. *Left:* Biopsy sampled from site interpreted as tumour, confirmed by histopathology. *Middle:* Biopsy sampled from site interpreted as

normal, confirmed by histopathology. *Right:* Biopsy sampled from site interpreted as tumour, but the pathologist saw no certain tumour tissue. **c** Screenshots from biopsy sampling after resection. *Left:* biopsy sampled from site interpreted as “tumour, uncertain”, tumour confirmed by histopathology. *Middle:* Biopsy sampled from site interpreted as normal, confirmed by histopathology. *Right:* Biopsy sampled from site interpreted as normal, but histopathology showed tumour

Ten biopsies were prepared as frozen sections. The sections were stained with hematoxylin and eosin. A senior neuropathologist (SHT) examined the biopsies according to the WHO classification [1]. All histopathological analyses were performed without prior knowledge of the image information. The biopsies were classified as “tumour”/“infiltration zone”/“not tumour”. All but three of the patients had a postoperative MRI within 48 h.

#### Statistical methods

To calculate specificity, sensitivity, PPV and NPV, the cells in the original  $3 \times 4$  result table from each phase (Table 2) were combined to create a  $2 \times 2$  table for each phase of the operation: Biopsies deemed “normal” and “normal, uncertain” by the surgeon were combined, and likewise biopsies deemed “tumour” and “tumour, uncertain” were combined.

Furthermore, biopsies that the pathologist classified as “infiltration zone” were combined with those classified as “tumour”. The ROC curves were constructed by calculating sensitivity and specificity for the three different possible cut-off points for surgeon’s judgment, one ROC curve for each phase of resection (Fig. 3).

## Results

Of 301 total biopsies acquired, 186 were included in our analyses. Table 1 shows the number of biopsies included/excluded in each phase of surgery. The histopathological diagnoses of the biopsies and the corresponding ultrasound findings for each of the stages of resection are shown in Table 2. The calculated values for specificity, sensitivity, NPV and PPV are listed in Table 3. Before resection, both sensitivity and specificity were 95%, while PPV and NPV were 98% and 90%, respectively. During resection, sensitivity was 88% but specificity had dropped to 42%. PPV and NPV was 73% and 67% respectively. After resection, sensitivity was 26% and specificity was 88%, while PPV and NPV both were 62%. The ROC curve for ultrasound in each stage of surgery is displayed in Fig. 3, and the area under the curve (AUC) is stated in the figure legend.

Although comparison of ultrasound and MRI was not a part of the study protocol, 16 of the 19 patients had early postoperative MRI (within 72 h). In 13 of these 16 patients the neurosurgeon also assessed the resection grade at the end of resection using 3D ultrasound. Among these, ten patients were considered either 90–95% or >95% resected. Two of the 10 patients had residual tumour on early postoperative MRI; one patient considered 90–95% resected and another considered >95% resected. The other eight patients had no residual tumour found on early postoperative MRI. In the remaining three patients (of the 13 with both early postoperative MRI and resection grade assessment), residual tumour was intentionally left behind because of unacceptable risk of neurological damage. Two of them had residual tumour on postoperative MRI, while one was considered to possibly have residual tumour.

Sixteen of the 19 patients had a good outcome with no new neurological deficits.

Two of the patients had a fair outcome with mild new neurological deficits, and one patient had a poor outcome,

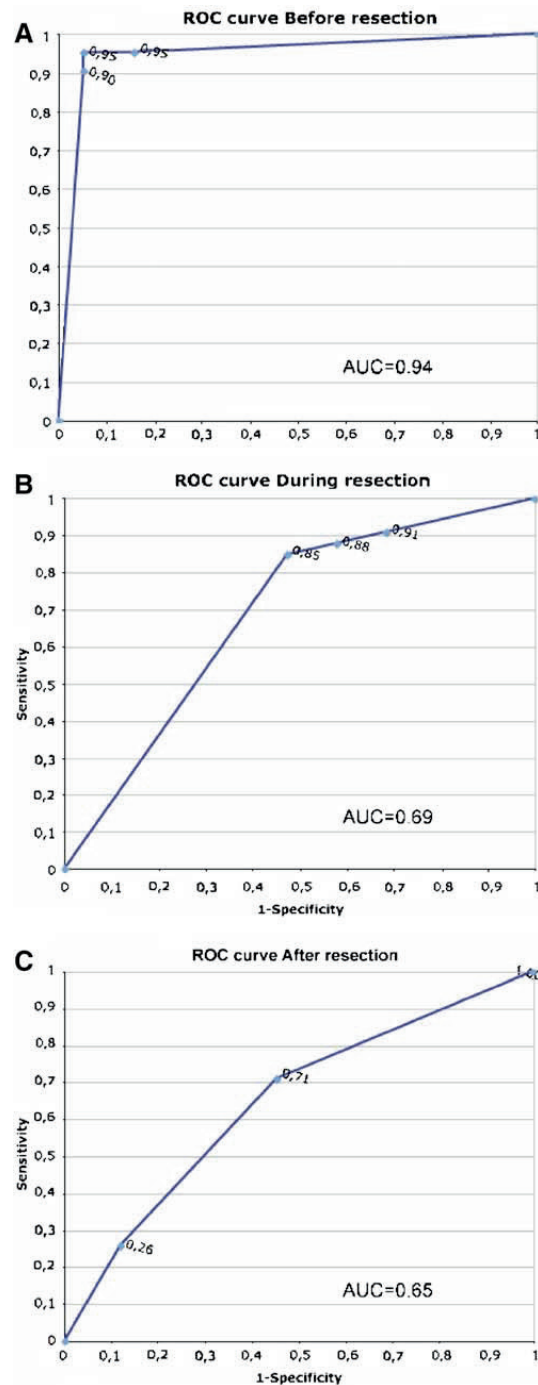


**Fig. 3** ROC curves. ROC curves for the ability of ultrasound to distinguish tumour from normal tissue. **a** ROC curve before resection, showing high accuracy (AUC=0.94). **b** ROC curve during resection. Compared to the ROC curve before resection the accuracy of ultrasound is decreased. (AUC=0.69). **c** ROC curve after resection. Compared to the ROC curve before and during resection, the accuracy is further decreased (AUC=0.65)

**Table 1** Biopsies

Parameter		Included	Excluded	Total
Total number of biopsies for patients included in study	Before resection	61	56	117
	During resection	52	47	99
	After resection	73	12	85
Average number of biopsies per patient	Before	3.2	2.9	NA
	During	2.7	2.5	NA
	After	3.8	0.6	NA
Total number of biopsies (overall)				301

The table shows the number of biopsies sampled in each phase of the resection, and the number of biopsies excluded and included. In the lower part of the table the average number of biopsies in each patient is shown.

with hemiparesis and aphasia. None of the patients had complications related to the procedure.

## Discussion

### General considerations

Delineation of gliomas poses a challenge to any imaging modality, as tumour cells infiltrate the normal brain tissue beyond the solid tumour border. In this sense, definition of a specific tumour border is impossible. For practical purposes, however, to delineate a glioblastoma usually means to outline the solid part of a tumour, of which removal is the goal of surgical resection.

Several authors have evaluated different diagnostic imaging modalities for delineation of gliomas, comparing image findings with histopathology [3, 5–7, 13, 16, 22, 23, 28, 32]. Also infiltrated brain tissue may be detected by new imaging techniques [28, 32]. In neuronavigation, intraoperative imaging is now increasingly recognized as important to amend for inaccuracy due to brain shift, and facilitate detection of residual tumour. Ultrasound and MRI are the commonly used modalities in this regard [12, 15, 26, 27, 36, 39]. However, it is not entirely known to what degree intraoperative factors affect intraoperative imaging, and the studies comparing image findings with histopathology in the

intraoperative setting are scarce. Reporting on intraoperative MRI, Sutherland [34], found that intraoperatively, the contrast-enhancing margin advanced beyond the preoperatively defined contrast limits, and that biopsy samples from this zone contained tumour tissue. Knauth [14] argue that surgically induced contrast enhancement may be misinterpreted as residual tumour in intraoperative MRI, but only in one case was this confirmed with a biopsy, obtained in a contrast-enhancing area which proved to contain normal tissue. Surgically induced contrast enhancement in intraoperative MRI at the resection border, mimicking residual tumour, is also mentioned by other authors [26, 33, 39]. In ultrasound, reverberations, refraction of the ultrasound beam, artefacts due to slice thickness among others, may all cause imaging artefacts which may be misleading. During tumour resection, air bubbles, debris, blood, and the rough surface of the tumour cavity wall probably increase the occurrence of imaging artefacts in ultrasound. In addition other, unknown factors may affect the ultrasound images during the course of a tumour resection. Comparing ultrasound findings after (completed) resection, Chacko [4] found that biopsies taken from the tumour margins agreed with ultrasound image findings in the majority of samples, however, there were instances (16%) when the ultrasound reported tumour while the biopsies were negative. LeRoux et al. [18] used intraoperative ultrasound to facilitate gross total resection of brain tumours and obtained biopsies from the resection

**Table 2** Image finding/histopathology of biopsies according to resection phase

Resection phase	Histopathological diagnosis	Interpretation of ultrasound image			
		“Normal”	“Normal, uncertain”	“Tumour, uncertain”	“Tumour”
Before resection	Tumour	0	0	0	32
	Infiltration	2	0	2	6
	Normal	16	2	0	1
During resection	Tumour	1	0	0	22
	Infiltration	2	1	1	6
	Normal	6	2	2	9
After resection	Tumour	4	4	7	0
	Infiltration	5	10	1	0
	Normal	23	14	5	0

The table shows the interpretation of the ultrasound image in columns and the histopathological diagnosis in rows, for each of the three subsequent phases of resection.

**Table 3** Sensitivity, specificity, PPV and NPV of ultrasound for distinguishing tumour from normal tissue according to resection phase

Stage of surgery	Values	
Before resection	Sensitivity	0.95
	Specificity	0.95
	PPV	0.98
	NPV	0.90
During resection	Sensitivity	0.88
	Specificity	0.42
	PPV	0.73
	NPV	0.67
After resection	Sensitivity	0.26
	Specificity	0.88
	PPV	0.62
	NPV	0.62

The sensitivity, specificity, PPV and NPV of ultrasound in each of the subsequent resection phases is shown.

cavity wall after completed resection. They found that among 15 tumours not invading eloquent cortex and thus feasible for total resection, 11 cases (73%) had margins without solid tumour involvement although scattered tumour cells were found. Woydt et al. [40] published a study in 1996, to evaluate ultrasound findings after completed microsurgical resection of gliomas. Biopsies were obtained in (1) hyperechoic areas adjacent to the resection cavity and (2) the hyperechoic rim of the resection cavity. In group 1 (hyperechoic areas adjacent to resection cavity), high-grade glioma cases showed that 90% of biopsies contained tumour tissue, and the rest contained infiltrated tissue. For low-grade glioma cases 85% of biopsies in this group contained tumour tissue, the rest contained infiltrated tissue. Biopsies obtained at the hyperechoic rim (group 2) were heterogeneous, 26% revealed solid tumour tissue, 35% infiltration zone and 39% brain tissue (high-grade and low-grade gliomas combined). Our research group published a study in 2005 [38], comparing ultrasound findings with histopathology by obtaining tissue samples obtained in the tumour border zone before starting the resection. The ultrasound findings were in agreement with the histopathology in 77% of biopsies from glioblastoma cases and 83% and 74% for anaplastic astrocytomas and low-grade astrocytomas, respectively.

In the present paper we report on our results evaluating the ability of intraoperative ultrasound for delineation of glioblastomas before, during and after resection by comparing image findings from image guided biopsies with histopathology.

#### Discussion of findings

The conditions for ultrasound imaging *before resection* are probably close to optimal, and imaging artefacts should be at a minimum level. Before resection, sensitivity was 95% and specificity also was 95%. The PPV and NPV were 98%

and 90%, respectively. This result shows that the ultrasound was highly accurate in delineating glioblastomas prior to resection. The sensitivity and specificity is slightly improved compared to our own study from 2005 [38]. This may be because of increased experience with ultrasound. The result also demonstrates that the sensitivity and specificity of ultrasound for predicting tumour/normal tissue, although operator dependent, is in the range of other, state of the art imaging techniques [16, 23, 28]. Thus, the sensitivity and specificity of ultrasound diagnosis in this phase serve as a baseline for comparison with subsequent phases.

*During resection*, a partial resection had been performed, with a resection cavity and some residual tumour left. The resection cavity wall, having a rough surface, as well as debris, small air bubbles, and blood all contribute to ultrasound imaging artefacts. The values of sensitivity and PPV were 87% and 73%; the specificity and NPV were 42% and 67%. The striking finding is a considerable decrease in specificity. This may be explained by a considerable amount of false positive biopsies; in nine biopsies, which contained normal tissue (as diagnosed by the pathologist), the diagnosis on ultrasound was “tumour”, and two were classified as “tumour, uncertain”. Several factors may explain the high false positive rate, both imaging artefacts and inherent error sources in the method of the study (discussed below). These numbers show that there may be some overestimation of tumour in this phase of surgery, but on the other hand, chances of overlooking areas with residual tumour tissue seem to be low (still high sensitivity).

*After resection*, leaving a cavity with the solid part of the tumour removed, biopsies were sampled in the resection cavity wall only. The same sources of imaging artefacts as discussed above also apply to this phase. The calculated values of sensitivity and PPV were 26% and 62%, while the values of specificity and NPV were 88% and 62%, respectively. The specificity was acceptable; reflecting that normal tissue in the majority of cases was correctly classified on ultrasound, important for patient safety. A sensitivity of 26% is discouraging, but calls for further considerations. First, the number of biopsies deemed “tumour” and “tumour, uncertain” were low in this stage of resection for obvious reasons. Also noteworthy is the high number of biopsies deemed “normal” and “normal, uncertain”, which contained either tumour tissue (four deemed “normal” and another four considered “normal, uncertain”) or tumour-infiltrated tissue (five deemed “normal” and ten deemed “normal, uncertain”). We are not surprised to find infiltrated brain tissue and small tumour remnants in the resection cavity wall, due to the infiltrating nature of glioblastomas. In their paper from 1996, Woydt et al. [40] reported that biopsies obtained from the “hyperechoic rim” of a resection cavity contained solid tumour (26%), infiltration zone (35%) and brain tissue (39%). For

comparison, biopsies taken from the resection cavity (regardless of image finding) wall after resection in this study have a similar, although slightly more favourable distribution; solid tumour 21%; infiltration zone 22% and normal tissue 58%. Comparison of 3D ultrasound findings at the end of resection and early postoperative MRI was not a part of the study. Still, the fact that two of ten patients considered either >95% or 90–95% resected had residual tumour on early postoperative MRI may likewise reflect difficulties in interpreting 3D ultrasound after resection, or limitations of the 3D ultrasound itself.

*In summary*, the diagnostic accuracy of ultrasound for delineating glioblastomas was lower in the subsequent phases of surgery than before resection. During surgery there seemed to be some overestimation of tumour, but residual tumour was rarely missed. After resection, small tumour remnants and infiltrated tissue appeared as normal tissue on ultrasound, lowering the sensitivity. Still in most cases biopsies containing normal tissue were correctly classified with ultrasound.

#### Limitations of the study

Important limitations of the study method must be recognized due to the fact that the 3D ultrasound technique used in this study still is not real time; the biopsy sampling in itself, although performed as gently as possible, may cause some motion of tissue. Furthermore, in some cases that the walls of the resection cavity seemed to collapse a little inwardly when removing the saline after 3D ultrasound image acquisition to what degree these effects have affected the results in this study is not known.

Small and traumatized biopsy specimens in some cases prevented optimal histological examination. The surgeon did not have the opportunity to classify tissue as infiltrated brain tissue, while the pathologist did: Whether this introduces a bias is unknown.

The diagnostic accuracy of ultrasound is user dependent. The majority of biopsies were assessed by a surgeon with long experience using 3D ultrasound (GU), and the rest of the biopsies were assessed by a surgeon with shorter, but significant experience using ultrasound. Interobserver variability analysis on the interpretation of 3D ultrasound images was not done, and this is an important limitation of the current study. In our view, interpreting 3D ultrasound is dependent on interactive navigation, and using 2D snapshots postoperatively may not be sufficient for analysis of interobserver variability. We were not able to record biopsy positions in the 3D ultrasound dataset for postoperative review and analysis.

Systematic comparison of 3D ultrasound at the end of the resection and postoperative MRI was not done as it was not part of the study protocol.

#### Ethical aspects

The ethical aspects of intentional sampling of biopsies in the outer border of the tumour, as seen in the US images, were given consideration. Biopsies from outside of the US indicated border were never sampled in eloquent areas.

We did not see any complications that could be related to the biopsy sampling procedure.

#### Conclusions

Our study shows that while ultrasound is highly accurate in delineating glioblastomas before resection it appears less accurate during and after resection. During resection there seem to be some overestimation of tumour, while small tumour remnants and infiltrated tissue in the cavity wall is underestimated after resection. Due to inherent error sources in the study design, the results must be interpreted with caution. Intraoperative 3D ultrasound still seems a reasonably reliable modality for guidance of the resection of glioblastomas as the sensitivity during resection and the specificity after completed resection are acceptable.

#### References

1. Albert FK, Forsting M, Sartor K, Adams HP, Kunze S (1994) Early postoperative magnetic resonance imaging after resection of malignant glioma: objective evaluation of residual tumour and its influence on regrowth and prognosis. *Neurosurgery* 34:45–60 discussion 60–41
2. Burger PC, Heinz ER, Shibata T, Kleihues P (1988) Topographic anatomy and CT correlations in the untreated glioblastoma multiforme. *J Neurosurg* 68:698–704
3. Chacko AG, Kumar NKS, Chacko G, Athyal R, Rajshekhar V (2003) Intraoperative ultrasound in determining the extent of resection of parenchymal brain tumours—a comparative study with computed tomography and histopathology. *Acta Neurochirurgica* 145:743–748
4. Croteau D, Scarpace L, Hearshen D, Gutierrez J, Fisher JL, Rock JP, Mikkelsen T (2001) Correlation between magnetic resonance spectroscopy imaging and image-guided biopsies: semiquantitative and qualitative histopathological analyses of patients with untreated glioma. *Neurosurgery* 49:823–829
5. Daumas-Duport C, Mounsgaignon V, Blond S, Munari C, Musolino A, Chodkiewicz JP, Missir O (1987) Serial stereotactic biopsies and CT scan in gliomas: correlative study in 100 astrocytomas, oligo-astrocytomas and oligodendrocytomas. *J Neurooncol* 4: 317–328
6. Ganslandt O, Stadlbauer A, Fahlbusch R, Kamada K, Buslei R, Blumcke I, Moser E, Nimsky C (2005) Proton magnetic resonance spectroscopic imaging integrated into image-guided surgery: correlation to standard magnetic resonance imaging and tumor cell density. *Neurosurgery* 56:291–298 discussion 291–298
7. Grønningsæter Å, Kleven A, Ommedal S, Årseth TE, Lie T, Lindseth F, Langø T, Unsgård G (2000) SonoWand, an ultra-

- sound-based neuronavigation system. *Neurosurgery* 47:1373–1380
8. Hammoud MA, Ligon BL, elSouki R, Shi WM, Schomer DF, Sawaya R (1996) Use of intraoperative ultrasound for localizing tumors and determining the extent of resection: a comparative study with magnetic resonance imaging. *J Neurosurg* 84:737–741
  9. Hirschberg H, Samset E, Hol PK, Tillung T, Lote K (2005) Impact of intraoperative MRI on the surgical results for high-grade gliomas. *Minim Invasive Neurosurg* 48:77–84
  10. Iseki H, Muragaki Y, Nakamura R, Ozawa N, Taniguchi H, Hori T, Takakura K (2005) Intelligent operating theater using intraoperative open-MRI. *Magn Reson Med Sci* 4:129–136
  11. Katisko JP, Koivukangas JP (2007) Optically neuronavigated ultrasonography in an intraoperative magnetic resonance imaging environment. *Neurosurgery* 60:373–380 discussion 380–371
  12. Kelly PJ, Daumas-Duport C, Scheithauer BW, Kall BA, Kispert DB (1987) Stereotactic histologic correlations of computed tomography- and magnetic resonance imaging-defined abnormalities in patients with glial neoplasms. *Mayo Clin Proc* 62:450–459
  13. Kleihues P, Cavenee WK (eds) (2000) Pathology and genetics of tumours of the nervous system: world health organization classification of tumours. IARC, Lyon
  14. Knauth M, Aras N, Wirtz CR, Dorfler A, Engelhorn T, Sartor K (1999) Surgically induced intracranial contrast enhancement: potential source of diagnostic error in intraoperative MR imaging. *AJNR Am J Neuroradiol* 20:1547–1553
  15. Koivukangas J, Louhisalmi Y, Alakuijala J, Oikarinen J (1993) Ultrasound-controlled neuronavigator-guided brain surgery. *J Neurosurg* 79:36–42
  16. Kracht LW, Miletic H, Busch S, Jacobs AH, Voges J, Hoevels M, Klein JC, Herholz K, Heiss WD (2004) Delineation of brain tumor extent with [<sup>11</sup>C]-methionine positron emission tomography: local comparison with stereotactic histopathology. *Clin Cancer Res* 10:7163–7170
  17. Lacroix M, Abi-Said D, Fourney DR, Gokaslan ZL, Shi W, DeMonte F, Lang FF, McCutcheon IE, Hassenbusch SJ, Holland E, Hess K, Michael C, Miller D, Sawaya R (2001) A multivariate analysis of 416 patients with glioblastoma multiforme: prognosis, extent of resection, and survival. *J Neurosurg* 95:190–198
  18. LeRoux PD, Winter TC, Berger MS, Mack LA, Wang K, Elliott JP (1994) A comparison between preoperative magnetic resonance and intraoperative ultrasound tumor volumes and margins. *J Clin Ultrasound* 22:29–36
  19. Letteboer MM, Willems PW, Viergever MA, Niessen WJ (2005) Brain shift estimation in image-guided neurosurgery using 3-D ultrasound. *IEEE Trans Biomed Eng* 52:268–276
  20. Lindner D, Trantakis C, Renner C, Arnold S, Schmitgen A, Schneider J, Meixensberger J (2006) Application of intraoperative 3D ultrasound during navigated tumor resection. *Minim Invasive Neurosurg* 49:197–202
  21. Lindseth F, Lango T, Bang J, Nagelhus Hernes TA (2002) Accuracy evaluation of a 3D ultrasound-based neuronavigation system. *Comput Aided Surg* 7:197–222
  22. Lunsford LD, Martinez AJ, Latchaw RE (1986) Magnetic resonance imaging does not define tumor boundaries. *Acta Radiol Suppl* 369:154–156
  23. McKnight TR, von dem Bussche MH, Vigneron DB, Lu Y, Berger MS, McDermott MW, Dillon WP, Graves EE, Pirzkall A, Nelson SJ (2002) Histopathological validation of a three-dimensional magnetic resonance spectroscopy index as a predictor of tumor presence. *J Neurosurg* 97:794–802
  24. Nimsky C, Ganslandt O, Buchfelder M, Fahlbusch R (2006) Intraoperative visualization for resection of gliomas: the role of functional neuronavigation and intraoperative 1.5 T MRI. *Neurol Res* 28:482–487
  25. Nimsky C, Ganslandt O, Cerny P, Hastreiter P, Greiner G, Fahlbusch R (2000) Quantification of, visualization of, and compensating for brain shift using intraoperative magnetic resonance imaging. *Neurosurgery* 47:1070–1080
  26. Nimsky C, Ganslandt O, Hastreiter P, Fahlbusch R (2001) Intraoperative compensation for brain shift. *Surg Neurol* 56:357–364 discussion 364–355
  27. Nimsky C, Ganslandt O, von Keller B, Romstock J, Fahlbusch R (2004) Intraoperative high-field-strength MR imaging: implementation and experience in 200 patients. *Radiology* 233:67–78
  28. Price SJ, Jena R, Burnet NG, Hutchinson PJ, Dean AF, Pena A, Pickard JD, Carpenter TA, Gillard JH (2006) Improved delineation of glioma margins and regions of infiltration with the use of diffusion tensor imaging: an image-guided biopsy study. *AJNR Am J Neuroradiol* 27:1969–1974
  29. Reinges MHT, Nguyen HH, Krings T, Hutter BO, Rohde V, Gilsbach JM (2004) Course of brain shift during microsurgical resection of supratentorial cerebral lesions: limits of conventional neuronavigation. *Acta Neurochirurgica* 146:369–377
  30. Rubin JM, Dohrmann GJ (1985) Efficacy of intraoperative US for evaluating intracranial masses. *Radiology* 157:509–511
  31. Sergeeva O, Uhlemann F, Schackert G, Hergeth C, Morgenstern U, Steinmeier R (2006) Integration of intraoperative 3D-ultrasound in a commercial navigation system. *Zentralbl Neurochir* 67:197–203
  32. Stadlbauer A, Ganslandt O, Buslei R, Hammen T, Gruber S, Moser E, Buchfelder M, Salomonowitz E, Nimsky C (2006) Gliomas: histopathologic evaluation of changes in directionality and magnitude of water diffusion at diffusion-tensor MR imaging. *Radiology* 240:803–810
  33. Steinmeier R, Fahlbusch R, Ganslandt O, Nimsky C, Buchfelder M, Kaus M, Heigl T, Lenz G, Kuth R, Huk W (1998) Intraoperative magnetic resonance imaging with the magnetom open scanner: concepts, neurosurgical indications, and procedures: a preliminary report. *Neurosurgery* 43:739–747 discussion 747–738
  34. Sutherland GR, Kaibara T, Louw D, Hoult DI, Tomanek B, Saunders J (1999) A mobile high-field magnetic resonance system for neurosurgery. *J Neurosurg* 91:804–813
  35. Unsgaard G, Gronningsaeter A, Ommedal S, Nagelhus Hernes TA (2002) Brain operations guided by real-time two-dimensional ultrasound: new possibilities as a result of improved image quality. *Neurosurgery* 51:402–411 discussion 411–402
  36. Unsgaard G, Ommedal S, Muller T, Gronningsaeter A, Nagelhus Hernes TA (2002) Neuronavigation by intraoperative three-dimensional ultrasound: initial experience during brain tumor resection. *Neurosurgery* 50:804–812 discussion 812
  37. Unsgaard G, Rygh OM, Selbekk T, Muller TB, Kolstad F, Lindseth F, Hernes TA (2006) Intra-operative 3D ultrasound in neurosurgery. *Acta Neurochir (Wien)* 148:235–253
  38. Unsgaard G, Selbekk T, Brostrup Muller T, Ommedal S, Torp SH, Myhr G, Bang J, Nagelhus Hernes TA (2005) Ability of navigated 3D ultrasound to delineate gliomas and metastases—comparison of image interpretations with histopathology. *Acta Neurochir (Wien)* 147:1259–1269 discussion 1269
  39. Wirtz CR, Knauth M, Staubert A, Bonsanto MM, Sartor K, Kunze S, Tronnier VM (2000) Clinical evaluation and follow-up results for intraoperative magnetic resonance imaging in neurosurgery. *Neurosurgery* 46:1112–1120 discussion 1120–1112
  40. Woydt M, Krone A, Becker G, Schmidt K, Roggendorf W, Roosen K (1996) Correlation of intra-operative ultrasound with histopathologic findings after tumour resection in supratentorial gliomas. A method to improve gross total tumour resection. *Acta Neurochir (Wien)* 138:1391–1398

**Comment**

There are only few papers analyzing the validity of intraoperative ultrasound findings. One possibility is to correlate the intraoperative ultrasound images with early postoperative MR images to see whether there are any discrepancies in the evaluation of tumour resection. This does not account for that a tumour margin in MR images does not exactly reflect the biological tumour margin, which actually does not exist. Morten et al. correlated histopathology findings with intraoperative ultrasound to analyze whether intraoperative ultrasound is able to distinguish tumour and normal brain. Navigated tissue samples were taken at various stages of surgery at the tumour border. This study clearly shows that intraoperative ultrasound is a reliable tool to evaluate the extent of a tumour at the beginning of surgery. However,

after resection of major tumour parts sensitivity dramatically decreased, surgically induced changes at the tumour border led to false image interpretation, reducing the value of intraoperative ultrasound being used for resection control. To which extent this effect also depends on the ultrasound technology is an open question. Ultrasound imaging has undergone impressive improvements in the last years, so that these shortcomings might be solved in the near future. The authors are to be encouraged to continue their innovative work; the combination of intraoperative ultrasound with histology compared with early postoperative MR images will result in further information on the validity of intraoperative ultrasound.

*Christopher Nimsky*  
Erlangen, Germany

